

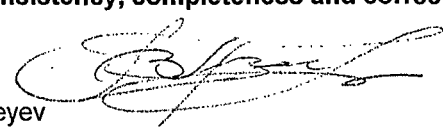



Enclosure 37 to TN E-29128

Transnuclear Calculation MP197HB-0401, Revision 2
associated with RAI 3-21 (Non-proprietary)

 AREVA TRANSNUCLEAR INC.	Form 3.2-1 Calculation Cover Sheet TIP 3.2 (Revision 4)	Calculation No.: MP197HB-0401						
		Revision No.: 2						
		Page: 1 of 112						
DCR NO (if applicable) : NUH09-006, Rev. 0	PROJECT NAME: MP197HB Transport Packaging Design							
PROJECT NO: 61003	CLIENT: Transnuclear, Inc.							
CALCULATION TITLE: <p style="text-align: center;">Thermal Analysis of MP197HB Transport Cask for Normal Conditions of Transport</p> SUMMARY DESCRIPTION: <p>1) Calculation Summary</p> <p>This calculation determines the maximum component temperatures of MP197HB transport cask for normal conditions of transport (NCT) for 100°F, -20°F, and -40°F ambient temperatures. The temperature distribution of the DSC shell is determined to be used for detail analysis of the basket. The maximum accessible surface temperature is also evaluated in this calculation.</p> <p>2) Storage Media Description</p> <p>Secure network server initially, then redundant tape backup</p>								
If original issue, is licensing review per TIP 3.5 required? Yes <input type="checkbox"/> No <input checked="" type="checkbox"/> (explain below) Licensing Review No.: N/A								
This calculation is performed to support a 10CFR71 transport license application that will be reviewed and approved by the NRC. Therefore, a 10CFR72.48 licensing review per TIP 3.5 is not applicable.								
Software Utilized: ANSYS	Version: 8.1							
Calculation is complete: Originator Name and Signature: Kamran Tavassoli 	Date: 03/09/10							
Calculation has been checked for consistency, completeness and correctness: Checker Name and Signature: Slava Guzeyev 	Date: 03/09/2010							
Calculation is approved for use: Project Engineer Name and Signature: Steven Streutker 	Date: 4/9/10							

REVISION SUMMARY

REV.	DATE	DESCRIPTION	AFFECTED PAGES	AFFECTED Computational I/O
0	03/27/09	Initial Issue	All	All
1	04/29/09	Changes due to Internal Review	All affected pages are indicated by revision bars	None
2	4/9/10	To address RAI questions a justification of the assumption that the personnel barrier is out of out streams from the cask is added in Section 5.6.1.	1-7, 9-12, 57, 58, 60-65, and 88	One Spreadsheet (BL thk.xls) is added. See Table 8-4

TABLE OF CONTENTS

	<u>Page</u>
1.0 Purpose.....	7
2.0 References.....	9
3.0 Assumptions and Conservatism.....	12
4.0 Design Input.....	16
4.1 Thermal Properties of Materials.....	16
4.2 Surface Properties of Materials.....	23
4.3 Design Criteria.....	23
5.0 Methodology.....	25
5.1 Effective Heat Transfer Coefficient for External Fins.....	40
5.2 Effective Conductivity for Helium Gap between DSC and TC/Sleeve.....	45
5.3 Effective Conductivity for DSC Top and Bottom Cover Plates.....	49
5.4 Effective Conductivity for TC Slide Rails.....	54
5.5 Effective Conductivity for Inner Sleeve.....	55
5.5.1 Axial Effective Conductivity.....	55
5.5.2 Radial Effective Conductivity.....	56
5.6 Maximum Accessible Surface Temperature.....	57
5.6.1 Evaluation of Thermal Boundary Layer Thickness on Cask.....	60
6.0 Results.....	66
6.1 Maximum Temperatures.....	66
6.2 Maximum Accessible Surface Temperature.....	76
6.3 Heat Balance.....	77
7.0 Conclusion.....	82
8.0 Listing of Computer Files.....	85
APPENDIX A Shapes of External Fins and Inner Sleeve.....	89
APPENDIX B Total Heat Transfer Coefficients.....	94
APPENDIX C Justification of Gamma Shield / Outer Shell Gap.....	97
APPENDIX D Justification of Cask Shield Shell / Aluminum Finned Shell Gap.....	100
APPENDIX E Mesh Sensitivity.....	104
APPENDIX F Sensitivity Analysis for Temperatures at Contact Area between Slide Rails and DSC Shell.....	105
APPENDIX G Thermal Analysis Results for MP197HB loaded with 37PTH DSC and 23.2 kW Heat Load for Structural Analysis Input.....	107
APPENDIX H Thermal Analysis Results for MP197HB loaded with 69BTH DSC and 32 kW Heat Load without External Fins.....	108

LIST OF TABLES

	<u>Page</u>
Table 1-1 DSC Types and Heat Loads in MP197HB	8
Table 3-1 Nominal DSC Dimensions in MP197HB Model.....	15
Table 4-1 List of Materials in ANSYS Model	17
Table 4-2 Stainless Steel Properties	18
Table 4-3 Low Alloy Steel Properties	18
Table 4-4 Carbon Steel Properties.....	19
Table 4-5 Aluminum Alloys Properties	19
Table 4-6 Lead Properties	19
Table 4-7 Non-Metallic Solids Properties	20
Table 4-8 Helium Thermal Conductivity	20
Table 4-9 Air Thermal Properties	21
Table 4-10 Thermal Conductivity for SS304 and A36 in Various ASME Years.....	22
Table 5-1 Normal Conditions of Transport for MP197HB.....	25
Table 5-2 Solar Heat Flux	26
Table 5-3 Decay Heat Flux	27
Table 5-4 Distance between DSC and TC Centerlines	28
Table 5-5 Effective Heat Transfer Coefficients for External Fins @ 100°F Ambient	42
Table 5-6 Effective Heat Transfer Coefficients for External Fins @ -20°F Ambient	43
Table 5-7 Effective Heat Transfer Coefficients for External Fins @ -40°F Ambient	43
Table 5-8 Radial Effective Conductivity for Helium in DSC Shell/TC Inner Shell Gap	47
Table 5-9 Radial Effective Conductivity for Helium in DSC Shell/TC Inner Sleeve Gap	48
Table 5-10 Axial Effective Conductivities for Bottom Shield Plug and Top Inner Cover Plate	51
Table 5-11 Axial Effective Conductivities for Cover Plates of 24PT4 DSC	52
Table 5-12 Axial Effective Conductivities for Lead Shield Plugs of 24PT4 DSC	53
Table 5-13 Effective Conductivities for TC Slide Rail.....	54
Table 5-14 Effective Conductivity of Inner Sleeve	56
Table 5-15 Variation of Grashof, Prandtl, and Rayleigh Numbers	63
Table 5-16 Variation of C_f and f in Calculation of Nu_L	64
Table 5-17 Variation of Nu_L/Nu_D	64
Table 5-18 Thickness of the Thermal Boundary Layer	65
Table 6-1 Maximum Temperatures of TC Component / DSC Shell for Hot NCT (100°F and Insolation)	66
Table 6-2 Average TC Component Temperatures for Hot NCT (100°F and Insolation).....	70
Table 6-3 Comparison of Maximum DSC Shell Temperatures	74
Table 6-4 Maximum Component Temperatures for Cold NCT (69BTH, 32 kW, No Insolation)	75
Table 6-5 Maximum Component Temperatures for Cold NCT (37PTH, 22.0 kW, No Insolation)	76
Table 6-6 Insolation Boundary Conditions for MP197HB.....	78

Table 6-7	Heat Balance for MP197HB.....	81
Table 7-1	Maximum Temperatures of TC Component / DSC Shell for Hot NCT	83
Table 7-2	Maximum Temperatures of TC Component / DSC Shell for Cold NCT	84
Table 8-1	List of Geometry Files	85
Table 8-2	Summary of ANSYS Runs	86
Table 8-3	Associated Files and Macros	87
Table 8-4	List of Spreadsheets	88
Table C-1	Thermal Expansion Coefficients	97
Table C-2	Density of Lead	97
Table D-1	Surface Properties for Aluminum and Stainless Steel Plates.....	102
Table D-2	Contact Resistances between Shield Shell and Finned Aluminum Shell	102
Table E-1	Maximum Temperatures for Coarse and Fine Model of MP197HB TC.....	104
Table F-1	Temperatures at Contact between TC Rail and DSC Shell for Sensitivity Analysis	106
Table G-1	Maximum Component Temperatures for MP197HB loaded with 37PTH DSC and 23.2 kW Heat Load.....	107
Table H-1	Maximum Component Temperatures of TC and 69BTH DSC with 32 kW Heat Load within MP197HB with No External Fins	109

LIST OF FIGURES

	<u>Page</u>
Figure 5-1 Transport Configuration for MP197HB Cask.....	30
Figure 5-2 Location of DSC within MP197HB TC.....	31
Figure 5-3 Finite Element Model of MP197HB with 69BTH DSC	32
Figure 5-4 MP197HB Finite Element Model, Components.....	33
Figure 5-5 Gaps in MP197HB Transport Cask Model.....	34
Figure 5-6 MP197HB Finite Element Model, Cross Section.....	35
Figure 5-7 Gaps in Cross Section	36
Figure 5-8 Typical Decay Heat and Insolation Boundary Conditions	37
Figure 5-9 Typical Convection and Radiation Boundary Conditions	38
Figure 5-10 Typical Convection and Radiation Boundary Conditions – Details.....	39
Figure 5-11 Sub-Model of the External Fins for MP197HB TC.....	44
Figure 5-12 Sub-Model for Helium Gap Effective Conductivity Calculation.....	45
Figure 5-13 Schematic View of Cask and Personnel Barrier	59
Figure 6-1 Temperature Profiles for MP197HB Transport Cask NCT, 100°F, Insolation, 69BTH DSC, 32 kW.....	68
Figure 6-2 Temperature Profiles for MP197HB Transport Cask NCT, 100°F, Insolation, 24PTH DSC, 26 kW.....	69
Figure 6-3 Comparison of DSC Shell Temperature Profiles for 61BTH DSC	72
Figure 6-4 Comparison of DSC Shell Temperature Profiles for 24PTH DSC	73
Figure A-1 Assumed Geometry of External Fins in Thermal Model.....	90
Figure A-2 Assumed Geometry of Inner Sleeve in Thermal Model	91
Figure A-3 Designed Geometry of External Fins	92
Figure A-4 Designed Geometry of the Inner Sleeve	93
Figure D-1 Conforming Rough Surfaces [15].....	103
Figure H-1 Temperature Profiles for MP197HB Transport Cask NCT, 100°F, Insolation, 69BTH DSC, 32 kW, No External Fins	110
Figure H-2 Temperature Profiles for 69BTH DSC Components NCT, 100°F, HLZC #4 [25] in TC w/o External Fins.....	111

1.0 PURPOSE

The purpose of this calculation is to determine the maximum component temperatures and the DSC shell temperature distribution for MP197HB transport cask (TC) under normal conditions of transport (NCT) with 100°F ambient temperature and insolation. The maximum accessible surface temperature of the TC under shade is also evaluated in this calculation.

The temperature distributions under cold NCT with -20°F and -40°F ambient temperatures, and no insolation are determined to be used in structural analysis.

MP197HB transport cask includes optional features such as aluminum inner sleeve to accommodate DSC types with outer diameters smaller than 69.75" and an aluminum shell with external circular fins to accommodate heat loads over 26 kW. The optional features along with the DSC types and their maximum heat loads considered for transportation in MP197HB are summarized in Table 1-1.

Based on Table 1-1, the maximum decay heat load for transport of DSC types 61BTH Type 1, 61BT, 32PT, and 24PT4 are considered at their maximum heat load for storage conditions.

The maximum decay heat load for transport of DSC types 32PTH, 32PTH Type 1, 32PTH1 Type 1, and 24PTH Type 1 (24PTH-S or 24PTH-L with aluminum inserts) and Type 2 (24PTH-S, 24PTH-L, or 24PTH-S-LC without aluminum inserts) are considered equal to 26.0 kW which is the maximum heat load for MP197HB without external fins.

The maximum decay heat load for 24PTH-S-LC (without aluminum inserts) is 24 kW [3]. Therefore, the analysis of 24PTH DSC Type 2 with 26 kW heat load is bounding for 24PTH-S-LC with 24 kW heat load.

The maximum decay heat load for transport of DSC types 61BTH Type 2 and 32PTH1 Type 2 are considered equal to 24.0 kW in order to maintain the maximum DSC shell temperature below the values reported in [5] for normal transfer conditions. The maximum decay heat load for 37PTH DSC is considered equal to 22.0 kW for transport operations.

DSC types 61BTHF and 24PTHF contain failed fuel and have possibly lower heat loads than DSC types 61BTH and 24PTH, respectively. Nevertheless, it is considered in this calculation that the heat loads for DSC types 61BTHF and 24PTHF are the same as those for DSC types 61BTH and 24PTH, respectively.

To address RAI questions, a discussion is added in Section 5.6.1 to justify the assumption that the personnel barrier is exposed to hot air stream from the cask.

The shapes of inner sleeve and external fins considered in this calculation are discussed in APPENDIX A.

Calculation

Calculation No.: MP197HB-0401

Revision No.: 2

Page: 8 of 112

To provide thermal input for structural evaluation, a heat load of 23.2 kW was considered for 37PTH DSC. Since the considered heat load of 23.2 kW is higher than the design heat load of 22.0 kW, this approach is conservative for structural evaluation of 37PTH DSC. The maximum component temperatures for 37PTH DSC with 23.2 kW are summarized in APPENDIX G.

Table 1-1 DSC Types and Heat Loads in MP197HB

	DSC type	DSC OD (in)	Sleeve	External Fins	Max. Heat Load for Storage (kW)	Max. Heat Load for Transport (kW)
1	69BTH	69.75	No	No	N/A	26.0
2				Yes	N/A	29.2
3				Yes	N/A	32.0
4	61BTH Type 1 ⁽¹⁾	67.25	Yes	No	22.0 [5]	22.0
5	61BTH Type 2 ⁽¹⁾	67.25	Yes	No	31.2 [5]	24.0
6	61BT	67.25	Yes	No	18.3 [3]	18.3
7	37PTH	69.75	No	No	N/A	22.0
8	32PTH / 32PTH Type 1	69.75	No	No	34.8 [6]	26.0
9	32PTH1 Type 1	69.75	No	No	40.8 [5]	26.0
10	32PTH1 Type 2	69.75	No	No	31.2 [5]	24.0
11	32PT	67.19	Yes	No	24.0 [3]	24.0
12	24PTH Type 1 ⁽¹⁾ (24PTH-S or -L w/ Al inserts)	67.19	Yes	No	40.8 [3]	26.0
13	24PTH Type 2 ⁽¹⁾ (24PTH-S or -L w/o Al inserts)	67.19	Yes	No	31.2 [3]	26.0
14	24PTH Type 2 ⁽¹⁾ (24PTH-S-LC)	67.19	Yes	No	24.0 [3]	24.0 ⁽²⁾
15	24PT4	67.19	Yes	No	24.0 [4]	24.0

Note (1): DSC types 61BTHF and 24PTHF has the same dimensions and use the same MP197HB features as DSC types 61BTH and 24PTH, respectively.

Note (2): The analysis for 24PTH-S-LC DSC is bounded by 24PTH DSC Type 2 with 26 kW heat load.

2.0 REFERENCES

- 1 U.S. Code of Federal Regulations, Part 71, Title 10, "Packaging and Transportation of Radioactive Material".
- 2 Project MP197HB, "Design Criteria Document (DCD) for the NUHOMS® MP197HB Transport Package", Transnuclear, Inc., Document No. MP197HB.0101, Rev. 2.
- 3 Updated Final Safety Analysis Report for the Standardized NUHOMS® Horizontal Modular Storage System for Irradiated Nuclear Fuel, NUH-003, Rev. 11.
- 4 Updated Final Safety Analysis Report for the Standardized Advanced NUHOMS® Horizontal Modular Storage System for Irradiated Nuclear Fuel, ANUH-01.0150, Rev. 3.
- 5 Safety Analysis Report for the Standardized NUHOMS® Horizontal Modular Storage System for Irradiated Nuclear Fuel, Amendment 10, Rev. 5.
- 6 Final Safety Analysis Report for NUHOMS® HD Horizontal Modular Storage System for Irradiated Nuclear Fuel, Rev. 1.
- 7 Rohsenow, Hartnett, Cho, "Handbook of Heat Transfer", 3rd Edition, 1998.
- 8 ASME Boiler and Pressure Vessel Code, Section II, Part D, "Material Properties", 2004 with 2006 Addenda.
- 9 Rohsenow, Hartnett, "Handbook of Heat Transfer Fundamentals", 2nd Edition, 1985.
- 10 Calculation, "NUHOMS-61B, Finite Element Model for Thermal Analysis", Transnuclear, Inc., Calculation No. 1093-20, Rev. 0.
- 11 Siegel, Howell, "Thermal Radiation Heat Transfer", 4th Edition, 2002.
- 12 Bucholz, J. A., *Scoping Design Analysis for Optimized Shipping Casks Containing 1-, 2-, 3-, 5-, 7-, or 10-Year old PWR Spent Fuel*, Oak Ridge National Laboratory, January, 1983, ORNL/CSD/TM-149.
- 13 Perry, Chilton, "Chemical Engineers' Handbook", 5th Edition, 1973.
- 14 ANSYS computer code and On-Line User's Manuals, Version 8.1.
- 15 M. M. Yovanovich, J. R. Culham, P. Teertstra, "Calculating Interface Resistance", Electronics Cooling, Vol. 3, No. 2, May 1997.
- 16 Amiss, J. M., et al., "Machinery's Handbook", 24th Edition, Industrial Press, 1992 - Fig. 5, pg 672.

- 17 Aluminum Association, Inc., "Aluminum Standards and Data", 10th Edition, 1990 - Table 2.1, pg 33.
- 18 Not Used.
- 19 Gordon England Company, "Microhardness Test",
<http://www.gordonengland.co.uk/hardness/microhardness.htm>
- 20 U.S. Code of Federal Regulations, Part 72, Title 10, "Licensing Requirements for the Independent Storage of Spent Nuclear Fuel and High-Level Radioactive Waste".
- 21 Calculation, "NUHOMS[®]-61BTH DSC Thermal Evaluation for Storage and Transfer Conditions", Transnuclear, Inc., Calculation No. NUH61BTH-0403, Rev. 0.
- 22 Calculation, "NUHOMS[®]-24PTH DSC Thermal Evaluation for Storage and Transfer Conditions", Transnuclear, Inc., Calculation No. NUH24PTH-0403, Rev. 5.
- 23 ASME Boiler and Pressure Vessel Code, Section II, Part D, "Material Properties", 1998 with 2000 addenda.
- 24 Kumar, Madras, "Thermal Degradation Kinetics of Isotactic and Atactic Polypropylene," Journal of Applied Polymer Science, Vol. 90, 2206-2213, 2003.
- 25 Calculation, "Thermal Analysis of Baskets for Normal Conditions of Transport in MP197HB Transport Cask", Transnuclear, Inc., Calculation No. MP197HB-0402, Rev. 1.
- 26 Calculation, "NUHOMS MP197HB Transport Cask Weight Properties Calculation", Transnuclear, Inc., Calculation No. MP197HB-0200, Rev. 0.
- 27 Safety Analysis Report for NUHOMS[®]-MP197 Transport Packaging, Rev. 4.
- 28 Henninger, J. H., "Solar Absorptance and Thermal Emittance of Some Common Spacecraft Thermal-Control Coatings," NASA Scientific and Technical Information Branch, NASA Reference Publication 1121, 1984.
- 29 Eckert, "Introduction to the Transfer of Heat and Mass", 1st Edition, 1950.
- 30 Eckert and Jackson, "Analysis of Turbulent Free-Convection Boundary Layer on Flat Plate", NASA Technical Reports, Report Number NACA-TN-2207, 1950.
- 31 Kays, Crawford, and Weigand, "Convective Heat and Mass Transfer", 4th Edition, 2005.
- 32 Holman, "Heat Transfer", 8th Edition, 1997.
- 33 Kreith, "Principles of Heat Transfer", 3rd Edition, 1973.

- 34 Misumi, Suzuki, and Kitamura, "Fluid Flow and Heat Transfer of Natural Convection around Large Horizontal Cylinders: Experiments with Air", *Heat Transfer—Asian Research*, 32 (4), 2003.

3.0 ASSUMPTIONS AND CONSERVATISM

The following assumptions are considered in the MP197HB model.

DSC types without spacer are centered axially in the transport cask. For DSC types with the spacer, a 0.5" gap is considered between the DSC outer top cover plate and the cask lid. These assumptions reduce the axial heat transfer and maximize the DSC shell temperature, which in turn result in higher fuel cladding temperature.

Heat load is simulated by heat flux distributed uniformly over the basket length on the radial inner surface of the DSC shell.

Since the transfer operation occurs in horizontal position, the lower halves of the cask cylindrical surfaces are not exposed to insolation. No solar heat flux is considered over these surfaces. To remove any uncertainty about the solar impact on the vertical surfaces, the entire surface areas of vertical surfaces are considered for application of the solar heat flux.

For the finned cask, insolation is applied only over the radial surfaces of the shield shell and fins. Insolation over the vertical surfaces of the fins is ignored. This approach is justified since the shadow of the exposed fins covers most of the other fins and the cask outer surface.

No convection is considered within the cask cavity.

No convection is considered between the cask ends and the thermal shields.

No heat transfer is considered within the bearing block.

No heat transfer is considered through spacers for short DSC types.

Heat dissipations from lateral surfaces of the skid straps, inner radial surface of impact limiter recess, thermal shield outer rings, and neutron shield end caps are conservatively neglected, see Figure 5-10.

No thermal radiation to ambient is considered for the cask surfaces in contact with the transport skid saddles. These areas are shown in Figure 5-9 and Figure 5-10.

Radiation heat exchange is considered between the DSC and the cask inner shell / inner sleeve by calculating effective conductivities for helium in this region. As discussed in Section 4.2, a conservative emissivity of 0.587 is considered for the painted surfaces of the cask inner shell for this calculation.

It is assumed that the personnel barrier is out of the hot streams from the cask. This assumption is justified in Section 5.6.1.

The following gaps are considered in the MP197HB transport cask model:

- 0.0625" axial gap between thermal shield and impact limiter shell

- 0.0625" axial gap between the three inches high, thermal shield standoffs and the cask top or bottom end surfaces
- 0.10" diametrical gap between cask lid and cask inner shell
- 0.01" axial gap between cask lid and cask flange
- 0.01" axial gap between ram closure plate and cask bottom plate
- 0.01" radial gaps between neutron shield boxes and surrounding shells
- 0.025" radial gap between gamma shield and cask outer shell
- 0.01" radial gaps between the cask inner shell and aluminum sleeve
- 0.01" radial gap between the finned aluminum shell and the cask shield shell
- 0.0625" axial gaps between the DSC bottom shield plug and bottom cover plates
- 0.0625" axial gaps between the DSC top inner cover and the adjacent top shield plug and top outer cover plate
- 0.025" axial gaps between the lead shield plugs and encapsulating plates for 24PT4 DSC
- 0.01" gaps between trunnion replacement plugs and the trunnion attachment blocks.

The 0.0625" gaps between thermal shield, impact limiter shell, and cask top or bottom end surfaces are based on assumption in MP197 SAR [27] and account for the 0.06" thick weld overlay conservatively.

The 0.01" gap between cask lid/ cask flange and ram closure plate/cask bottom plate account for thermal resistance between bolted components. The 0.01" radial gaps between the neutron shield boxes and the surrounding shells is also based on assumptions in MP197 SAR [27].

The gap of 0.025" assumed between gamma shield and cask outer shell is justified in APPENDIX C.

The radial gap of 0.01" assumed between the finned aluminum shell and the cask shield shell is justified in APPENDIX D.

The 0.0625" and 0.025" axial gaps between DSC end plates maximize the radial heat transfer through DSC shell toward the cask to bound the maximum component temperatures conservatively.

The width of TC slide rail is 3". For conservatism, a gap of 0.01" with a contact width of 0.12" is considered between the TC slide rails and the DSC shell at 168° and 192° orientations. The 0° orientation is located at the top of the horizontal TC as shown in [26], Appendix B, Sketch B.5. The sensitivity of the maximum component temperatures to the size of this gap is discussed in APPENDIX F.

The finned shell is divided into three axial sections with one inch distance between adjacent sections and no finned shell is considered over the trunnion plugs in the model. Since the finned shell is designed as a continuous shell which covers the trunnion plugs, the model which has fewer fins is conservative for thermal analysis of transport cask under NCT.

APPENDIX H provides results for the most limiting case of 69BTH payload with 32 kW and no external fins on the cask. This appendix demonstrates the conservatism provided by adding the external fins into the design.

The conservatism involved in the calculation of the maximum accessible surface temperature is discussed in Section 5.6.

The nominal dimensions considered for DSCs in MP197HB model are listed in Table 3-1. For each basket type, the shortest cavity length is considered for the analysis to bound the maximum decay heat flux.

To provide thermal input for structural evaluation, a heat load of 23.2 kW (along with 22.0 kW) is considered for 37PTH DSC. Since the heat load of 23.2 kW is higher than the design heat load of 22.0 kW, this assumption is conservative for structural evaluation of 37PTH DSC.

Table 3-1 Nominal DSC Dimensions in MP197HB Model

Parameter ⁽¹⁾	69BTH	61BT / 61BTH Type 1	61BTH Type 2	37PTH ⁽²⁾	32PTH / 32PTH1 ⁽³⁾	32PT ⁽⁴⁾	24PTH ⁽⁵⁾	24PT4
Outer Top Cover	2.00	1.25	1.50	2.00	2.00	1.50	1.50	1.25
Inner Top Cover	2.00	0.75	1.25	2.00	2.00	1.25	1.25	6.75 ⁽⁶⁾
Top Shield Plug	5.75	7.00	6.25	5.75	8.00	7.50	6.25	
Total Top End	9.75	9.00	9.00	9.75	12.00	10.25	9.00	8.00
Inner Bottom Cover	2.25 ⁽⁸⁾	0.75	1.75	2.25 ⁽⁸⁾	2.25	1.75	1.75	2.00
Bottom Shield Plug	3.00 ⁽⁸⁾	5.00	4.00	3.00 ⁽⁸⁾	4.50	5.25	4.00	4.75 ⁽⁶⁾
Outer Bottom Cover	2.00	1.75	1.75	2.00	2.00	1.75	1.75	
Total Bottom End	7.25	7.50	7.50	7.25	8.75	8.75	7.50	6.75
Cavity Length	178.41	179.50	179.50	164.38	164.38	167.10	169.60	180.20
Canister Length (w/o grapple) ⁽⁷⁾	195.41	196.00	196.00	181.38	185.13	186.10	186.10	194.95
Basket height	164	164	164	162	162.00	166.10	168.60	179.13

Note (1): DSC types 61BTHF and 24PTHF has the same dimensions as DSC types 61BTH and 24PTH, respectively.

Note (2): The shortest cavity length for 37PTH baskets belongs to 37PTH-S.

Note (3): The shortest cavity length for 32PTH, 32PTH, type 1 and 32PTH1 Type 1 & 2 baskets belongs to 32PTH1-S.

Note (4): The shortest cavity length for 32PT baskets belongs to 32PT-S125.

Note (5): The shortest cavity length for 24PTH baskets belongs to 24PTH-S.

Note (6): Shield plugs of 24PT4 DSC are lead encapsulated in plates of stainless steel 316, see [4]

Note (7): The canister length in the model is the sum of total top end, total bottom end, and cavity length.

Note (8): The thicknesses of inner bottom cover plate and bottom shield plug for 69BTH and 37PTH DSCs are designed as 1.75" and 3.5", respectively. Since the bottom shield plug (carbon steel) has a higher conductivity than inner bottom cover plate (stainless steel), considering a smaller thickness of 3" for bottom shield plug and higher thickness of 2.25" for inner bottom cover plate is conservative which increases the thermal resistance across these two plates.

4.0 DESIGN INPUT

4.1 Thermal Properties of Materials

Materials used in the transport cask model are listed in Table 4-1.

Thermal conductivity values used in this calculation are listed in Table 4-2 through Table 4-9.

Various ASME code years are called for DSCs in MP197HB in [2], Table 2-1. Except for 24PT4, the other DSC types are covered by ASME code from 1998 to 2006.

The shell and cover plates of all DSC types except for 24PT4 consist of stainless steel SA-240, type 304 (SS304). There are no changes in thermal conductivity of SS304 in ASME 1998 to 2006 in temperature range from 70 to 700°F. This range properly covers the DSC shell temperature for all DSC types in this calculation.

The shield plugs of all DSC types except for 24PT4 consist of carbon steel A36. The changes in the A36 conductivity between ASME code years 1998 to 2006 are limited to $\pm 0.9\%$ as shown in Table 4-10. Since relative large gaps of 0.0625" are considered between the DSC shield plugs and the cover plates, this small change has no significant effect on the thermal evaluation.

The conductivity values in various ASME code years for SA-240, type 304 and A36 are compared in Table 4-10.

The thermal properties for 24PT4 DSC are taken from UFSAR ANUH [4]. These properties are based on ASME code 1992 through 1994 addenda and used in this calculation without any changes.

Table 4-1 List of Materials in ANSYS Model

Component	Mat # in ANSYS Model	Material
DSC shell	1	SA-240, type 304, SA-240, type 316 for 24PT4
DSC bottom inner cover plate	2	SA-240, type 304 SA-240, type 316 for 24PT4 with axial gaps ⁽¹⁾
DSC bottom shield plug	3	A36 with axial gaps ⁽¹⁾
	6	Lead for 24PT4 with axial gaps ⁽¹⁾
DSC top inner cover plate	4	SA-240, type 304 with axial gaps ⁽¹⁾ SA-240, type 316 for 24PT4
	5	A36
DSC top shield plug	9	Lead for 24PT4 with axial gaps ⁽¹⁾
DSC outer cover plates	7	SA-240, type 304 SA-240, type 316 for 24PT4
	67	SA-240, type 316 for 24PT4 ⁽¹⁾
Inner sleeve	8	6061 aluminum with gaps ⁽²⁾
Cask slide rails	10	Nitronic 60 ⁽³⁾
Cask inner shell	11	SA-203, Gr. E
Gamma shield	12	ASTM B-29 (Lead)
Cask outer shell	13	SA-203, Gr. E
Cask bottom plate	14	SA-350-LF3
Cask bearing block	15	SA-182-F6NM
Cask lid	16	SA-350-LF3 or SA-203, Gr. E
Neutron shield boxes	17	6063 aluminum
Neutron shield resin	18	Epoxy resin – VYAL B
Ram closure plate	19	SA-203, Gr. E ⁽⁴⁾
Thermal shield	20	Aluminum (Al 6061 is used for analysis)
Impact limiter material	21	Wood
Trunnion plug – plates	22	SA-240, type 304
Trunnion block	23	SA-350-LF3
Impact limiter shell and gussets	24	SA-240, type 304
Shield shell	25	SA-516-70
External fins and shell	26	6061 aluminum
Skid straps	28	SA-240, type 304
TC Cavity gas	31	Helium
Gamma shield / Outer shell gap	33	Air
Cask gaps	34	Air
DSC shell / TC inner shell gap	37 / 38	Helium with radiation ⁽⁵⁾
Trunnion plug – resin	40	Polypropylene

Note (1): Axial air gaps are integrated into the component. The effective conductivity for these components in the axial direction is calculated in Section 5.3.

Note (2): Effective conductivities are calculated for inner sleeve in Section 5.5.

Note (3): A gap of 0.01" is considered between the slide rail and the DSC shell. The effective conductivity of slide rail is calculated in Section 5.4.

Note (4): A stainless steel weld is overlaid on the ram closure surfaces in contact with the cask bottom plate. For conservatism, ram closure plate is considered as SA-240, type 304 in this analysis.

Note (5): Effective conductivities are calculated for this gap in Section 5.2.

Table 4-2 Stainless Steel Properties

Stainless Steel	Thermal conductivity SA-240, Type 304 / Nitronic 60 ASME, Group J [8], [2]		Thermal conductivity SA-240, Type 316 for 24PT4 DSC UFSAR ANUH [4], [2]		
	Temperature (°F)	(Btu/hr-ft-°F)	(Btu/hr-in-°F)	(Btu/hr-ft-°F)	(Btu/hr-in-°F)
70	8.6	0.717	7.7	0.642	
100	8.7	0.725	7.9	0.658	
200	9.3	0.775	8.4	0.700	
300	9.8	0.817	9.0	0.750	
400	10.4	0.867	9.5	0.792	
500	10.9	0.908	10.0	0.833	
600	11.3	0.942	10.5	0.875	
700	11.8	0.983	11.0	0.917	
800	12.3	1.025	11.5	0.958	
900	12.7	1.058			
1000	13.1	1.092			

Table 4-3 Low Alloy Steel Properties

Low Alloy Steel	Thermal conductivity SA-182-F6NM ASME, Group G [8]	
Temperature (°F)	(Btu/hr-ft-°F)	(Btu/hr-in-°F)
70	14.2	1.183
100	14.2	1.183
200	14.3	1.192
300	14.4	1.200
400	14.5	1.208
500	14.5	1.208
600	14.6	1.217
700	14.6	1.217
800	14.7	1.225
900	14.7	1.225
1000	14.7	1.225

Table 4-4 Carbon Steel Properties

Carbon Steel	Thermal conductivity SA-516-70 or A36 ASME, Group B [8], [2]		Thermal conductivity SA-203, Gr. E or SA-350-LF3 ASME, Group C [8], [2]	
	Temperature (°F)	(Btu/hr-ft-°F)	(Btu/hr-in-°F)	(Btu/hr-ft-°F)
70	27.3	2.275	23.7	1.975
100	27.6	2.300	23.6	1.967
200	27.8	2.317	23.5	1.958
300	27.3	2.275	23.4	1.950
400	26.5	2.208	23.1	1.925
500	25.7	2.142	22.7	1.892
600	24.9	2.075	22.2	1.850
700	24.1	2.008	21.6	1.800
800	23.2	1.933	21.0	1.750
900	22.3	1.858	20.3	1.692
1000	21.1	1.758	19.7	1.642

Table 4-5 Aluminum Alloys Properties

Aluminum	Thermal conductivity Al 6061 ASME [8], [2]		Thermal conductivity Al 6063 ASME [8], [2]	
Temperature (°F)	(Btu/hr-ft-°F)	(Btu/hr-in-°F)	(Btu/hr-ft-°F)	(Btu/hr-in-°F)
70	96.1	8.008	120.8	10.067
100	96.9	8.075	120.3	10.025
150	98.0	8.167	119.7	9.975
200	99.0	8.250	119.0	9.917
250	99.8	8.317	118.5	9.875
300	100.6	8.383	118.1	9.842
350	101.3	8.442	118.0	9.833
400	101.9	8.492	117.6	9.800

Table 4-6 Lead Properties

Lead			
Temperature (K)	Conductivity [9] (W/m-K)	Temperature (°F)	Conductivity (Btu/hr-in-°F)
200	36.7	-100	1.767
250	36.0	-10	1.733
300	35.3	80	1.700
400	34.0	260	1.637
500	32.8	440	1.579
600	31.4	620	1.512

Table 4-7 Non-Metallic Solids Properties

Neutron Shield Resin (Vyal B)	Trunnion Plug Resin (PP)	Wood
Conductivity (Btu/hr-in-°F)	Conductivity (Btu/hr-in-°F)	Conductivity (Btu/hr-in-°F)
0.039 ⁽¹⁾	0.0067 [13], Table 23-10	0.0019 ⁽²⁾

Note (1): Minimum conductivity of VYAL B is taken from [6], Section 4.2, Item 5.

Note (2): Minimum conductivity of wood is discussed in [10], Appendix B.

Table 4-8 Helium Thermal Conductivity

Temperature (K)	Thermal conductivity (W/m-K)	Temperature (°F)	Thermal conductivity (Btu/hr-in-°F)
300	0.1499	80	0.0072
400	0.1795	260	0.0086
500	0.2115	440	0.0102
600	0.2466	620	0.0119
800	0.3073	980	0.0148
1000	0.3622	1340	0.0174
1050	0.3757	1430	0.0181

The above data are calculated base on the following polynomial function from [7] or [2]

$$k = \sum C_i T_i \quad \text{for conductivity in (W/m-K) and T in (K)}$$

For 300 < T < 500 K		for 500 < T < 1050 K	
C0	-7.761491E-03	C0	-9.0656E-02
C1	8.66192033E-04	C1	9.37593087E-04
C2	-1.5559338E-06	C2	-9.13347535E-07
C3	1.40150565E-09	C3	5.55037072E-10
C4	0.0E+00	C4	-1.26457196E-13

Table 4-9 Air Thermal Properties

Temperature (K)	Thermal conductivity (W/m-K)	Temperature (°F)	Thermal conductivity (Btu/hr-in-°F)
200	0.01822	-100	0.0009
250	0.02228	-10	0.0011
300	0.02607	80	0.0013
400	0.03304	260	0.0016
500	0.03948	440	0.0019
600	0.04557	620	0.0022
800	0.05698	980	0.0027
1000	0.06721	1340	0.0032

The above data are calculated base on the following polynomial function from [7] or [2]

$$k = \sum C_i T_i \quad \text{for conductivity in (W/m-K) and T in (K)}$$

For 250 < T < 1050 K	
C0	-2.2765010E-03
C1	1.2598485E-04
C2	-1.4815235E-07
C3	1.7355064E-10
C4	-1.0666570E-13
C5	2.4766304E-17

Specific heat, viscosity, density and Prandtl number of air are used to calculate heat transfer coefficients in APPENDIX B based on the following data from [7] or [2].

$$c_p = \sum A_i T_i \quad \text{for specific heat in (kJ/kg-K) and T in (K)}$$

For 250 < T < 1050 K	
A0	0.103409E+1
A1	-0.2848870E-3
A2	0.7816818E-6
A3	-0.4970786E-9
A4	0.1077024E-12

$$\mu = \sum B_i T_i \quad \text{for viscosity (N-/m}^2\text{)} \times 10^6 \text{ and T in (K)}$$

For 250 < T < 600 K		For 600 < T < 1050 K	
B0	-9.8601E-1	B0	4.8856745
B1	9.080125E-2	B1	5.43232E-2
B2	-1.17635575E-4	B2	-2.4261775E-5
B3	1.2349703E-7	B3	7.9306E-9
B4	-5.7971299E-11	B4	-1.10398E-12

$$\rho = P/RT \quad \text{for density (kg/m}^3\text{) with P=101.3 kPa; R = 0.287040 kJ/kg-K; T = air temp in (K)}$$

$$Pr = c_p \mu / k \quad \text{Prandtl number}$$

Table 4-10 Thermal Conductivity for SS304 and A36 in Various ASME Years

	SA-240, type 304 (Group J)			A-36 (Group B)		
	ASME 2004 w/ 2006 Addenda [8], [2]	ASME 1998 w/ 2000 Addenda [23], [2]	Deviation	ASME 2004 w/ 2006 Addenda [8], [2]	ASME 1998 w/ 2000 Addenda [23], [2]	Deviation
Temp	TC	TC		TC	TC	
(°F)	(Btu/hr-ft-°F)	(Btu/hr-ft-°F)		(Btu/hr-ft-°F)	(Btu/hr-ft-°F)	
70	8.6	8.6	0.0%	27.3	27.5	0.7%
100	8.7	8.7	0.0%	27.6	27.6	0.0%
200	9.3	9.3	0.0%	27.8	27.6	-0.7%
300	9.8	9.8	0.0%	27.3	27.2	-0.4%
400	10.4	10.4	0.0%	26.5	26.7	0.8%
500	10.9	10.9	0.0%	25.7	25.9	0.8%
600	11.3	11.3	0.0%	24.9	25.0	0.4%
700	11.8	11.8	0.0%	24.1	24.0	-0.4%
800	12.3	12.2	-0.8%	23.2	23.0	-0.9%
		max	0.0%		max	0.8%
		min	-0.8%		min	-0.9%

4.2 Surface Properties of Materials

Reference [11] gives an emissivity between 0.92 to 0.96 and a solar absorptivity between 0.09 and 0.23 for white paints. To account for dust and dirt and to bound the problem, the thermal analysis uses a solar absorptivity of 0.3 and an emissivity of 0.9 for white painted surfaces of the neutron shield shell.

Emissivity of rolled stainless steel plates is 0.578 as considered in [12]. The emissivity for rolled steel sheets is 0.657 as reported in [13], Table 10-17. The transport cask inner shell is painted white. For conservatism, the emissivity value of 0.587 is considered for both the DSC shell (stainless steel) and the transport cask inner shell (painted carbon steel) in calculation of thermal radiation exchange between these shells.

Solar absorptance values of 0.39 and 0.47 are given in [28] for rolled and machined stainless steel plates, respectively. For conservatism, it is assumed that the absorptivity and the emissivity of stainless steel are equal in this calculation. Solar absorptivity and emissivity of 0.587 are used for the exposed impact limiters and skid strap surfaces.

Emissivity of anodized aluminum is between 0.84 and 0.72 for temperatures between 296K and 484K (between 73°F and 411°F) and its solar absorptivity is between 0.12 and 0.16 [7, Table A.7.2]. An emissivity of 0.70 and a solar absorptivity of 0.16 are considered for the finned aluminum shell of MP197HB cask in this analysis.

Although an emissivity of 0.7 can be considered for the anodized surface of the inner sleeve for the purposes of this calculation, the effective conductivity for helium between DSC and inner sleeve is conservatively set equal to the effective conductivity of helium between DSC shell and TC inner shell with surface emissivities of 0.587. The effective conductivity of helium between DSC shell and TC inner shell is calculated in Section 5.2.

For plain aluminum, an absorptivity of 0.1 is reported in [7], Table A.7.2. This value is used only for calculation of insolation over thermal shield in Section 6.3 and is not used in the finite element model of MP197HB.

4.3 Design Criteria

To establish the heat removal capability, several thermal design criteria are established for the MP197HB TC. These are:

- Seal temperatures must be maintained within specified limits to satisfy the leak tight function of transport cask back filled with helium. A maximum long-term seal temperature limit of 400°F (204°C) is considered for the Fluorocarbon O-Rings [2].
- To maintain the shielding property of the neutron shield during NCT, a maximum temperature of 320°F (160°C) is considered for the neutron shield resin [2].

- To prevent melting of the gamma shield (lead) during NCT, an allowable maximum temperature of 621°F (327.5°C – melting point of lead) is considered for the gamma shield [13].
- A temperature limit of 160°C (320°F) is considered for wood to maintain its crush properties for structural analysis [2].
- The accessible surface temperature of the packaging under normal conditions of transport shall be limited to 185°F in the shade [2].
- Based on [24], the onset of polypropylene thermal degradation associated with weight loss starts at 230 to 250°C (446 to 482°F). Although the breakdown of the polymer leading to volatile products begins above 300°C (572°F), no significant weight loss occurs below 350°C (662°F). A temperature limit of 445°F is considered conservatively for polypropylene to prevent thermal degradation of resin in trunnion plugs.

All materials of MP197HB can be subjected to a minimum environment temperature of -40°F (-40°C) without any adverse effects.

5.0 METHODOLOGY

A half-symmetric, three-dimensional finite element model of MP197HB transport cask is developed using ANSYS [14]. The model contains the cask shells, cask bottom plate, cask lid, impact limiters, DSC shell, and DSC end plates without the basket. The DSC dimensions correspond to nominal DSC dimensions listed in Table 3-1 for variations of the MP197HB model.

SOLID70 elements are used to model the components including the gaseous gaps. Impact limiter gussets, cask slide rails, and trunnion plug plates are modeled using SHELL57 elements. Surface elements SURF152 are used for applying the insulation boundary conditions.

Ambient conditions for NCT are taken from 10CFR71 [1] and applied on the boundaries of the cask model. These conditions are listed in Table 5-1.

Table 5-1 Normal Conditions of Transport for MP197HB

Case #	Ambient temperature (°F)	Insolance	Purpose
1	100	Yes	Maximum Component Temperatures
2	-20	No	Cold conditions for Structural Analysis
3	-40	No	Maximum Thermal Stress
4	100	No	Maximum Accessible Surface Temperature

A personnel barrier installed on the transport skid between the two impact limiters limits the accessible packaging surfaces to the impact limiter and barrier outer surfaces. The personnel barrier has an open area of at least 80%. Heat transfer between the cask and barrier will be minimal due to the small radiation view factor between the cask and the barrier. Due to large distance between the barrier and cask outer surface, the free convection heat transfer remains undisturbed. The transport configuration is shown in Figure 5-1.

The methodology to calculate the accessible surface temperature is described in Section 5.6.

Insolance is applied as a heat flux over the TC outer surfaces using average insolance values from 10CFR71 [1]. The insolance values are averaged over 24 hours and multiplied by the surface absorptivity factor to calculate the solar heat flux. The solar heat flux values used in MP197HB model are summarized in Table 5-2.

Table 5-2 Solar Heat Flux

Surface Material	Shape	Insolance over 12 hrs [1] (gcal/cm ²)	Solar Absorptivity ⁽¹⁾	Total solar heat flux averaged over 24 hrs (Btu/hr-in ²)
Stainless Steel	Curved	400	0.587 ⁽²⁾	0.2505
	Flat vertical	200	0.587 ⁽²⁾	0.1252
White Paint (shield shell)	Curved	400	0.30	0.1280
Anodized Aluminum	Curved	400	0.16	0.0683
Plain aluminum	Flat vertical	200	0.10	0.0213

Note (1): See Section 4.2 for surface properties.

Note (2): Solar absorptivity of stainless steel is taken equal to its emissivity.

The cask external fins are not considered explicitly in the TC model. Instead, an effective heat transfer coefficient is applied over the outer surface of the un-finned aluminum shell to simulate the heat dissipation from this area. The methodology to calculate the effective heat transfer coefficient for external fins is described in Section 5.1.

A radial gap of 0.01" is considered between the finned aluminum shell and the cask shield shell to account for the thermal resistance between these two shells. The size of this gap is justified in APPENDIX D.

Convection and radiation heat transfer from the un-finned cask surfaces are combined together as total heat transfer coefficients. The total heat transfer coefficients are calculated using free convection correlations from Rohsenow Handbook [7] and are incorporated in the model using ANSYS macros. These correlations are described in APPENDIX B. The ANSYS macros used in this calculation are listed in Section 8.0.

Decay heat load is applied as a uniform heat flux over the inner surface of the DSC shell covering the basket length.

$$q'' = \frac{Q}{\pi D_i L_b}$$

q'' = decay heat flux (Btu/hr-in²)

Q = decay heat load (Btu/hr) (to convert from kW multiply by 3412.3)

D_i = DSC inner diameter (in)

L_b = Basket length (in)

The applied decay heat values in the model are listed in Table 5-3

Table 5-3 Decay Heat Flux

DSC Type	Heat Load (kW) (Btu/hr)		D _i (in)	L _b (in)	Decay heat flux (Btu/hr-in ²)
69BTH	26.0	88,720	68.75	164	2.505
	29.2	99,639			2.813
	32.0	109,194			3.083
61BTH Type 1 ⁽¹⁾	22.0	75,071	66.25	164	2.199
61BTH Type 2 ⁽¹⁾	24.0	81,895	66.25	164	2.399
61BT	18.3	62,445	66.25	164	1.829
37PTH	22.0	75,071	68.75	162	2.146
32PTH / 32PTH Type 1	26.0	88,720	68.75	162	2.536
32PTH1 Type 1	26.0	88,720	68.75	162	2.536
32PTH1 Type 2	24.0	81,895	68.75	162	2.341
32PT	24.0	81,895	66.19	166.10	2.371
24PTH Type 1 & 2	26.0	88,720	66.19	168.60	2.531
24PT4	24.0	81,895	66.19	179.13	2.199

Note (1): DSC types 61BTHF and 24PTHF has the same dimensions and heat loads as DSC types 61BTH and 24PTH, respectively.

Radiation and conduction between the DSC and the TC inner shell / inner sleeve is considered by calculating effective conductivities for helium gaps between the above components. Calculation of the helium effective conductivities within this gap is described in Section 5.2.

During transportation, the DSC shell rests on four slide rails in the TC. These rails are flat stainless steel plates welded to the inner shell of the TC. The thickness of the slide rail is 0.12" when no inner sleeve is used. The slide rail at 180° orientation is 0.06" thick and does not contact the DSC shell. The same configuration is considered for the small diameter DSC and the inner sleeve.

The angle between the lower rail and the vertical plane is 12 degree. Considering this configuration shown in Figure 5-2, the distance between the centerline of DSC and centerline of the cask are calculated as follows.

$$R_2^2 = R_1^2 + x^2 - 2 R_1 x \cos(\alpha)$$

With

$$R_1 = D_{i, TC} / 2 - t_{rail}$$

$$R_2 = D_{o, DSC} / 2$$

$$\alpha = 12^\circ$$

x = Distance between the DSC and TC centerlines

$D_{i,TC}$ = Inner diameter of TC or inner sleeve

$D_{o,DSC}$ = DSC outer diameter

t_{rail} = cask slide rail thickness = 0.12"

The calculated values for x are listed in Table 5-4. In the ANSYS model, the DSC is shifted down by the amount of x in the Cartesian y-direction within the TC cavity.

Table 5-4 Distance between DSC and TC Centerlines

DSC Type	$D_{i,TC}$ (in)	$D_{o,DSC}$ (in)	R_1 (in)	R_2 (in)	α (degree)	x (in)
69BTH 37PTH 32PTH 32PTH1	70.5	69.75	35.130	34.875	12	0.261
61BT 61BTH 61BTHF	68	67.25	33.880	33.625	12	0.261
32PT 24PTH 24PTHF 24PT4	68	67.19	33.880	33.595	12	0.291

To simplify the model, the lower cask slide rails at 168° and 192° orientations are modeled using shell elements with the conductivity of Nitronic 60 and a helium gap of 0.01". The effects of the other cask slide rails are conservatively omitted. The slide rail width is 3". For conservatism, a contact width of 0.12" is considered between the lower rails and the DSC shell.

The axial gaps considered between DSC cover plates and shield plugs are integrated into bottom shield plug and top inner cover plates. The axial gaps considered for the lead shield plugs of 24PT4 are also integrated into the shield plug material. The axial effective conductivities are calculated for these components in Section 5.3. The conductivity in radial direction remained unchanged and equal to the conductivity of the corresponding material.

To reduce the complexity of the model, effective conductivities are calculated for the inner sleeve in axial and radial directions. The methodology to calculate the effective conductivity of the inner sleeve is described in Section 5.5. These effective conductivities are conservative since the number and the assumed gaps between the inner sleeve pieces are larger than those considered for the proposed inner sleeve.

The material properties used in the MP197HB model are listed in Section 4.0.

The geometry of the TC model and its mesh density are shown in Figure 5-3 through Figure 5-7. Mesh sensitivity of the MP197HB model is discussed in APPENDIX E.

Typical boundary conditions for TC model are shown in Figure 5-8 through Figure 5-10.

The seal o-rings are not explicitly considered in the models. The maximum seal temperatures are retrieved from the models by selecting the nodes at the locations of the corresponding seal o-rings. The nodal coordinates corresponding to seal locations are defined in the input files for running the MP197HB models listed in Table 8-2.

Except for DSC types 69BTH and 37PTH, all other DSC types listed in Table 1-1 are analyzed for storage/transfer conditions under 10CFR72 [20]. The safety analysis reports (SAR) for these DSC types under storage/transfer conditions are presented in [3], [4], [5], and [6].

The following approach is undertaken to determine the maximum heat load for all DSC types in MP197HB except for 69BTH and 37PTH DSCs.

- a) The MP197HB/DSC shell model is run with either the design basis total heat load for each particular DSC or the maximum allowable heat load in MP197HB without external fins (26 kW) to get the maximum DSC shell temperature ($T_{\text{DSC shell max}}$).
- b) If $T_{\text{DSC shell max}}$ is higher than $T_{\text{DSC shell max}}$ predicted by corresponding 10CFR72 SAR, the total heat load in the MP197HB/DSC model is reduced until $T_{\text{DSC shell max}}$ is below $T_{\text{DSC shell max}}$ predicted by corresponding 10CFR72 SAR.
- c) The DSC shell temperature profile in MP197HB model is compared with the corresponding profile in 10CFR72 SAR and is verified that the 10CFR72 SAR represents the bounding profile.
- d) Since 10CFR72 SAR represents the bounding case, the DSC component and fuel cladding temperatures for transport in MP197HB cask are bounded by the corresponding values in the 10CFR72 SAR. The thermal analysis results in 10CFR72 SAR are applicable for 10CFR, Part 71 conditions and no further DSC thermal analysis is required.

The maximum heat load for 69BTH and 37PTH DSCs are determined based on requirements defined under 10CFR71 [1] for MP197HB.

The final heat loads for each DSC type are those listed in Table 1-1.

Calculation

Calculation No.: MP197HB-0401

Revision No.: 2

Page: 30 of 112

Proprietary Information Withheld Pursuant to 10 CFR 2.390

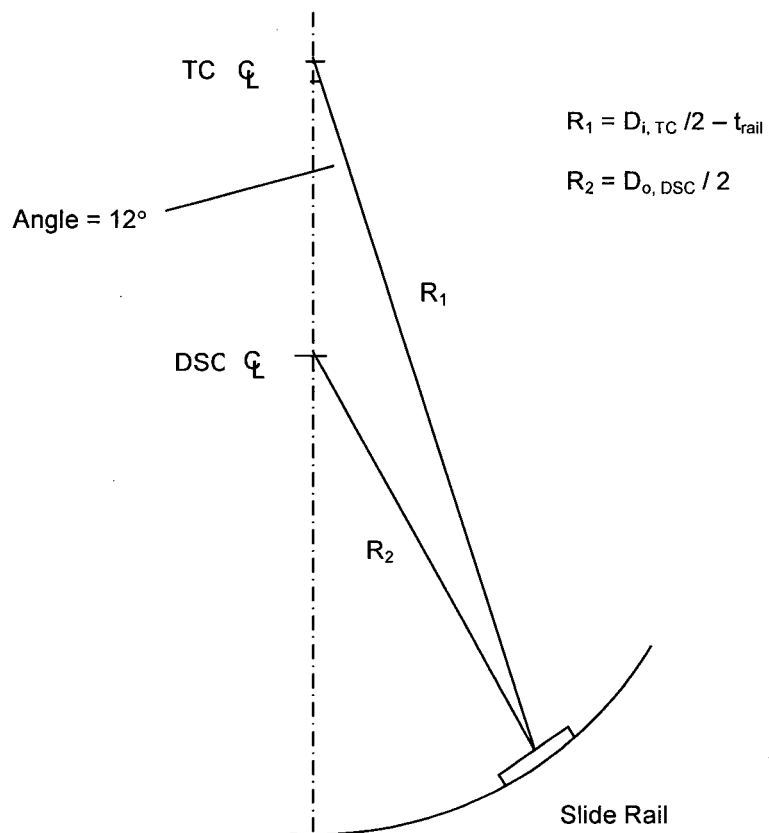
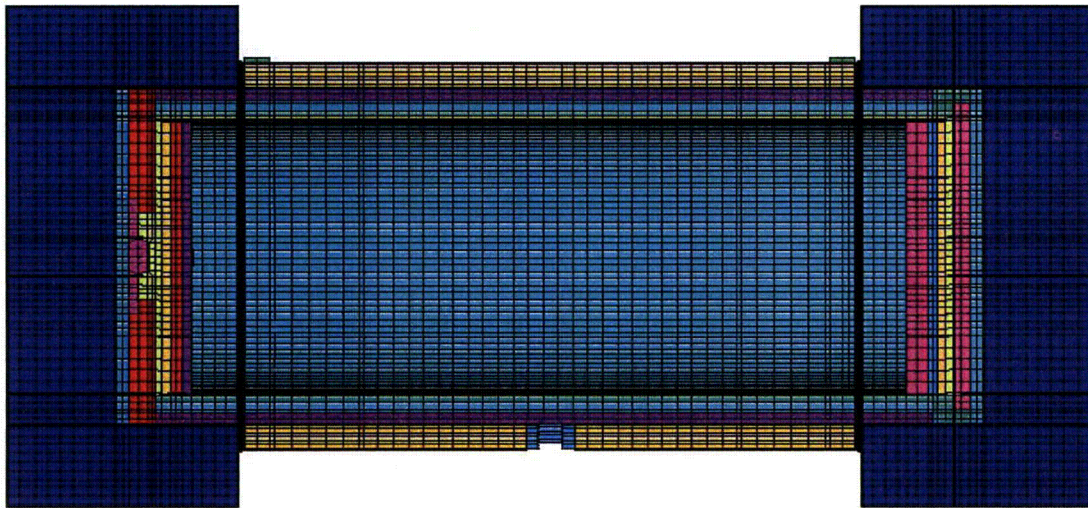
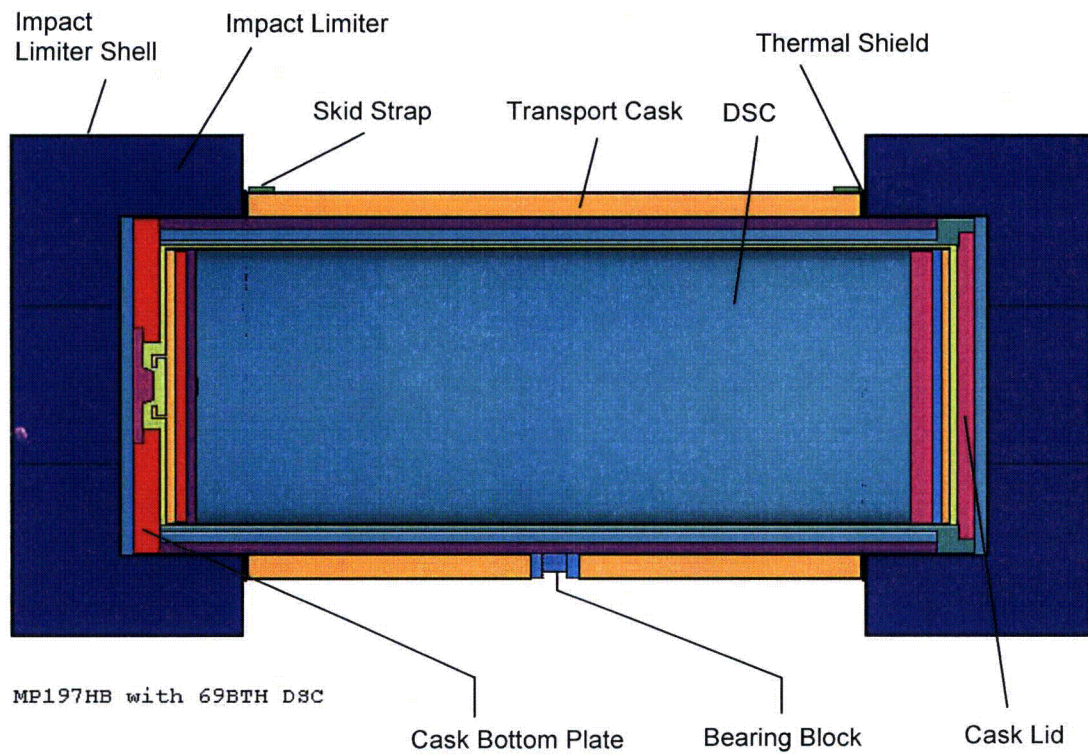


Figure 5-2 **Location of DSC within MP197HB TC**



MP197HB with 69BTH DSC



MP197HB with 69BTH DSC

Figure 5-3 Finite Element Model of MP197HB with 69BTH DSC

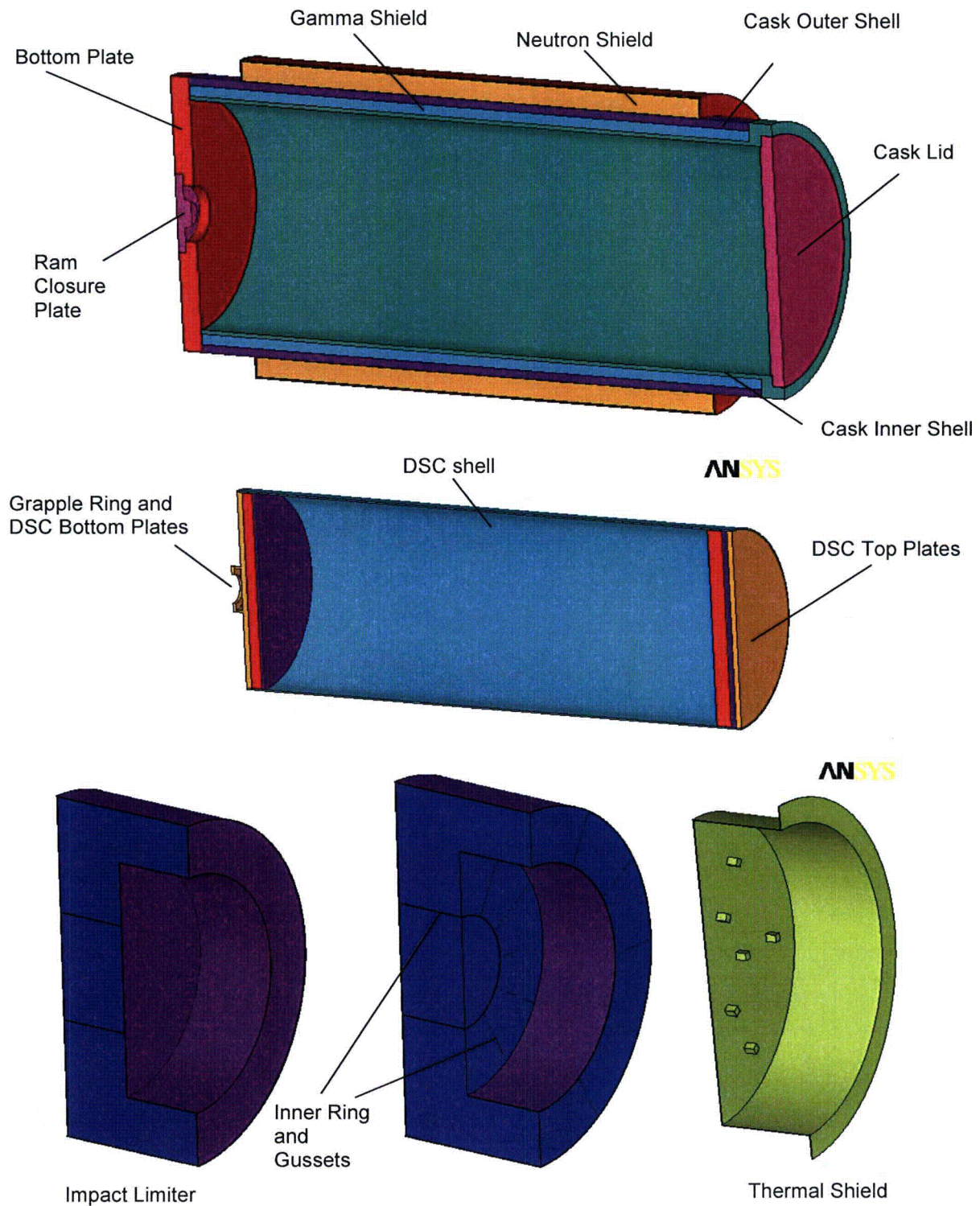


Figure 5-4

MP197HB Finite Element Model, Components

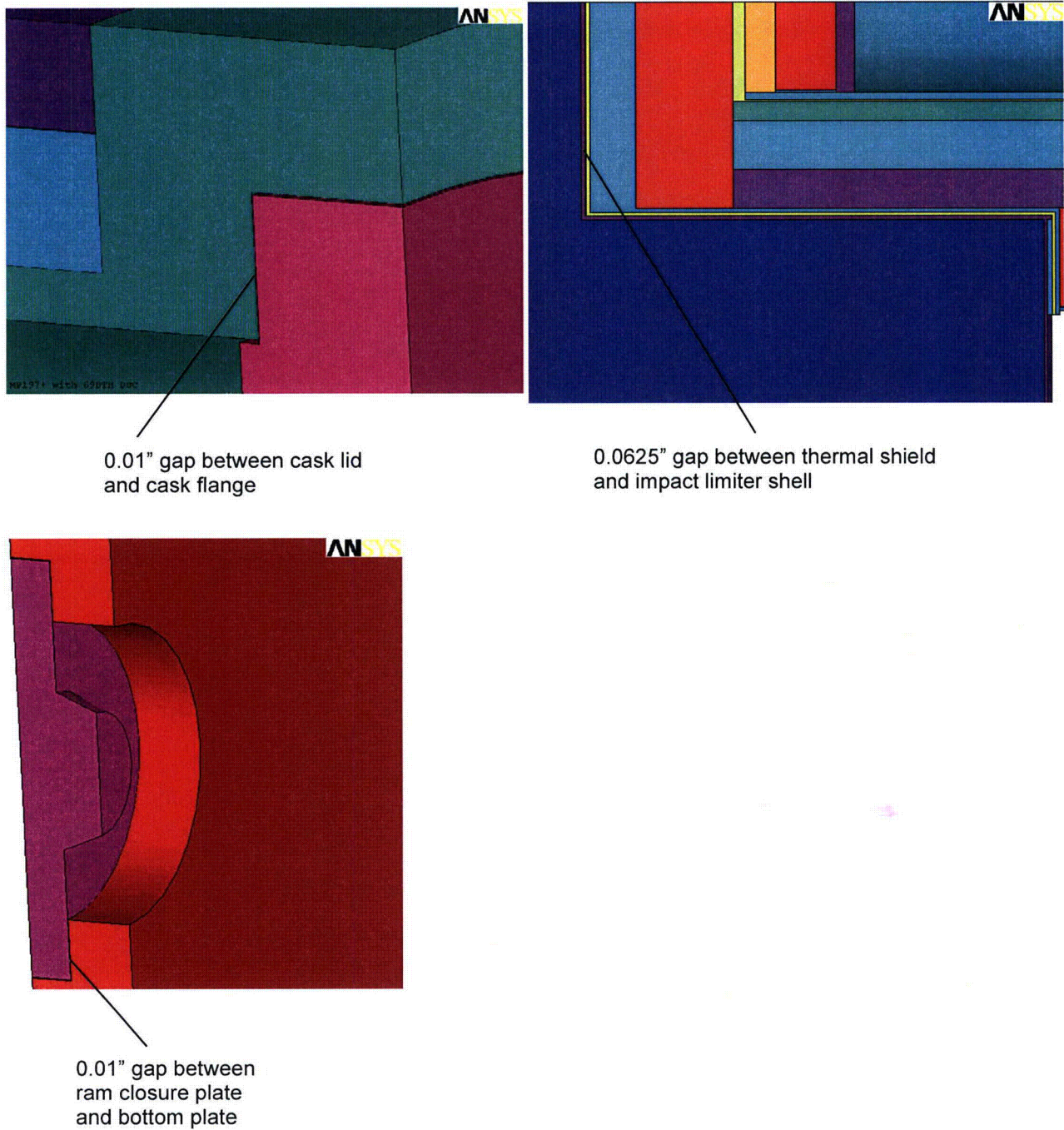


Figure 5-5 Gaps in MP197HB Transport Cask Model

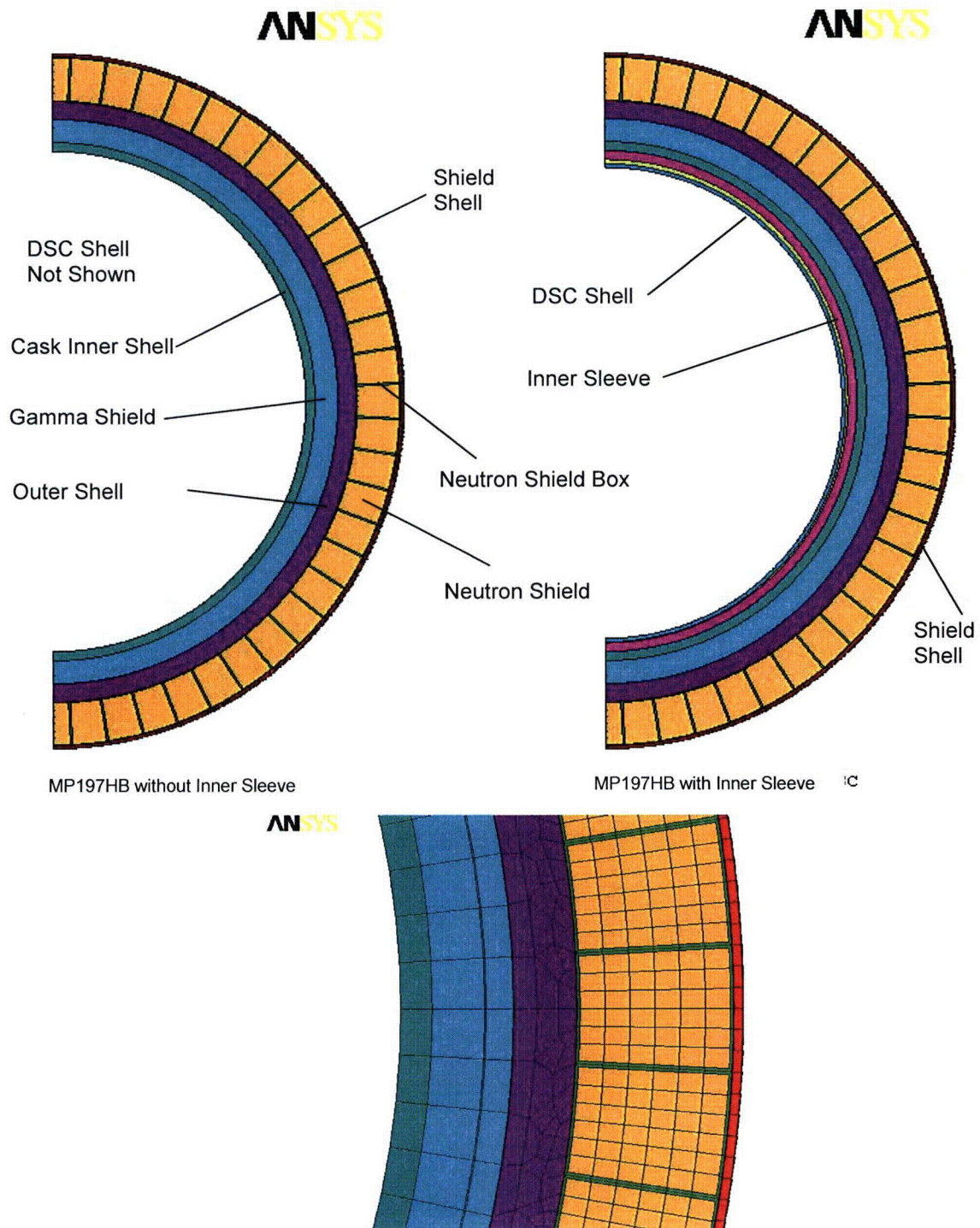


Figure 5-6 MP197HB Finite Element Model, Cross Section

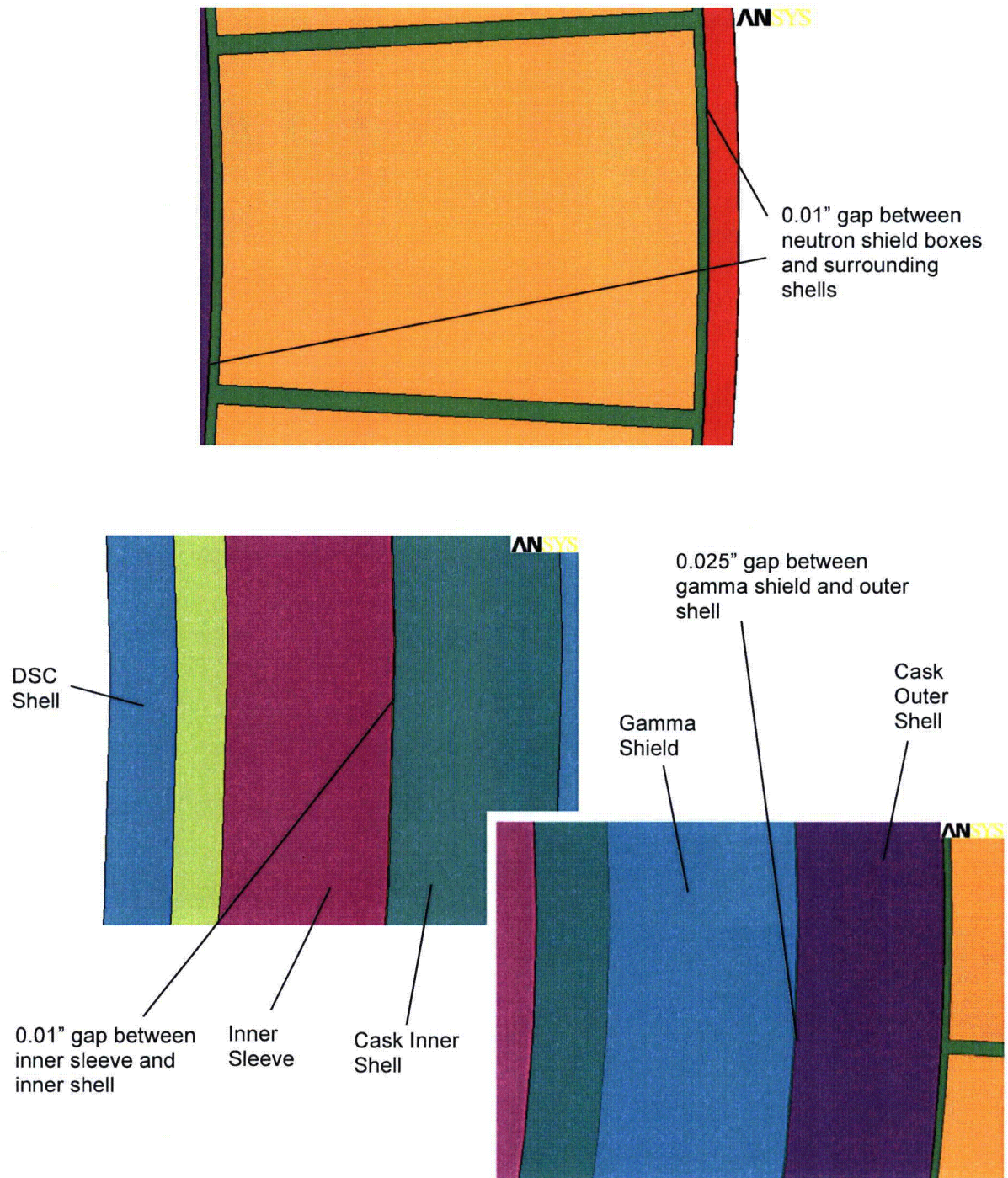
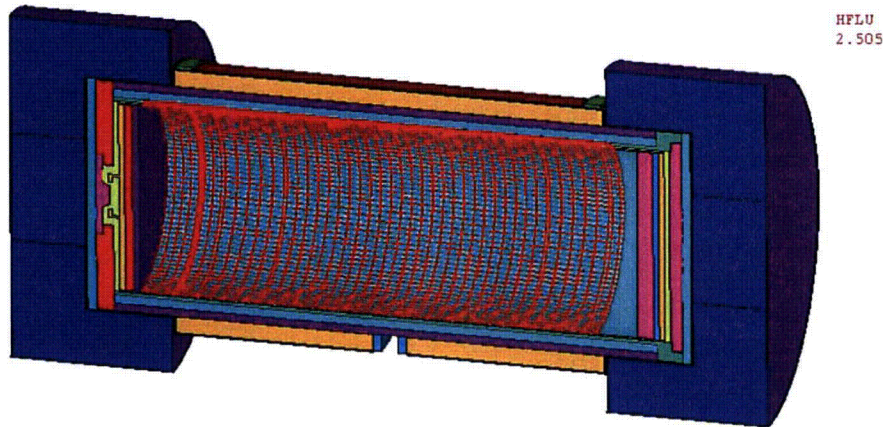
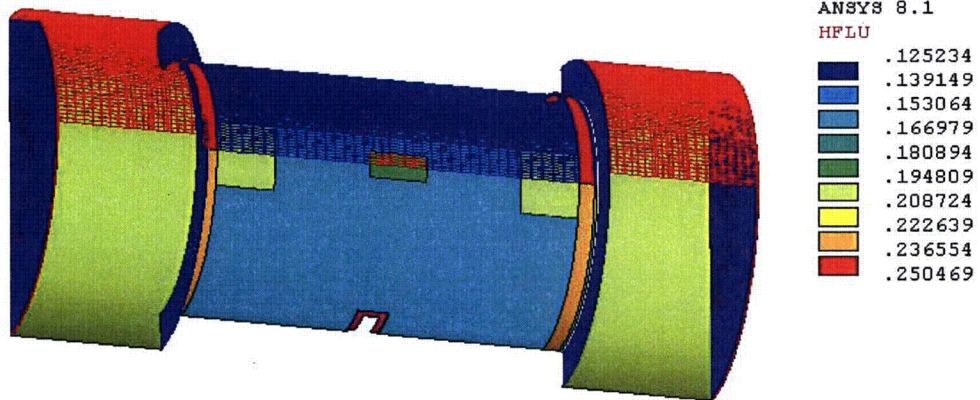


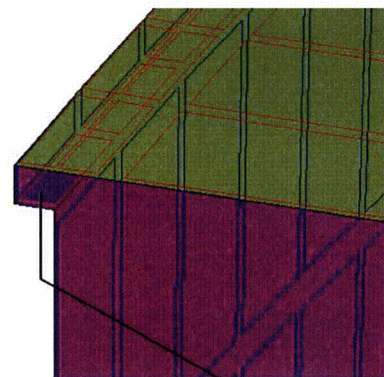
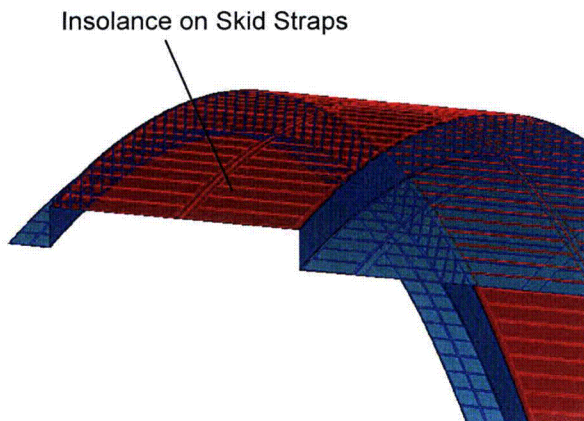
Figure 5-7 Gaps in Cross Section



Decay Heat Boundary Conditions for 69BTH DSC, 26 kW

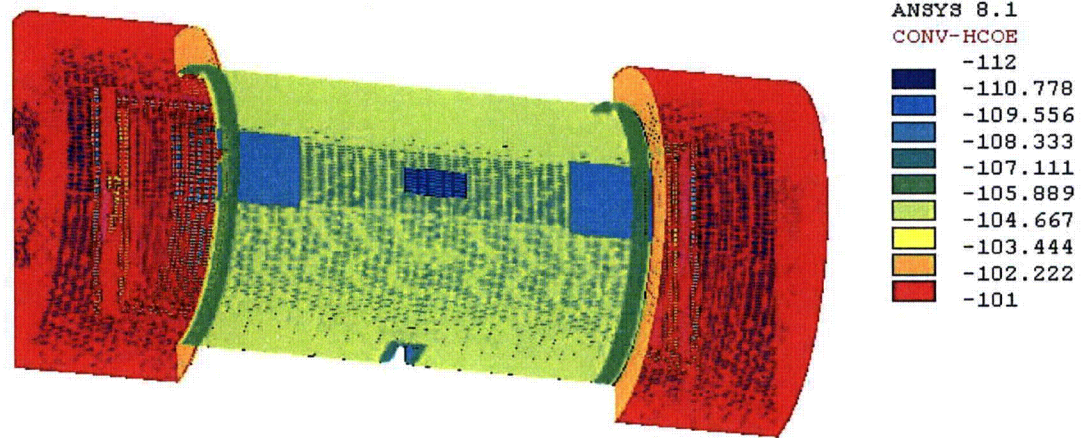


Insolance Boundary Conditions

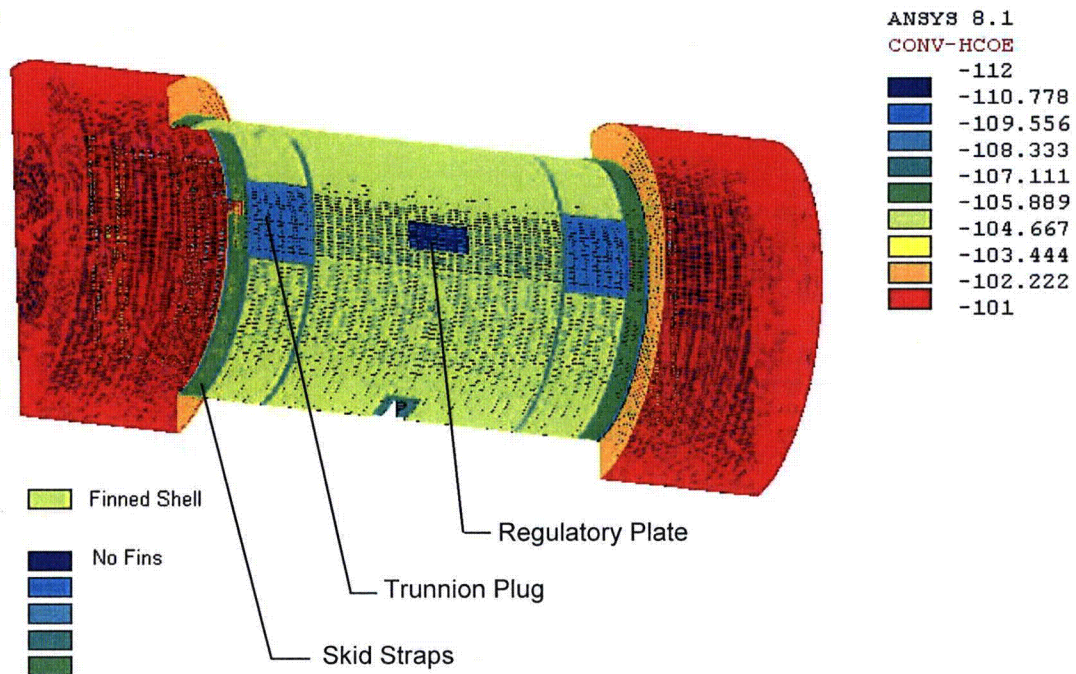


Insolance on Impact Limiter Recess

Figure 5-8 Typical Decay Heat and Insolance Boundary Conditions

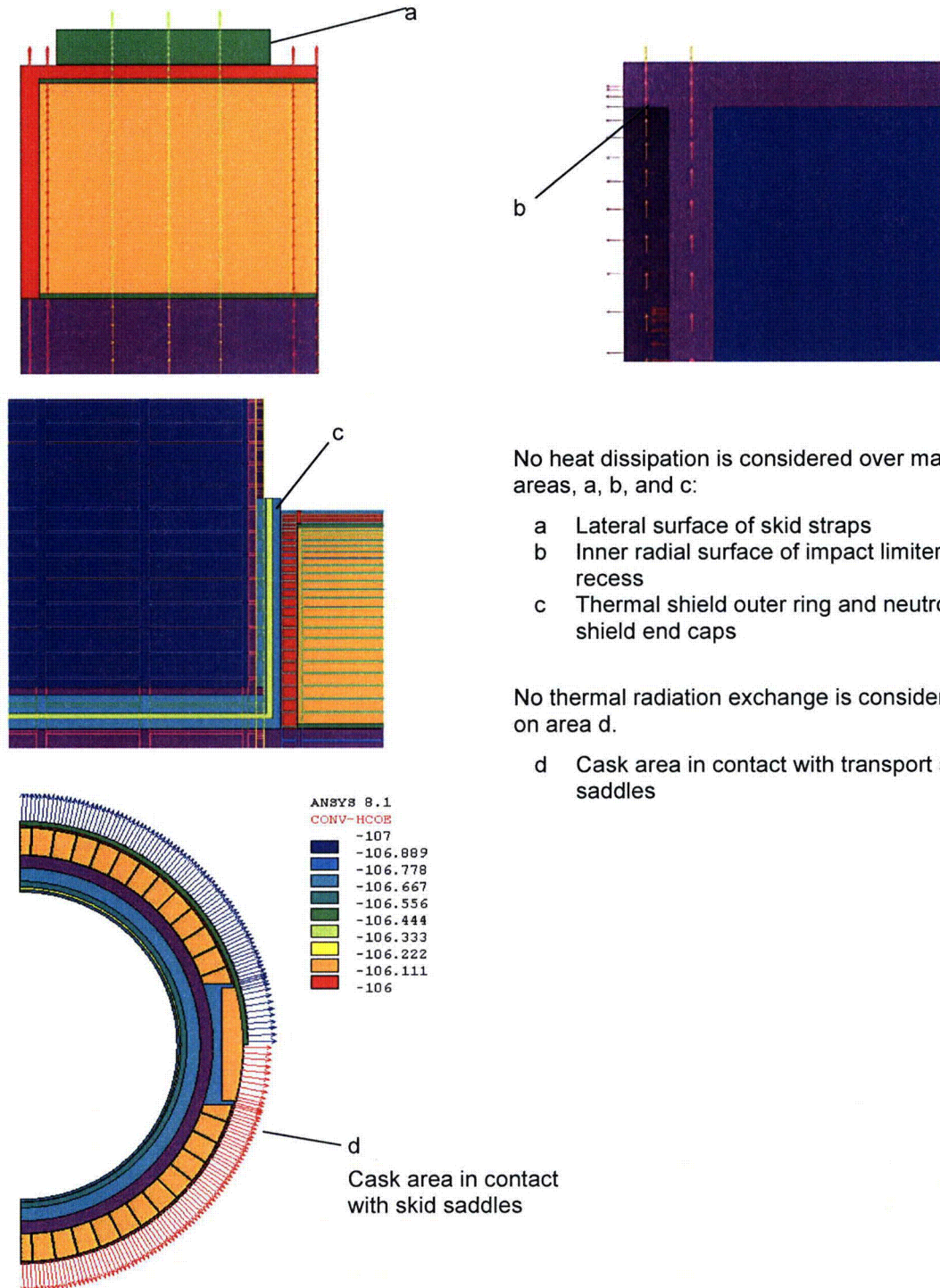


Convection and Radiation Boundary Conditions for MP197HB w/o External Fins



Convection and Radiation Boundary Conditions for MP197HB with External Fins

Figure 5-9 Typical Convection and Radiation Boundary Conditions



No heat dissipation is considered over marked areas, a, b, and c:

- a Lateral surface of skid straps
- b Inner radial surface of impact limiter recess
- c Thermal shield outer ring and neutron shield end caps

No thermal radiation exchange is considered on area d.

- d Cask area in contact with transport skid saddles

Figure 5-10 Typical Convection and Radiation Boundary Conditions – Details

5.1 Effective Heat Transfer Coefficient for External Fins

To reduce the complexity of the TC model, an effective heat transfer coefficient is calculated for the external fins based on the geometry shown in Figure A-1. Circular external fins are welded to an aluminum shell which will be installed over the outer surface of the TC shield shell to enhance heat dissipation for heat loads over 26 kW. An effective heat transfer coefficient is calculated for the external fins which includes the convection and radiation heat transfer to ambient. The following dimensions are considered for the fins.

- Fin height = 3.0"
- Fin thickness = 0.156"
- Fin pitch = 1.0"

A sub-model of the TC outer surface is developed for this purpose using ANSYS [14].

This sub-model considers a 30 degree segment of the aluminum shell with three circular external fins. Figure 5-11 shows the sub-model of the finned shell.

Convection boundary conditions are applied over the outer surfaces of the fins in the model using surface load (SF) commands in ANSYS [14]. SHELL57 elements are overlaid on the external surfaces of the fins to create radiation super-element. The radiation shell elements are shown in Figure 5-11. Thermal radiation from the outer surfaces is modeled using /AUX12 processor. Ambient temperature of 100°F, -20°F, and -40°F are considered for convection and radiation.

Based on discussions in Section 4.2, an emissivity of 0.70 is considered for the anodized aluminum for exposed finned surfaces.

Fixed temperature boundary conditions are applied over the inner surface of the aluminum shell. The amount of heat dissipation is retrieved from the model using reaction solution command (PRRSOL) in ANSYS [14]. The effective heat transfer coefficient is calculated as follows.

$$h_{eff} = \frac{Q_{react}}{A_{eff}(T_s - T_{amb})}$$

h_{eff} = effective heat transfer coefficient over finned surface (Btu/hr-in²)

Q_{react} = heat input entering the cask shield shell (reaction solution) retrieved from model (Btu/hr)

T_s = shield shell inner surface temperature (fixed temperature boundary conditions) (°F)

T_{amb} = ambient temperature (°F) = 100°F, -20°F, and -40°F

A_{eff} = outer surface area of the un-finned shield shell (in²).

Since the h_{eff} will be applied over the un-finned surface of the aluminum shell, A_{eff} is the area of the un-finned surface.

$$A_{eff} = \pi D_o (3 \times \text{fin pitch})(30 / 360) = \pi \times 98.25 \times 3 \times 1.0 \times (30/360) = 77.2 \text{ in}^2$$

Convection heat transfer coefficients are calculated using correlations from Rohsenow Handbook [7], page 4.39 and 4.40, equations 4.68 to 4.70b. The correlations used for convection coefficients are:

$$Nu = \frac{h S}{k}; \quad \zeta = \frac{D_o}{D_f}; \quad Ra = \frac{g \beta (T_w - T_{amb}) S^3}{\nu \alpha} \frac{S}{D_f}; \quad Pr = \frac{\nu}{\alpha}$$

D_o = outer diameter of un-finned surface = 98.25"

D_f = outer diameter of circular fins = $(98.25 + 2 \times 3.0) = 104.25$ "

S = fin pitch = 1.0"

g = gravitational constant = 9.81 (m/s²)

β = expansion coefficient = 1/T (1/K)

T = absolute temperature (K)

ν = kinematic viscosity (m²/s)

α = thermal diffusivity (m²/s)

k = air conductivity (W/m-K)

On fin tips:

$$Nu = c Ra^b \quad \text{for } 2 \leq Ra \leq 10^4 \text{ with } c \text{ and } b \text{ defined in Table 5-5.}$$

On fin lateral surfaces together with the supporting shell:

$$Nu = C_0 Ra_0^p \left\{ 1 - \exp \left[- \left(\frac{C_1}{Ra_0} \right)^{C_2} \right] \right\}^{C_3} \quad \text{for } 1.0 \leq \frac{D_f}{D_o} \leq 1.67$$

where

$$\begin{aligned} C_0 &= -0.15 + 0.3\zeta + 0.32\zeta^{16} \\ C_2 &= 0.04 + 0.9\zeta \\ p &= 0.25 + C_2 C_3 \end{aligned}$$

$$\begin{aligned} C_1 &= -180 + 480\zeta - 1.4 \zeta^{-8} \\ C_3 &= 1.3 (1 - \zeta) + 0.0017 \zeta^{-12} \\ Ra_0 &= Ra/\zeta \end{aligned}$$

Properties are evaluated at wall temperature as required in [7]. Air properties used for these correlations are listed in Table 4-9.

The results for the effective heat transfer coefficient are summarized in Table 5-5, Table 5-6, and Table 5-7 for ambient temperatures of 100°F, -20°F, and -40°F, respectively.

Table 5-5 Effective Heat Transfer Coefficients for External Fins @ 100°F Ambient

fin_h =	3.0	fin height (in)
fin_p =	1.0	fin pitch (in)
fin_t =	0.156	fin thickness (in)
fin_n =	3	No. of fins in model
D _o =	98.25	cask diameter (in)
D _f =	104.25	fin diameter (in)
D _f /D _o =	1.061	
A _{eff} =	77.2	area of un-finned surface (in ²)

From Rohsenow Handbook [7]

D _f /D _o	c	b
1.36	0.62	0.29
1.14	0.59	0.27
Extrapolated for this calculation based on above data		
1.061	0.579	0.263

File name *Heff fin 100.out*

T _s	T _{amb}	Q _{react}	A _{eff}	h _{eff}
(°F)	(°F)	(Btu/hr)	(in ²)	(Btu/hr-in ² -°F)
120	100	31.295	77.2	0.0203
140	100	71.639	77.2	0.0232
160	100	116.59	77.2	0.0252
180	100	165.15	77.2	0.0268
200	100	216.89	77.2	0.0281
220	100	271.55	77.2	0.0293
240	100	329.01	77.2	0.0305
260	100	388.75	77.2	0.0315
280	100	452.15	77.2	0.0326
300	100	518.00	77.2	0.0336
320	100	586.59	77.2	0.0346
340	100	658.05	77.2	0.0355

Table 5-6 Effective Heat Transfer Coefficients for External Fins @ -20°F Ambient

Geometrical data are the same as those in Table 5-5

File name Heff_Alfm_20.out

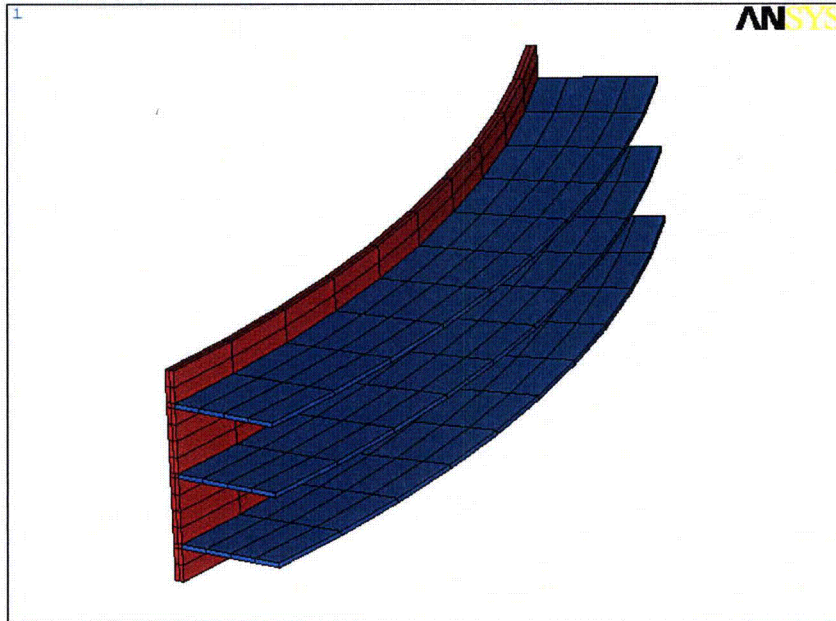
T _s	T _{amb}	Q _{react}	A _{eff}	h _{eff}
(°F)	(°F)	(Btu/hr)	(in ²)	(Btu/hr-in ² -°F)
0	-20	26.511	77.2	0.0172
20	-20	61.325	77.2	0.0199
40	-20	99.88	77.2	0.0216
60	-20	141.15	77.2	0.0229
80	-20	184.56	77.2	0.0239
100	-20	229.46	77.2	0.0248
120	-20	278.04	77.2	0.0257
140	-20	329.65	77.2	0.0267
160	-20	382.98	77.2	0.0276
180	-20	437.79	77.2	0.0284
200	-20	494.84	77.2	0.0291
220	-20	553.94	77.2	0.0299

Table 5-7 Effective Heat Transfer Coefficients for External Fins @ -40°F Ambient

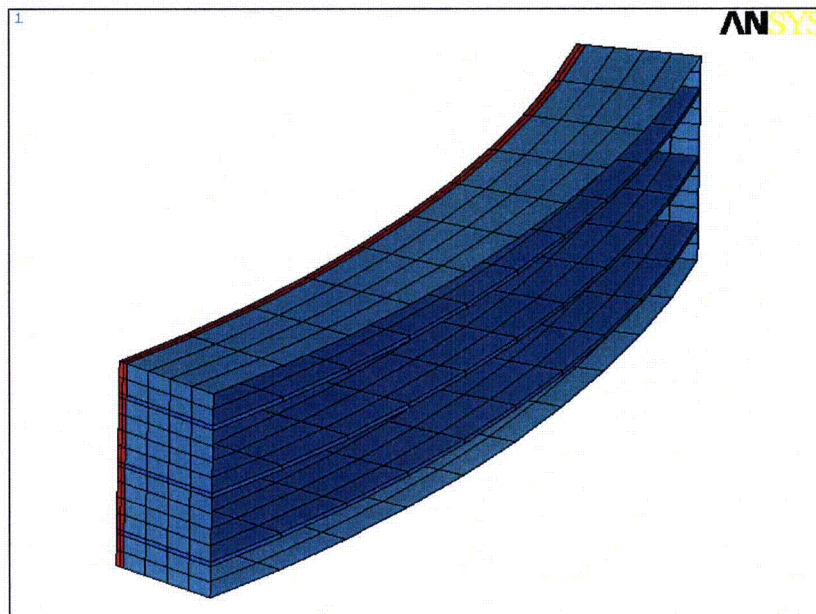
Geometrical data are the same as those in Table 5-5

File name Heff_Alfm_40.out

T _s	T _{amb}	Q _{react}	A _{eff}	h _{eff}
(°F)	(°F)	(Btu/hr)	(in ²)	(Btu/hr-in ² -°F)
-20	-40	26.044	77.2	0.0169
0	-40	60.344	77.2	0.0196
20	-40	98.33	77.2	0.0212
40	-40	139.00	77.2	0.0225
60	-40	181.83	77.2	0.0236
80	-40	226.42	77.2	0.0245
100	-40	272.53	77.2	0.0252
120	-40	321.95	77.2	0.0261
140	-40	374.39	77.2	0.0270
160	-40	427.93	77.2	0.0277
180	-40	483.57	77.2	0.0285
200	-40	541.13	77.2	0.0292



Solid Elements



Shell Elements for Radiation

Figure 5-11 Sub-Model of the External Fins for MP197HB TC

5.2 Effective Conductivity for Helium Gap between DSC and TC/Sleeve

Effective conductivities are calculated for helium between the DSC and the TC inner shell / inner sleeve to account for conduction and radiation between these components. An emissivity of 0.587 is considered for rolled steel shells.

The inner surface of the inner sleeve is anodized. Based on discussion in Section 4.2, an emissivity of 0.7 is considered for anodized surface of inner sleeve.

The effective conductivity of helium within the gap between the DSC shell and TC inner shell is calculated based on a detailed sub-model of this region. This sub-model considers a 10" high, 30 degree segment of the shells. Conductivity of helium is considered for the gap between the shells. Radiation between surfaces is modeled using /AUX12 processor. Figure 5-12 shows the sub-model of the DSC shell and the TC inner shell.

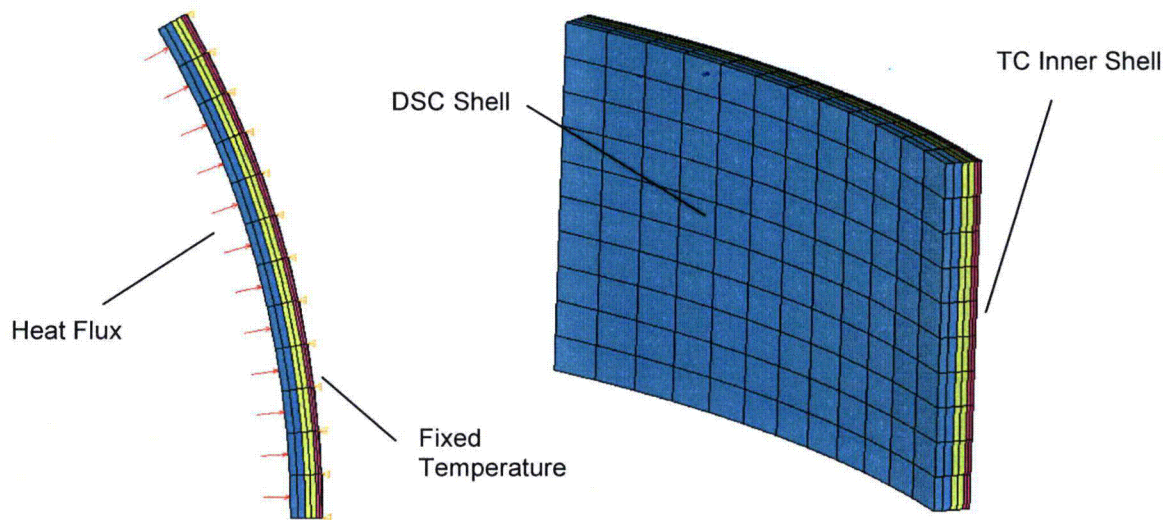


Figure 5-12 Sub-Model for Helium Gap Effective Conductivity Calculation

In the DSC/TC sub-model, a heat flux of 2.813 Btu/hr-in² equivalent to 29.2 kW (see Table 5-3) is applied on the radial surface of the innermost shell (DSC shell) and fixed temperature boundary conditions are applied over the radial surface of the outermost shell (TC inner shell).

The nodes of the gap between the DSC shell and TC inner shell build up the radiation super element (MATRIX50). To avoid convergence problems, the heat flux or fixed temperature

boundary conditions are not applied directly on the nodes of the radiation super element. Instead the heat flux is applied on the innermost nodes of the DSC shell and the fixed temperatures are applied on the outermost nodes of the TC shell.

The effective conductivity is calculated as follows.

$$k_{eff} = \frac{(q_{react} \times 360/30) \ln(D_{i,TC}/D_{o,DSC})}{2\pi \times 10 \times (T_{DSC} - T_{TC})}$$

Where,

q_{react} = reaction solution retrieved from the model (Btu/hr)

$D_{i,TC}$ = inner diameter of TC inner shell = 70.5"

$D_{o,DSC}$ = outer diameter of DSC for 69BTH, 37PTH, 32PTH, and 32PTH1 = 69.75"

T_{TC} = temperature of the TC inner shell innermost nodes (°F)

T_{DSC} = average temperature of DSC shell (°F)

The conductivity of SA-240, type 304 is considered for the TC inner shell in this sub-model. Since the TC inner shell material is SA-203, Gr. E and has higher conductivity than SA-240, type 304, this approach is conservative.

Due to high conductivity of the metallic shells, the temperature gradient across the shells is very small (< 1°F). Therefore the actual temperature gradient across the gap is slightly lower than the temperature gradient between the shells ($T_{DSC} - T_{TC}$) considered in the above equation. This results in a slightly underestimated effective conductivity across the gap, which is conservative for the purpose of this calculation.

The average temperature of the DSC shell is retrieved from the model using "ETABLE" commands in ANSYS [14]. The fixed temperature boundary condition applied on the outermost node of TC shell is considered as TC temperature.

The q_{react} depends on the applied heat flux. Since the effect of q_{react} is accounted for in the equation for k_{eff} , the calculated k_{eff} values can be used for other heat loads considered in this analysis.

The effective conductivity values for the helium within the gap between the DSC shell and the TC inner shell are summarized in Table 5-8.

Table 5-8 Radial Effective Conductivity for Helium in DSC Shell/TC Inner Shell Gap

Between DSC Shell and Cask Inner Shell
(Mat # 37 in the ANSYS model)

File name *Keff_gap.out*
Keff_gc.out

D_{o,DSC} = 69.75 DSC OD (in)
D_{i,TC} = 70.50 Cask ID (in)
L = 10 Model height (in)

T _{DSC} (°F)	T _{TC} (°F)	q _{react} (Btu/hr)	T _{avg} (°F)	k _{eff} (Btu/hr-in-°F)
110	-20	506	45	0.0080
153	30	506	92	0.0084
195	80	506	138	0.0090
237	130	506	183	0.0097
279	180	506	230	0.0104
296	200	506	248	0.0108
339	250	506	294	0.0116
382	300	506	341	0.0126
426	350	506	388	0.0136
470	400	506	435	0.0148
515	450	506	482	0.0160
560	500	506	530	0.0173
606	550	506	578	0.0187
652	600	506	626	0.0202
698	650	506	674	0.0217
745	700	506	722	0.0233
791	750	506	771	0.0251

The calculated effective conductivity in Table 5-8 is applied only in radial direction for the gap between the DSC shell and the TC inner shell. The conductivity in axial direction is set equal to helium conductivity for conservatism.

As shown in Table 5-4, the gap size between the 61BTH or 61BT DSC shell and the inner sleeve is equal to the gap size between the large diameter DSC shells (69BTH, 37PTH, 32PTH, and 32PTH1) and the TC inner shell. Since the emissivity of stainless steel is lower than emissivity of anodized aluminum, the above effective conductivity calculated for the gap between the large diameter DSC and TC inner shell can be used conservatively for the gap between the DSC and the inner sleeve for DSC types 61BTH and 61BT.

For small diameter DSC types, 32PT, 24PTH, and 24PT4, an effective conductivity is calculated for the gap between the DSC shell and TC inner sleeve using the same methodology described above with the following data.

D_{i,sleeve} = inner diameter of TC inner sleeve = 68.0"
D_{o,DSC} = outer diameter of small diameter DSC types = 67.19"

$\epsilon_{DSC} = 0.587$ (emissivity of steel or stainless steel, see Section 4.2)

$\epsilon_{sleeve} = 0.7$ (emissivity of anodized aluminum, see Section 4.2)

The effective conductivity values for the helium within the gap between the small DSC shell and the TC inner sleeve are listed in Table 5-9.

Table 5-9 Radial Effective Conductivity for Helium in DSC Shell/TC Inner Sleeve Gap

Between DSC Shell and Cask Inner Sleeve
(Mat # 38 in the ANSYS model)

File name *Keff_sl.out*

$D_{o,DSC} = 67.19$ DSC OD (in)
 $D_{i,Sleeve} = 68.00$ Cask ID (in)
 $L = 10$ Model height (in)

T_{DSC} (°F)	T_{Sleeve} (°F)	q_{react} (Btu/hr)	T_{avg} (°F)	k_{eff} (Btu/hr-in-°F)	k_{eff} in Model ⁽¹⁾ (Btu/hr-in-°F)
297	200	487	249	0.0115	0.0102
339	250	487	295	0.0125	0.0111
382	300	487	341	0.0136	0.0121
425	350	487	388	0.0148	0.0132
469	400	487	435	0.0161	0.0144
514	450	487	482	0.0175	0.0156
559	500	487	529	0.0191	0.0170
604	550	487	577	0.0207	0.0185
650	600	487	625	0.0225	0.0201
696	650	487	673	0.0244	0.0217
742	700	487	721	0.0263	0.0235
789	750	487	770	0.0285	0.0254

Note (1): For conservatism, approximately 90% of the calculated effective conductivity values are considered in the model.

This analysis uses the effective conductivity values in Table 5-8 for the gaps between the DSC shell and TC inner sleeve for 32PT, 24PTH, and 24PT4 DSC types only in radial direction. The conductivity in axial direction is set equal to helium conductivity for conservatism.

5.3 Effective Conductivity for DSC Top and Bottom Cover Plates

Axial air gaps of 0.0625" are considered between the carbon steel/stainless steel shield plugs and cover plates for all DSC types. These gaps account for contact resistance and fabrication imperfections between these components and adjacent plates. In addition, axial gaps of 0.025" are considered on both sides of lead shield plugs for 24PT4 DSC.

For simplification of the model, the axial air gaps of 0.0625" are integrated into DSC bottom shield plug and DSC top inner cover plate for all DSC types except for 24PT4.

Single axial air gaps of 0.0625" are integrated into DSC bottom inner cover plate and DSC top outer cover plate for 24PT4 DSC. The axial gaps of 0.025" are also integrated into the lead shield plugs of 24PT4 DSC.

An effective conductivity in the axial direction is calculated for these components. The conductivities of these components remain unchanged in the radial direction.

The gaps and the plates built up serial thermal resistances in the axial direction. The effective conductivity through these serial pieces is:

$$k_{eff} = \frac{\frac{t_{plate} + n \cdot t_{gap}}{k_{plate} + \frac{n \cdot t_{gap}}{k_{air}}}}$$

Where,

k_{eff} = effective conductivity in axial direction (Btu/hr-in-°F)

t_{plate} = thickness of targeted plate

(bottom shield plug and top inner cover plate for all DSC types except 24PT4)

(bottom inner cover plate, top outer cover plate, and lead shield plugs for 24PT4 DSC)

t_{gap} = 0.0625" between steel shield plugs and stainless steel plates

0.025" between lead shield plugs and stainless steel plates

k_{plate} = conductivity of A36 steel for bottom shield plug (all DSC except 24PT4)

conductivity of SS304 steel for top cover plate (all DSC except 24PT4)

conductivity of SS316 steel for top outer cover and bottom inner cover plates for 24PT4

conductivity of lead for lead shield plugs of 24PT4 DSC (Btu/hr-in-°F)

k_{air} = conductivity of air (Btu/hr-in-°F)

n = number of gaps

= 2 for gaps between shield plugs and cover plates for all DSC types except 24PT4

=1 for gap between top shield plug and outer cover plate for 24PT4

=1 for gap between bottom shield plug and outer cover plate for 24PT4

=2 for gaps between lead shield plugs and encapsulating stainless steel plates for 24PT4

The conductivity values are taken from Section 4.1.

Based on data in Table 3-1, the smallest thickness of DSC shield plug is 3" and the smallest thickness for DSC top cover plate is 0.75". These values are considered to calculate the axial effective conductivities conservatively for all DSC types except for 24PT4. The thicknesses of cover plates for 24PT4 are as follows.

24PT4 DSC top outer cover plate = 1.25"

24PT4 DSC bottom inner cover plate = 2.0"

24PT4 DSC top lead shield plug = 3.38"

24PT4 DSC bottom lead shield plug = 2.88"

The axial effective conductivities for bottom shield plug and top inner cover plates of all DSC types except 24PT4 are listed in Table 5-10.

The axial effective conductivities calculated for top/bottom inner cover plates and lead shield plugs of 24PT4 DSC are listed in Table 5-11 and Table 5-12, respectively.

Table 5-10 Axial Effective Conductivities for Bottom Shield Plug and Top Inner Cover Plate

Top inner cover plate for all DSC types except 24PT4

Plate thickness = 0.75 in

Gap thickness = 0.0625 in

Two axial gaps

Temp (°F)	k_SS304 [Table 4-2] (Btu/hr-in-°F)	Temp (K)	k_air [Table 4-9] (W/m-K)	k_air (Btu/hr-in-°F)	k_eff (Btu/hr-in-°F)
70	0.717	294.4	0.0257	0.0012	0.0086
100	0.725	311.1	0.0269	0.0013	0.0090
200	0.775	366.7	0.0308	0.0015	0.0103
300	0.817	422.2	0.0345	0.0017	0.0115
400	0.867	477.8	0.0381	0.0018	0.0127
500	0.908	533.3	0.0415	0.0020	0.0138
600	0.942	588.9	0.0449	0.0022	0.0149
700	0.983	644.4	0.0482	0.0023	0.0160
800	1.025	700.0	0.0514	0.0025	0.0171
900	1.058	755.6	0.0545	0.0026	0.0181
1,000	1.092	811.1	0.0576	0.0028	0.0191

Bottom shield plug for all DSC types except 24PT4 ⁽¹⁾

Plate thickness = 3 in

Gap thickness = 0.0625 in

Two axial gaps

Temp (°F)	k_A36 [Table 4-4] (Btu/hr-in-°F)	Temp (K)	k_air [Table 4-9] (W/m-K)	k_air (Btu/hr-in-°F)	k_eff (Btu/hr-in-°F)
70	2.275	294.4	0.0257	0.0012	0.030
100	2.300	311.1	0.0269	0.0013	0.032
200	2.317	366.7	0.0308	0.0015	0.037
300	2.275	422.2	0.0345	0.0017	0.041
400	2.208	477.8	0.0381	0.0018	0.045
500	2.142	533.3	0.0415	0.0020	0.049
600	2.075	588.9	0.0449	0.0022	0.053
700	2.008	644.4	0.0482	0.0023	0.056
800	1.933	700.0	0.0514	0.0025	0.060
900	1.858	755.6	0.0545	0.0026	0.063
1,000	1.758	811.1	0.0576	0.0028	0.067

Note (1): See Note 8 of Table 3-1 regarding 69BTH and 37PTH DSCs.

Table 5-11 Axial Effective Conductivities for Cover Plates of 24PT4 DSC

Top outer cover plate for 24PT4 DSC

Plate thickness = 1.25 in

Gap thickness = 0.0625 in

One axial gap

Temp (°F)	k_SS316 [Table 4-2] (Btu/hr-in-°F)	Temp (K)	k_air [Table 4-9] (W/m-K)	k_air (Btu/hr-in-°F)	k_eff (Btu/hr-in-°F)
70	0.642	294.4	0.0257	0.0012	0.025
100	0.658	311.1	0.0269	0.0013	0.026
200	0.700	366.7	0.0308	0.0015	0.030
300	0.750	422.2	0.0345	0.0017	0.033
400	0.792	477.8	0.0381	0.0018	0.037
500	0.833	533.3	0.0415	0.0020	0.040
600	0.875	588.9	0.0449	0.0022	0.043
700	0.917	644.4	0.0482	0.0023	0.046
800	0.958	700.0	0.0514	0.0025	0.049

Bottom inner cover plate for 24PT4 DSC

Plate thickness = 2 in

Gap thickness = 0.0625 in ⁽¹⁾

One axial gap

Temp (°F)	k_SS316 [Table 4-2] (Btu/hr-in-°F)	Temp (K)	k_air [Table 4-9] (W/m-K)	k_air (Btu/hr-in-°F)	k_eff (Btu/hr-in-°F)
70	0.642	294.4	0.0257	0.0012	0.038
100	0.658	311.1	0.0269	0.0013	0.040
200	0.700	366.7	0.0308	0.0015	0.046
300	0.750	422.2	0.0345	0.0017	0.051
400	0.792	477.8	0.0381	0.0018	0.056
500	0.833	533.3	0.0415	0.0020	0.061
600	0.875	588.9	0.0449	0.0022	0.066
700	0.917	644.4	0.0482	0.0023	0.071
800	0.958	700.0	0.0514	0.0025	0.075

Note (1): The axial gap between the bottom inner cover plate and the bottom shield plug is integrated in the axial effective conductivity for bottom shield plug (see Table 5-12). Considering an additional gap for the bottom inner cover maximizes the DSC shell temperature in the radial direction and is therefore conservative for steady state analysis.

Table 5-12 Axial Effective Conductivities for Lead Shield Plugs of 24PT4 DSC

Top shield plug for 24PT4 DSC

Plate thickness = 3.38 in

Gap thickness = 0.025 in

Two axial gaps

Temp (°F)	k _{lead} [Table 4-6] (Btu/hr-in-°F)	Temp (K)	k _{air} [Table 4-9] (W/m-K)	k _{air} (Btu/hr-in-°F)	k _{eff} (Btu/hr-in-°F)
-100	1.767	200	0.0182	0.0009	0.0582
-10	1.733	250	0.0223	0.0011	0.0706
80	1.700	300	0.0261	0.0013	0.0820
260	1.637	400	0.0330	0.0016	0.1024
440	1.579	500	0.0395	0.0019	0.1206
620	1.512	600	0.0456	0.0022	0.1371

Bottom shield plug for 24PT4 DSC

Plate thickness = 2.88 in

Gap thickness = 0.025 in

Two axial gaps

Temp (°F)	k _{lead} [Table 4-6] (Btu/hr-in-°F)	Temp (K)	k _{air} [Table 4-9] (W/m-K)	k _{air} (Btu/hr-in-°F)	k _{eff} (Btu/hr-in-°F)
-100	1.767	200	0.0182	0.0009	0.0500
-10	1.733	250	0.0223	0.0011	0.0607
80	1.700	300	0.0261	0.0013	0.0706
260	1.637	400	0.0330	0.0016	0.0883
440	1.579	500	0.0395	0.0019	0.1042
620	1.512	600	0.0456	0.0022	0.1187

5.4 Effective Conductivity for TC Slide Rails

A helium gap of 0.01" is considered between the slide rail and DSC shell to account for the contact resistance. For simplification of the model, this gap is integrated into slide rail and an effective conductivity is calculated for this component. The calculated effective conductivity for slide rail is applied conservatively in all directions.

The gap and the slide rail built up serial thermal resistances along the rail height. The effective conductivity through these serial pieces is:

$$k_{eff} = \frac{t_{rail} + t_{gap}}{\frac{t_{rail}}{k_{rail}} + \frac{t_{gap}}{k_{He}}}$$

Where,

k_{eff} = effective conductivity (Btu/hr-in-°F)

t_{rail} = thickness of TC slide rail = 0.12"

t_{gap} = thickness of gap = 0.01"

k_{rail} = conductivity of TC slide rails (Nitronic 60)

k_{He} = conductivity of helium (Btu/hr-in-°F)

The conductivity values are taken from Section 4.1. The effective conductivities for TC slide rail are listed in Table 5-13.

Table 5-13 Effective Conductivities for TC Slide Rail

Slide rail thickness = 0.12 in

Gap thickness = 0.01 in

Temp (°F)	k_{SS304} [Table 4-2] (Btu/hr-in-°F)	Temp (K)	k_{He} [Table 4-8] (W/m-K)	k_{He} (Btu/hr-in-°F)	k_{eff} (Btu/hr-in-°F)
70	0.717	294.4	0.1482	0.0071	0.076
100	0.725	311.1	0.1533	0.0074	0.079
200	0.775	366.7	0.1697	0.0082	0.087
300	0.817	422.2	0.1861	0.0090	0.095
400	0.867	477.8	0.2038	0.0098	0.104
500	0.908	533.3	0.2236	0.0108	0.113
600	0.942	588.9	0.2429	0.0117	0.122
700	0.983	644.4	0.2610	0.0126	0.131
800	1.025	700.0	0.2781	0.0134	0.139
900	1.058	755.6	0.2945	0.0142	0.147
1,000	1.092	811.1	0.3104	0.0149	0.154

5.5 Effective Conductivity for Inner Sleeve

To reduce the complexity of the TC model, an effective conductivity is calculated for the inner sleeve based on the shape shown in Figure A-2. The following dimensions are considered for the inner sleeve in the thermal model.

Sleeve ID =	68	in
Sleeve OD =	70.5	in
Total length =	196	in
No. of pieces in axial direction =	4	
No. of segments in radial direction =	40	
Axial gap =	0.188	in
Radial gap =	0.25	in

Although the above dimensions differ from the designed dimensions, they result in lower effective conductivities for the aluminum inner sleeve as discussed in APPENDIX A. The assumed dimensions are therefore conservative.

5.5.1 Axial Effective Conductivity

Along one segment of the sleeve, there are four sections of aluminum pieces with 0.1875" gaps between them in the axial direction (see Figure A-2, at bottom). The thermal resistance through these serial pieces is:

$$R_{axl,1} = 4 R_{Al} + 3 R_{gap}$$

$$R_{axl,1} = \frac{L_t}{k_{eff} \cdot A}; \quad R_{Al} = \frac{L_{Al}}{k_{Al} \cdot A}; \quad R_{gap} = \frac{L_{gap}}{k_{He} \cdot A}$$

$$L_t = 196''$$

$$L_{gap} = 0.1875''$$

$$L_{Al} = (196 - 3 \times 0.1875) / 4 = 48.86''$$

k_{eff} = effective conductivity of one axial segment (Btu/hr-in-°F)

k_{Al} = conductivity of aluminum (Btu/hr-in-°F)

k_{He} = conductivity of helium (Btu/hr-in-°F)

A = surface area of one segment (in²)

Rearranging the above equations gives:

$$k_{eff,axl,1} = \frac{L_t}{\left(\frac{4 L_{Al}}{k_{Al}} + \frac{3 L_{gap}}{k_{He}} \right)}$$

The axial segments are parallel to each other. Due to low conductivity of helium in comparison to aluminum, helium conductivity can be conservatively ignored. The total axial effective conductivity is then proportional to the ratio of the surface area for the aluminum segments in cross section to the total cross-sectional area of the inner sleeve, which is equivalent to the ratio of aluminum segment angle to the nominal angle (see Figure A-2).

$$k_{eff,axl} = k_{eff,axl,1} \times \frac{\theta_{Al}}{\theta_{nom}}$$

with $\theta_{nom} = \frac{360}{40} = 9^\circ$

$$\theta_{Al} = \theta_{nom} - \frac{gap_{rad}}{D_{o,sleeve}} \times \frac{180}{\pi} = 8.6^\circ$$

gap_{rad} = radial gap = 0.25"
D_{o,sleeve} = 70.5"

5.5.2 Radial Effective Conductivity

Forty aluminum segments in the radial direction build up parallel resistances perpendicular to the direction of heat flow from center to periphery. Again, the total radial effective conductivity can be set proportional to the ratio of the angle for one aluminum segment (θ_{Al}) to the nominal angle of each segment (θ_{nom}).

$$k_{eff,rad} = k_{Al} \times \frac{\theta_{Al}}{\theta_{nom}}$$

The effective conductivity values calculated for sleeve are summarized in Table 5-14.

Table 5-14 Effective Conductivity of Inner Sleeve

Temperature	$k_{Al}^{(1)}$	$k_{He}^{(2)}$	$k_{eff,axl,1}$	$k_{eff,axl}$	$k_{eff,rad}$
(°F)	(Btu/hr-in-°F)	(Btu/hr-in-°F)	(Btu/hr-in-°F)	(Btu/hr-in-°F)	(Btu/hr-in-°F)
70	8.008	0.0071	1.894	1.808	7.646
100	8.075	0.0074	1.947	1.859	7.710
150	8.167	0.0077	2.030	1.938	7.798
200	8.250	0.0081	2.111	2.016	7.878
250	8.317	0.0085	2.190	2.091	7.941
300	8.383	0.0090	2.276	2.173	8.005
350	8.442	0.0094	2.362	2.255	8.061
400	8.492	0.0098	2.445	2.335	8.109

Note (1): See Table 4-5 for aluminum properties.

Note (2): Interpolated / extrapolated between data in Table 4-8

5.6 Maximum Accessible Surface Temperature

The cask model is run without insolation to determine the accessible surface temperature of the impact limiters in the shade. A heat load of 32 kW and boundary conditions at 100°F and no insolation are considered in the cask model to bound the maximum accessible surface temperature under shade.

The personnel barrier is exposed to thermal radiation from the cask shield shell / finned shell and dissipates heat via thermal radiation and natural convection to ambient. Since the personnel barrier is far apart from the cask shield shell, it is not exposed to the hot air streams from the cask. This assumption is justified in Section 5.6.1.

The heat balance for the personnel barrier is shown schematically in Figure 5-13. The following conservative assumptions are considered to simplify the heat balance.

- Convection heat dissipation from the barrier is omitted completely
- Radiation heat dissipation to ambient from barrier surfaces facing the cask are omitted
- The maximum cask shield shell temperature is considered for the entire shield shell / finned shell surface
- An emissivity of 0.9 is considered for the cask outer surface. Based on discussion in Section 4.2, the emissivities for shield shell and finned shell are 0.9 and 0.7, respectively. The emissivity of 0.9 bounds these values.

The simplified heat balance for the personnel barrier is as follows.

$$q_{in,rad} = q_{out,rad}$$

$$q_{in,rad} = \frac{\sigma (T_{shell}^4 - T_{PB}^4)}{\frac{1 - \epsilon_{shell}}{\epsilon_{shell} A_{shell}} + \frac{1}{F_{PB-shell} A_{PB}} + \frac{1 - \epsilon_{PB}}{\epsilon_{PB} A_{PB}}}$$

$$q_{out,rad} = q_{1,rad,amb} + q_{2,rad,amb}, \quad q_{1,rad,amb} = 0 \text{ (conservatively, omitted in this analysis)}$$

$$q_{2,rad,amb} = \frac{\sigma (T_{PB}^4 - T_{\infty}^4)}{\frac{1 - \epsilon_{PB}}{\epsilon_{PB} A_{PB}} + \frac{1}{F_{PB-\infty} A_{PB}}}$$

σ = Stefan-Boltzmann constant = 0.119E-10 (Btu/hr-in²-°R⁴)

T_{shell} = maximum cask shield shell temperature (°R)

T_{PB} = maximum personnel barrier temperature (°R)

T_{∞} = ambient temperature = 100 °F = 560 °R

ϵ_{shell} = emissivity of TC outer surface = 0.9

ϵ_{PB} = emissivity of personnel barrier SS304 = 0.587 (see discussion in Section 4.2)

$F_{PB-shell}$ = view factor from personnel barrier to cask shield shell

$F_{PB-\infty}$ = view factor from personnel barrier (not facing cask) to ambient = 1.0

A_{PB} = surface area of personnel barrier (in²)

A_{shell} = surface area of cask shield shell (in²)

The dimensions of the cask shield shell (D_{shell}) and personnel barrier (l_{PB}) are 97.75" and 52.38", respectively as shown in Figure 5-1.

$$\frac{A_{shell}}{A_{PB}} = \frac{\pi D_{shell} / 2}{l_{PB}} = \frac{\pi \times 97.75 / 2}{52.38} = 2.931$$

The view factor of a long strip element to a parallel cylinder is given in [7], Chapter 7, Appendix B, Page 7.80 as follows. The dimensions are shown schematically in Figure 5-13 for reference.

$$F_{d1-2} = \frac{Y}{X^2 + Y^2}$$

With

$Y = y/r$, $X = x/r$

$y = 58"$ (Figure 5-1)

$r = 97.75/2 = 48.875"$ (Figure 5-1)

Integration of the above incremental view factor over the length of the strip barrier gives the view factor of the strip to the cask.

$$F_{1-2} = \frac{1}{l_{PB}} \int_0^{l_{PB}} \left(\frac{Y}{X^2 + Y^2} \right) dx$$

Considering $L = l_{PB}/r$ and $dX = dx/r$, gives the view factor of the personnel barrier to the cask.

$$F_{1-2} = \frac{1}{L} \int_0^L \left(\frac{Y}{X^2 + Y^2} \right) dX = \frac{1}{L} \left(\tan^{-1} \frac{L}{Y} \right) = \frac{r}{l_{PB}} \tan^{-1} \left(\frac{l_{PB}}{y} \right) = 0.685$$

Since the personnel barrier has an open area of 80%, a factor of 0.2 should be considered to calculate the view factor of the personnel barrier mesh to the cask.

$$F_{PB-shell} = F_{1-2} \times 0.2 = 0.137$$

Substitution of the above values in the heat balance of the personnel barrier gives the maximum temperature of the personnel barrier as reported in Section 6.2.

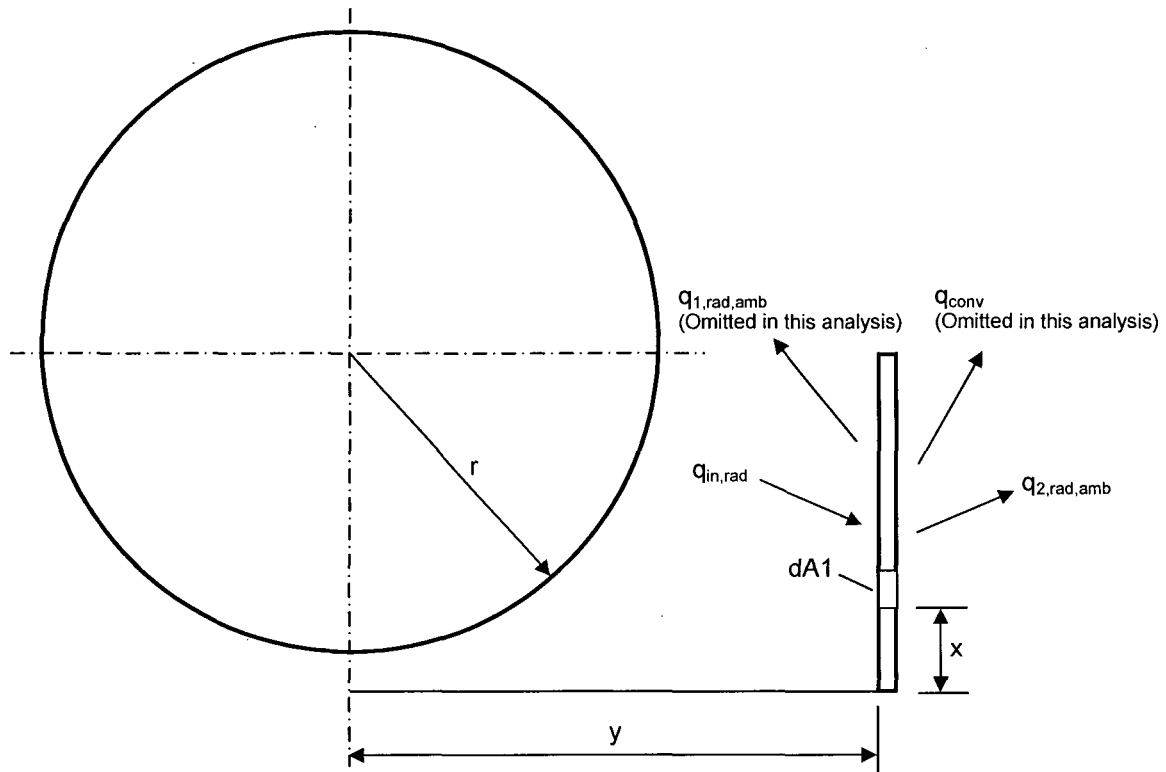


Figure 5-13 Schematic View of Cask and Personnel Barrier

5.6.1 Evaluation of Thermal Boundary Layer Thickness on Cask

The assumption that the personnel barrier is not exposed to hot air stream from the cask shield shell can be justified by calculation of the thermal boundary layer thickness around the lower half of the cask. This calculation demonstrates that the thermal boundary layer thickness is smaller than the shortest distance between the personnel barrier and the cask and therefore the personnel barrier remains out of the hot air stream from the cask.

The large diameter of the cask and the relative large temperature difference between the cask outer surface and ambient temperature suggest that the free convection over the cylinder is a turbulent flow.

The theoretical and experimental studies of the free convection and its related thermal boundary layer thickness are widely available and well documented ([29], [31], [32], and [33]). These correlations can be used to determine the free convection thermal boundary layer thickness over the horizontal MP197HB cask. These studies show that the thickness of the free convection thermal boundary layer is inversely proportional to a power of the local Nusselt number for laminar or turbulent flows.

$$\frac{\delta}{x} = \frac{C f(Pr)}{Nu_x^m} \quad (1)$$

δ = local thermal boundary layer thickness

x = local position

$f(Pr)$ = a function of Prandtl number

Nu_x = local Nusselt number

m and c = constant values

For instance, the theoretical calculation in reference [32] determines the following equation for a free convection laminar flow over flat vertical plates.

$$\frac{\delta}{x} = \frac{2}{Nu_x}$$

This equation means that $c = 2$, $f(Pr) = 1$, and $m = 1$ in equation (1).

The correlations to determine the free convection thermal boundary layer thickness and local and average Nusselt number over a vertical flat plate in turbulent flow are documented in references [30] and [31]. These correlations are shown below.

$$\frac{\delta_x}{x} = 0.565 Gr_x^{-0.1} Pr^{-8/15} (1 + 0.494 Pr^{2/3})^{0.1} \quad [30] \quad (2)$$

$$Gr_x = \frac{g \beta \Delta T x^3}{\nu^2}$$

$$Nu_x = 0.0295 \left[\frac{Pr^7}{(1 + 0.494 Pr^{2/3})^6} \right]^{1/15} Gr_x^{2/5} \quad [31]$$

$$Nu_L = 0.834 Nu_x \quad [31] \quad (3)$$

An examination of the above equations shows that the thermal boundary layer thickness is reversely proportional to the $Nu_x^{0.25}$ for turbulent free convection over a vertical flat plate.

Considering the relationship between the thermal boundary layer thickness and the local Nusselt number, the boundary layer thickness over a horizontal cylinder in free convection turbulent flow can be determined using the correlations over a vertical flat plate and the inverse ratio of the local Nusselt numbers. Since the correlations for the average Nusselt numbers of free convection for vertical flat plates and horizontal cylinders are known better than the local Nusselt numbers, the ratio of the local Nusselt numbers are extended to include the average Nusselt numbers and avoid elimination of any functions related to Prandtl number.

$$\frac{\delta_{D0}}{\delta_x} = \frac{\delta_L}{\delta_x} \cdot \frac{\delta_D}{\delta_L} \cdot \frac{\delta_{D0}}{\delta_D}$$

$$\frac{\delta_{D0}}{\delta_x} = \left(\frac{Nu_x}{Nu_L} \right)^p \left(\frac{Nu_L}{Nu_D} \right)^q \left(\frac{Nu_D}{Nu_{D0}} \right)^r \quad (4)$$

δ_{D0} = thermal boundary layer thickness at midsection of a horizontal cylinder ($\alpha = 0$)

δ_x = thermal boundary layer thickness at height of x for a vertical flat plate

Nu_x = local Nusselt number for a vertical flat plate at height x

Nu_L = average Nusselt number for a vertical flat plate at height L

Nu_{D0} = local Nusselt number at midsection of a horizontal cylinder ($\alpha = 0$)

Nu_D = average Nusselt number for a horizontal cylinder with outer diameter of D

p, q, and r = constant parameters

Based on the discussion for the thermal boundary layer thickness over a vertical flat plate above, the constant parameter p in equation (4) is 0.25.

An extensive study on free convection over large diameter, horizontal cylinders conducted in reference [34] shows that the onset of turbulent transition occurs at a point passing the midsection of the cylinder by five degree even for large Rayleigh numbers so that the free convection over the lower half of the cylinder remains laminar.

Since the personnel barrier designed for MP197HB cask is extended only to the midsection of the cask, the correlations for free convection laminar flow over horizontal cylinders can be used to determine the thermal boundary layer thickness at this location.

The free convection local Nusselt number over a horizontal cylinder in laminar flow in air is given in reference [33] as follows.

$$Nu_{D\alpha} = 0.604 Gr_D^{1/4} \phi(\alpha) \quad [33]$$

$$Gr_D = \frac{g\beta\Delta T D^3}{\nu^2}$$

α	-90°	-60°	-30°	0°	30°	60°	75°	90°
$\phi(\alpha)$	0.76	0.75	0.72	0.66	0.58	0.46	0.36	0
	Bottom half			Top half				

The local Nusselt number at the midsection of the cylinder at $\alpha = 0$ is:

$$Nu_{D0} = 0.604 Gr_D^{1/4} \times 0.66$$

Based on the above correlation, the average Nusselt number over the horizontal cylinder is:

$$Nu_D = \frac{1}{180} \int_{-90}^{90} Nu_{D\alpha} d\alpha = 0.604 Gr_D^{1/4} \times \frac{1}{180} \int_{-90}^{90} \phi(\alpha) d\alpha$$

The integration of $\phi(\alpha)$ over the range of -90° to 90° performed using the data in the above table gives:

$$Nu_D = 0.604 Gr_D^{1/4} \times 0.6025$$

Comparison of the correlations for Nu_{D0} and Nu_D gives:

$$Nu_D = \frac{0.6025}{0.66} Nu_{D0} = 0.913 Nu_{D0} \quad (5)$$

Since the equation (5) is based on free convection laminar flow, the constant parameter r in equation (4) is equal to 1.

The ratio of the average Nusselt numbers for vertical flat plate and horizontal cylinder can be determined using the corresponding correlations shown in Section APPENDIX B.

The thickness of the boundary layer at the midsection of the cask can be determined by substitution of the correlations for the local and average Nusselt numbers into equation (4). The height (L) of the vertical flat plate can be set equal to the outer diameter of the cask (D) for this evaluation. Average of the cask outer surface and ambient temperatures are considered in calculation of the Nusselt numbers.

As seen above, the correlations for the local and average Nusselt numbers depend on the Grashof and Prandtl numbers, which in turn depend on the cask outer surface temperature. A sensitivity analysis is performed to cover the effects of a wide range of cask temperatures from 200°F to 500°F on the thickness of free convection thermal boundary layer at the midsection of the cask. This sensitivity analysis starts with variation of Grashof and Prandtl numbers as summarized in Table 5-15.

Table 5-15 Variation of Grashof, Prandtl, and Rayleigh Numbers

$T_{\infty} = 100^{\circ}\text{F}$

For $L=D$

T_{cask}	T_{cask}	T_{∞}	T_{avg}	β	ν	Gr	Pr	Ra
(°F)	(K)	(K)	(K)	(1/K)	(m ² /s)	(---)	(---)	(---)
200	367	311	339	2.95E-03	2.235E-05	4.931E+10	0.71	3.490E+10
300	422	311	367	2.73E-03	2.849E-05	5.609E+10	0.70	3.948E+10
400	478	311	394	2.54E-03	3.516E-05	5.135E+10	0.70	3.602E+10
500	533	311	422	2.37E-03	4.232E-05	4.415E+10	0.70	3.091E+10

The values in Table 5-15 are calculated based on air properties taken from Table 4-9 at the average air temperature. As seen in Table 5-15, the Grashof number varies between 5.6E+10 and 4.4E+10, the Prandtl number varies between 0.70 and 0.71, and the Rayleigh number varies between 3.1E+10 and 4.0E+10 for the cask outer surface temperatures between 200°F and 500°F. Since the variation of Prandtl is relative small, an average Prandtl number of 0.70 is considered in the sensitivity analysis to calculate the average Nusselt numbers for a vertical flat plate (Nu_L) and a horizontal cylinder (Nu_D). To bound the variation of the Rayleigh number conservatively, the average Nusselt numbers Nu_L and Nu_D are evaluated for a wider range of Rayleigh numbers between 1E+10 and 1E+11.

As shown in APPENDIX B, the correlation for Nu_L depends on C_f^* and f factors, which in turn depend on Prandtl number and surface temperature, respectively. C_f^* is a weak function of Prandtl number. The variation of the f factor is determined for a cask outer surface temperature from 200°F to 500°F. The variations of these values are summarized in Table 5-16.

[illegible]

As shown in Table 5-17, the ratio of Nu_L to Nu_D varies between 0.973 and 1.029 for the range of considered Rayleigh numbers. An average value of 1.011 is considered for this ratio to use in equation (4). Since this ratio is close to one, the constant parameter q in equation (4) does not have any significant effect and can be omitted.

Substitution of the local and average Nusselt number ratios from equation (3), equation (5), and the table of Nu_L/Nu_D variations into equation (4) gives:

$$\delta_{D0} = (1/0.834)^{0.25} \times 1.011 \times 0.913 \delta_x$$

Using δ_x from equation (2) in the above equation determines the range of boundary layer thickness at the midsection of the cask as summarized in Table 5-18.

Table 5-18 Thickness of the Thermal Boundary Layer

$$T_{\infty} = 100^{\circ}\text{F}$$

$$L = D = 97.75''$$

T_{cask} (°F)	T_{cask} (K)	T_{∞} (K)	T_{avg} (K)	Gr (---)	Pr (---)	δ_x/L (---)	δ_x (in)	δ_{D0} (in)
200	367	311	339	4.931E+1 0	0.71	0.060	5.9	5.7
300	422	311	367	5.609E+1 0	0.70	0.059	5.8	5.6
400	478	311	394	5.135E+1 0	0.70	0.060	5.9	5.7
500	533	311	422	4.415E+1 0	0.70	0.061	6.0	5.7

As seen in Table 5-18, the variation of the thermal boundary layer thickness is small and its maximum value at the midsection of the cask is 5.7" for a uniform cask surface temperature of 500°F. Based on data shown in Section 5.6, the shortest distance between the outer surface of the cask and the personnel barrier is over 9".

$$\text{Shortest distance} = \text{distance to cask centerline} - \text{cask OD}/2 = y - r = 58 - 48.875 = 9.125''$$

The conservatively evaluated boundary layer thickness of 5.7" is much smaller than shortest distance between the outer surface of the cask and the personnel barrier. Therefore, the personnel barrier remains out of the hot air streams flowing around the cask outer surface.

6.0 RESULTS

6.1 Maximum Temperatures

Typical temperature distributions for the MP197HB finite element models are shown in Figure 6-1 and Figure 6-2.

The maximum component temperatures for hot NCT for ambient temperature of 100°F with insolation are listed in Table 6-1.

Table 6-1 Maximum Temperatures of TC Component / DSC Shell for Hot NCT (100°F and Insolation)

DSC type	69BTH			61BTH/ 61BTHF Type 1	61BTH/ 61BTHF Type 2	61BT	
Heat Load	32 kW	29.2 kW	26 kW	22 kW	24 kW	18.3 kW	
Inner sleeve	No	No	No	Yes	Yes	Yes	
External fins	Yes	Yes	No	No	No	No	
Component	T _{max} (°F)	T _{max} (°F)	T _{max} (°F)	T _{max} (°F)	T _{max} (°F)	T _{max} (°F)	Limit (°F)
DSC shell	484	458	451	414	435	372	---
DSC shell @ mid-length ⁽¹⁾	470	445	440	406	427	365	---
Inner sleeve	N/A	N/A	N/A	317	333	286	---
Cask inner shell	367	347	351	315	331	284	---
Gamma shield	366	345	349	314	330	283	621 [13]
Outer shell	352	332	337	306	321	276	---
Shield shell	305	289	299	272	285	248	---
Finned Shell	229	220	N/A	N/A	N/A	N/A	---
Cask lid	267	254	265	248	259	228	---
Cask bottom plate	353	334	338	307	322	277	---
Neutron Shield Resin ⁽²⁾	323	305	314	285	299	259	---
Trunnion Plug Resin ⁽²⁾	324	306	315	286	299	259	---
Cask lid seal	268	256	266	249	260	229	400 [2]
Ram plate seal	352	332	337	306	321	277	400 [2]
Drain port seal @ bottom	351	332	337	306	321	276	400 [2]
Test seal @ bottom	349	330	335	305	320	276	400 [2]
Vent & test seal @ top	267	254	265	248	259	228	400 [2]
Wood in Impact limiter	302	287	291	265	278	242	320 [2]

**Table 6-1 Maximum Temperatures of TC Component / DSC Shell
for Hot NCT (100°F and Insolation) – Continued**

DSC type	37PTH	32PTH / 32PTH Type1 / 32PTH1 Type 1	32PTH1 Type 2	32PT	24PTH / 24PTHF Type 1 & 2	24PT4	
Heat Load	22.0 kW	26 kW	24 kW	24 kW	26 kW	24 kW	
Inner sleeve	No	No	No	Yes	Yes	Yes	
External fins	No	No	No	No	No	No	
Component	T _{max} (°F)	T _{max} (°F)	T _{max} (°F)	T _{max} (°F)	T _{max} (°F)	T _{max} (°F)	Limit (°F)
DSC shell	408	444	423	443	464	428	---
DSC shell @ mid-length ⁽¹⁾	397	436	416	432	449	424	
Inner sleeve	N/A	N/A	N/A	329	347	319	---
Cask inner shell	314	337	322	326	344	317	---
Gamma shield	313	336	321	325	343	316	621 [13]
Outer shell	301	320	306	316	335	308	---
Shield shell	271	290	278	281	295	274	---
Cask lid	301	319	305	318	336	306	---
Cask bottom plate	246	276	265	268	282	309	---
Neutron Shield Resin ⁽²⁾	284	303	290	295	310	287	---
Trunnion Plug Resin ⁽²⁾	285	305	292	296	311	287	---
Cask lid seal	301	319	305	317	336	307	400 [2]
Ram plate seal	244	274	263	267	280	308	400 [2]
Drain port seal @ bottom	245	275	264	267	281	308	400 [2]
Test seal @ bottom	243	272	262	265	279	307	400 [2]
Vent & test seal @ top	300	318	305	317	336	306	400 [2]
Wood in Impact limiter	262	278	266	274	289	267	320 [2]

Note (1): This value is the maximum DSC shell temperature in the region where the fuel assemblies have the maximum peaking factor. The values for PWR DSCs are retrieved from the models using the macro "DSCmid_PWR.txt" listed in Table 8-3.

Note (2): See Table 6-2 for the highest volumetric average resin temperature and its temperature limit.

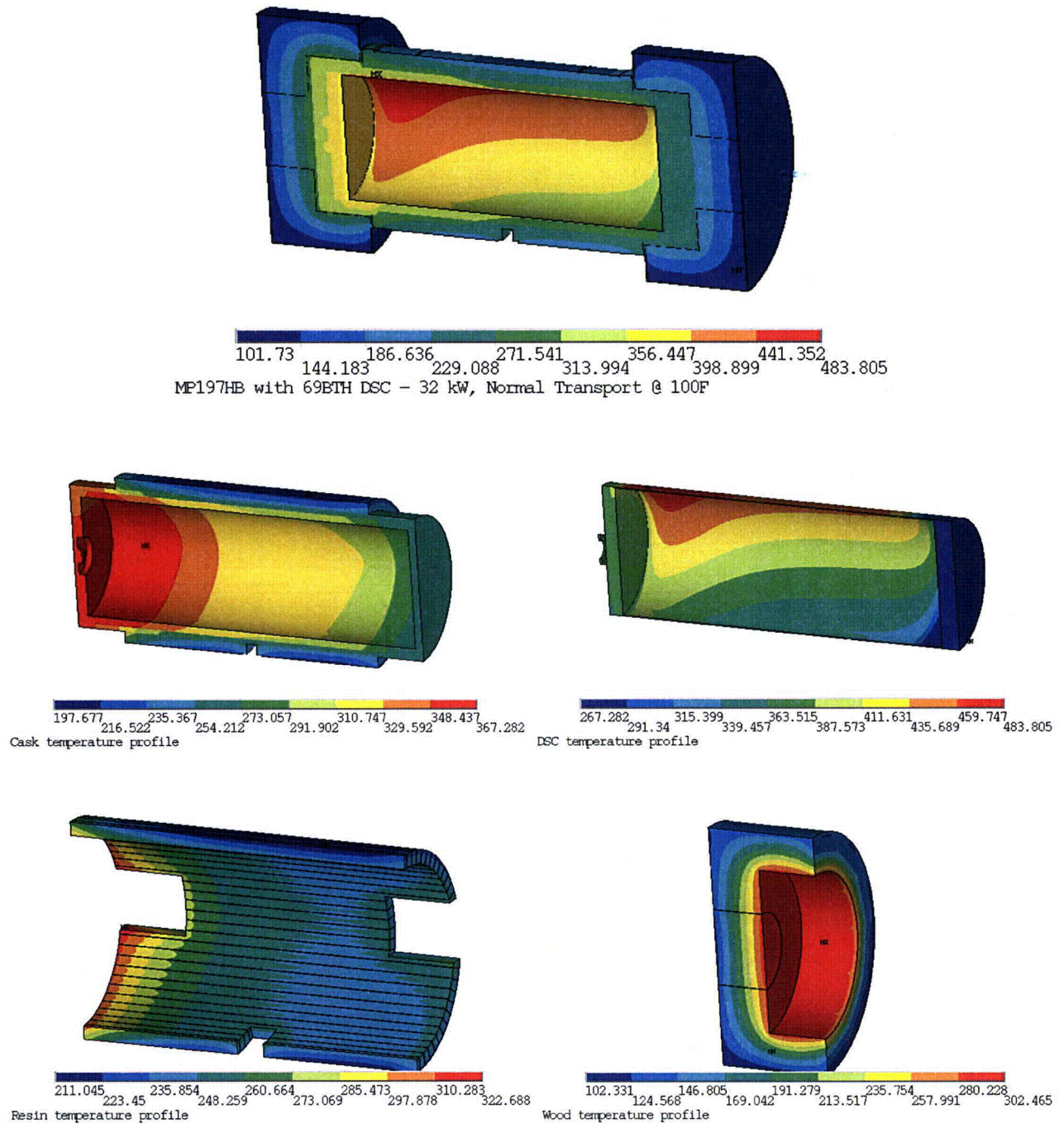


**Figure 6-1 Temperature Profiles for MP197HB Transport Cask
NCT, 100°F, Insolation, 69BTH DSC, 32 kW**

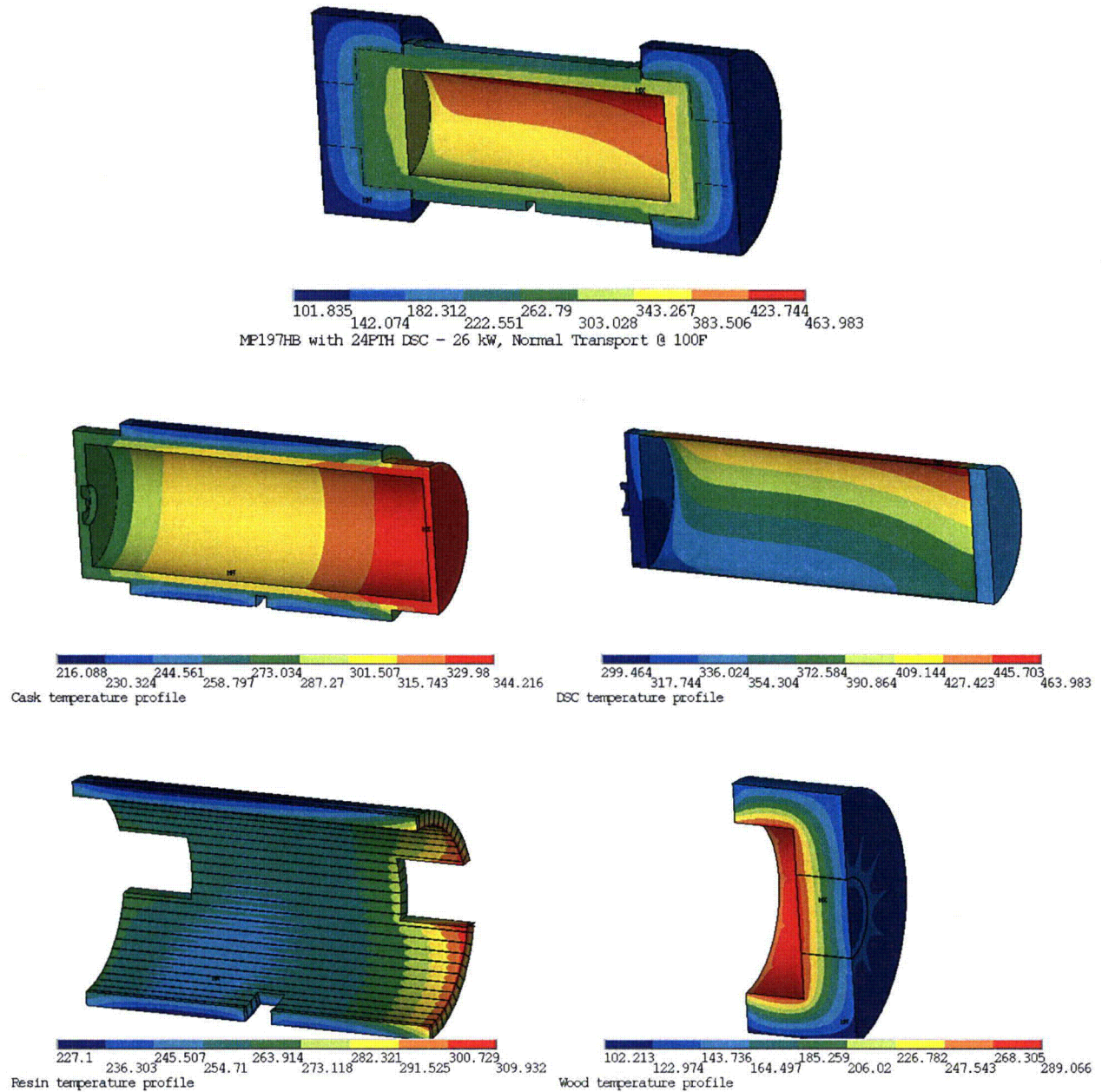


**Figure 6-2 Temperature Profiles for MP197HB Transport Cask
NCT, 100°F, Insolation, 24PTH DSC, 26 kW**

The average temperatures of helium within TC cavity, the average temperatures of TC inner shell, and the volumetric average temperatures of neutron shield and trunnion plug resins for NCT with 100°F ambient temperature and insolation are listed in Table 6-2.

The volumetric average temperatures of resins are calculated for elements at the hottest cross section of the resin with a thickness of one or two element.

**Table 6-2 Average TC Component Temperatures for Hot NCT
(100°F and Insolation)**

DSC Type	69BTH			61BTH/ 61BTHF Type 1	61BTH/ 61BTHF Type 2	61BT
Heat load	32 kW	29.2 kW	26 kW	22 kW	24 kW	18.3 kW
Inner sleeve	No	No	No	Yes	Yes	Yes
External fins	Yes	Yes	No	Yes	No	No
Component	T _{avg} (°F)	T _{avg} (°F)	T _{avg} (°F)	T _{avg} (°F)	T _{avg} (°F)	T _{avg} (°F)
Helium in TC cavity	339	321	328	301	316	273
TC inner shell	321	304	314	287	300	260
Neutron Shield Resin ⁽¹⁾	290	276	288	264	276	241
Trunnion Plug Resin ⁽²⁾	277	263	272	249	260	229

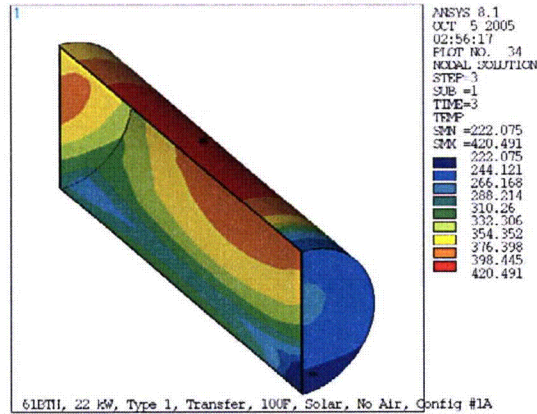
DSC Type	37PTH	32PTH / 32PTH Type1 / 32PTH1 Type 1	32PTH1 Type 2	32PT	24PTH/ 24PTHF Type 1 & 2	24PT4
Heat load	22.0 kW	26 kW	24 kW	24 kW	26 kW	24 kW
Inner sleeve	No	No	No	Yes	Yes	Yes
External fins	No	No	No	No	No	No
Component	T _{avg} (°F)	T _{avg} (°F)	T _{avg} (°F)	T _{avg} (°F)	T _{avg} (°F)	T _{avg} (°F)
Helium in TC cavity	269	301	288	281	297	313
TC inner shell	285	312	298	299	313	302
Neutron Shield Resin ⁽¹⁾	263	280	268	273	285	265
Trunnion Plug Resin ⁽²⁾	249	264	254	257	268	250

Note (1): This temperature is the volumetric, average temperature of the elements located at hottest cross section of the neutron shield resin. The temperature limit for neutron shield resin (Vyal B) is 320°F [2].

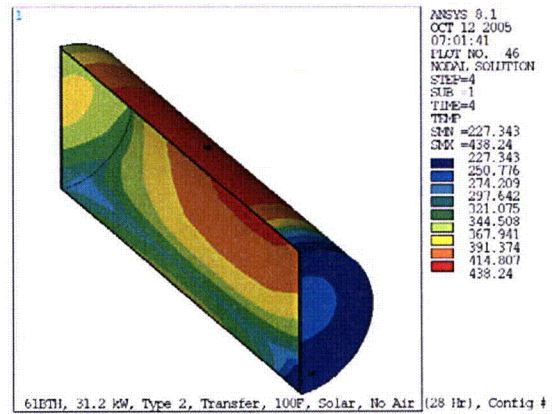
Note (2): This temperature is the volumetric, average temperature of the elements located at hottest cross section of the trunnion plug resin. Based on discussion in Section 4.3, a temperature limit of 445°F is selected for trunnion plug resin (Polypropylene).

The maximum DSC shell temperature for normal transfer conditions without air circulation occurs generally in the mid section of the DSC where the fuel assembly has its highest peaking factor while the maximum DSC shell temperature for NCT occurs toward the ends of the DSC shell where it is covered by impact limiters.

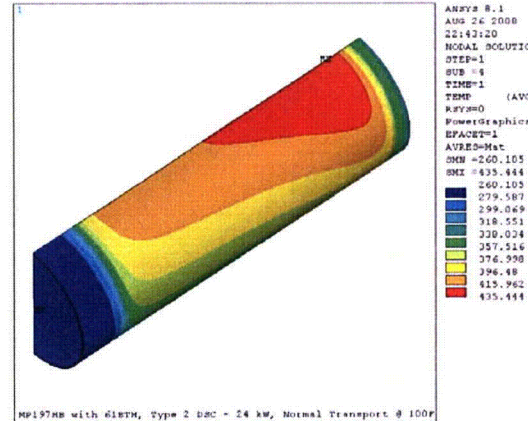
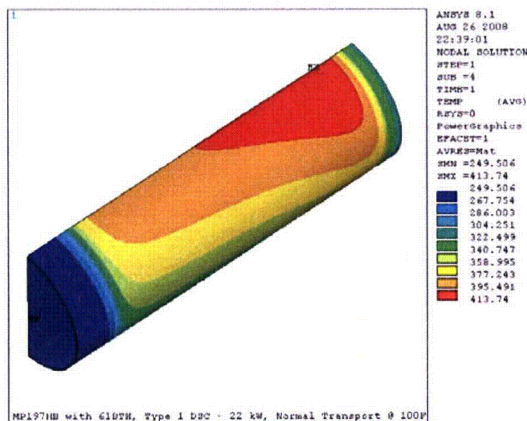
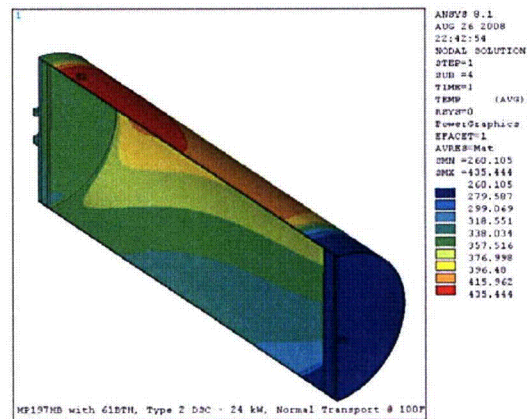
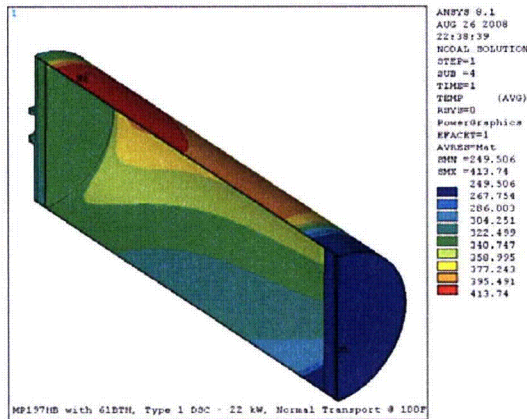
To illustrate this fact, the DSC shell temperature profiles for 61BTH DSC and 24PTH DSC under normal transfer conditions and NCT at 100°F ambient are compared in Figure 6-3 and Figure 6-4.



Transfer Conditions
61BTH Type 1, 22.0 kW, 100°F
from [21], Appendix A, Figure A-26



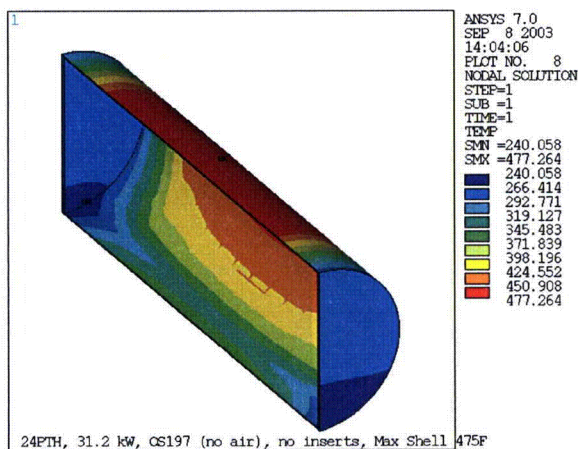
Transfer Conditions
61BTH Type 2, 31.2 kW, 100°F
from [21], Appendix A, Figure A-88



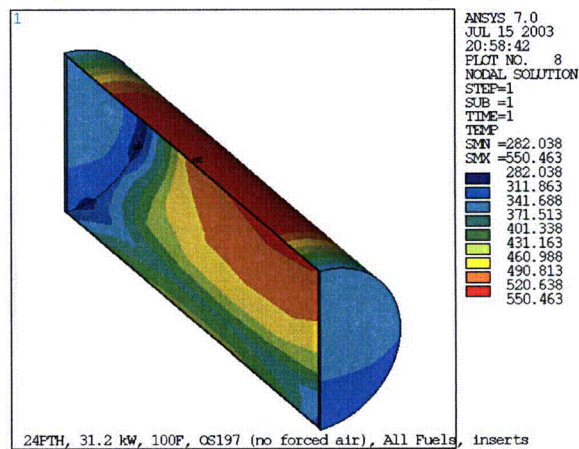
NCT, 61BTH Type 1, 22.0 kW, 100°F

NCT, 61BTH Type 2, 24.0 kW, 100°F

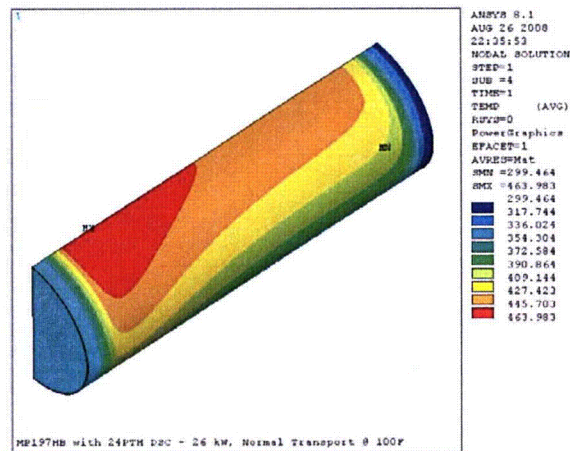
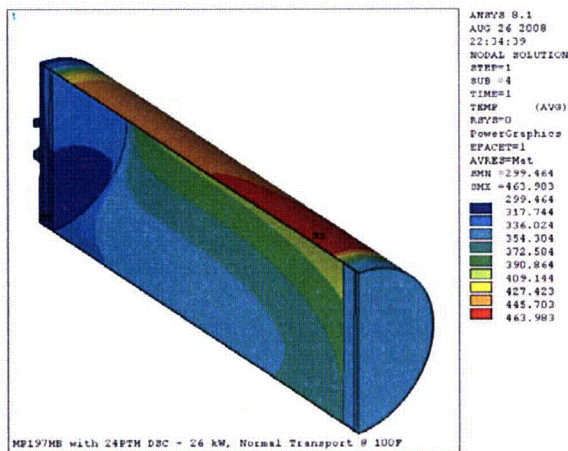
Figure 6-3 Comparison of DSC Shell Temperature Profiles for 61BTH DSC



Transfer Conditions
24PTH Type 2, 31.2 kW, 100°F
from [22], Appendix A, Figure A65.2



Transfer Conditions
24PTH Type 1, 31.2 kW, 100°F
from [22], Appendix A, Figure A62.2



NCT, 24PTH Type 1 or Type 2, 26.0 kW, 100°F

Figure 6-4 Comparison of DSC Shell Temperature Profiles for 24PTH DSC

Since the maximum DSC shell temperature for normal transfer conditions is higher and the hottest region of the DSC shell temperature overlaps the area of the highest peaking factors, the DSC shell temperature profile for normal transfer conditions gives the bounding values for the basket and fuel cladding temperatures, if the maximum shell temperature for normal transfer conditions is higher than the one for NCT.

The above statement is true when the maximum heat load for normal transfer conditions and NCT are equal. If the heat load for normal transfer conditions is also higher than the one for NCT, even lower basket and fuel cladding temperatures are expected for NCT.

Based on peaking factor profiles reported in [5], the maximum peaking factor region is located between ~36.1" and ~84.9" for BWR and between ~28.0" to ~100.0" for PWR fuel assemblies. These locations are measured from the bottom of active fuel length. The active fuel length starts approximately 7.5" and 4.0" measured from the bottom of the fuel assembly for BWR and PWR fuel assemblies, respectively. The maximum DSC shell temperature for each DSC type is retrieved at the above locations to give the maximum DSC shell temperature in the region of highest peaking factors, where maximum fuel cladding temperatures are expected.

The maximum DSC shell temperatures for NCT are compared with the corresponding data for normal transfer conditions in Table 6-3.

Table 6-3 Comparison of Maximum DSC Shell Temperatures

DSC type	Maximum DSC Shell Temperature		10 CFR 72 Model Reference
	Normal Conditions of Transport ⁽¹⁾ [Table 6-1] (°F)	Normal Transfer Conditions (°F)	
61BTH Type 1	414 / 406	418 [5], Table T.4-7 ⁽²⁾	[5], Section T.4.5.1
61BTH Type 2	435 / 427	441 [5], Table T.4-8 ⁽²⁾	[5], Section T.4.5.1
61BT	372 / 365	378 [3], Table K.4-2	[3], Section K.4.4.1
32PTH / 32PTH Type 1	444 / 436	475 [6], Table 4-1	[6], Section 4.3.1.1
32PTH1 Type 1	444 / 436	485 [5], Table U.4-11	[5], Section U.4.5.2
32PTH1 Type 2	423 / 416	429 [5], Table U.4-34	[5], Section U.4.5.2
32PT	443 / 432	445 [3], Table M.4-3	[3], Section M.4.4.1.6
24PTH Type 1 (24PTH-S or -L w/ Al inserts)	464 / 449	551 [3], Table P.4-11 ⁽²⁾	[3], Section P.4.5.2
24PTH Type 2 (24PTH-S or -L w/o Al inserts)	464 / 449	475 [3], Table P.4-10 ⁽²⁾	[3], Section P.4.5.2
24PTH Type 2 (24PTH-S-LC)	464 / 449 ⁽³⁾	475 [3], Table P.4-10 ⁽²⁾	[3], Section P.4.5.2
24PT4	428 / 424	439 [4], Table A.4.4-4	[4], Section 4.4.3.1

Note (1): The first value is the absolute maximum DSC shell temperature and the second value is the maximum DSC shell temperature where the fuel has the maximum peaking factor.

(2): The small differences between the maximum DSC shell temperatures in this table and those shown in Figure 6-3 and Figure 6-4 are caused by imperfections in the nodal temperature transfer from TC to DSC models for 61BTH and 24PTH DSCs in [21] and [22].

(3): The analysis for 24PTH-S-LC DSC with 24kW heat load is bounded by 24PTH DSC Type 2 with 26 kW heat load.

As seen in Table 6-3, the maximum DSC shell temperature for NCT at the mid section, where the highest peaking factors are located, is 4 to 15°F lower than the absolute maximum DSC shell temperature for the NCT and both of these values are lower than the maximum DSC shell temperature for normal transfer conditions. This concludes that the DSC shell temperature profiles for normal transfer conditions represent the bounding cases for the maximum basket and fuel cladding temperatures.

Table 6-3 shows that the maximum DSC shell temperature for NCT is lower than the corresponding value for normal transfer conditions for all DSC types. Therefore, the selected maximum heat loads listed in Table 1-1 are acceptable and the thermal analysis results for loaded DSCs in 10CFR72 SARs ([3], [4], [5], and [6]) are applicable for NCT. Except for 69BTH and 37PTH DSCs, no further DSC thermal analyses are required.

Based on Table 6-1, the results for the 69BTH DSC with 32 kW heat load bound the maximum MP197HB cask component and DSC shell temperatures. The maximum temperature gradients are also expected to be bounded by this case. Therefore, 69BTH DSC with 32 kW heat load case is selected to determine the maximum temperature gradients through MP197HB cask. The maximum component temperatures for cold NCT at -20°F and -40°F ambient temperatures without insolation are listed in Table 6-4.

**Table 6-4 Maximum Component Temperatures for Cold NCT
(69BTH, 32 kW, No Insolation)**

DSC type	69BTH, 32 kW, TC with External Fins and No Inner Sleeve	
Ambient Temperature	-20°F	-40°F
Component	T _{max} (°F)	T _{max} (°F)
DSC shell	405	392
Cask inner shell	267	250
Gamma shield	265	248
Outer shell	250	233
Shield shell	202	184
Finned Shell	124	105
Cask lid	162	145
Cask bottom plate	252	235
Neutron Shield Resin ⁽¹⁾	187	169
Trunnion Plug Resin ⁽²⁾	169	151
Wood in Impact limiter	193	175

Note (1): This temperature is the volumetric, average temperature of the elements located at hottest cross section of the neutron shield resin.

Note (2): This temperature is the volumetric, average temperature of the elements located at hottest cross section of the trunnion plug resin.

The temperature profiles for 37PTH DSC shell are also determined for cold NCT at -20°F and -40°F ambient temperatures without insolation to be used for basket thermal and structural evaluations. The maximum component temperatures for 37PTH at -20°F and -40°F ambient temperatures without insolation are listed in Table 6-5.

**Table 6-5 Maximum Component Temperatures for Cold NCT
(37PTH, 22.0 kW, No Insolation)**

DSC type	37PTH, 22.0 kW, TC without External Fins or Inner Sleeve	
Ambient Temperature	-20°F	-40°F
Component	T _{max} (°F)	T _{max} (°F)
DSC shell	328	315
Cask inner shell	219	203
Gamma shield	217	202
Outer shell	204	188
Shield shell	173	157
Cask lid	204	188
Cask bottom plate	146	130
Neutron Shield Resin ⁽¹⁾	164	148
Trunnion Plug Resin ⁽²⁾	145	128
Wood in Impact limiter	157	140

Note (1): This temperature is the volumetric, average temperature of the elements located at hottest cross section of the neutron shield resin.

Note (2): This temperature is the volumetric, average temperature of the elements located at hottest cross section of the trunnion plug resin.

The maximum component temperatures for 37PTH DSC with 23.2 kW under NCT are listed in APPENDIX G. The results of the analysis for 37PTH DSC with 23.2 kW are used only for structural evaluations.

6.2 Maximum Accessible Surface Temperature

With the installation of the personnel barrier, the accessible packaging surfaces are limited to the impact limiter and the barrier outer surfaces.

Based on requirements in [1] and [2], the maximum accessible surface temperature is determined for impact limiters considering the maximum decay heat load of 32 kW, ambient temperature of 100°F, and no insolation. The maximum accessible surface temperature of impact limiters under these conditions is 121°F.

The maximum temperature of the cask outer surface is 302°F and belongs to a part of shield shell uncovered by the external fins. This temperature is retrieved by selecting the outermost elements and nodes (element type # 3) from the cask ANSYS model. The maximum temperature of the personnel barrier is calculated based on the maximum temperature of the cask outer surface using the methodology described in Section 5.6. The maximum temperature of the personnel barrier is 152°F.

The maximum accessible surface temperatures are well below the limit of 185°F defined in Section 4.3.

6.3 Heat Balance

Insolance over various surfaces of MP197HB is calculated using the following equation.

$$Sol_A = q''_{sol} \cdot S_A \cdot \alpha \cdot F$$

Sol_A = insolance over surface A (Btu/hr)

q''_{sol} = solar heat flux from Table 5-2 for surface A (Btu/hr-in²)

S_A = surface area of surface A

α = solar absorptivity for surface A

F = exposure factor for surface A (1 for vertical surfaces, 0.5 for other surfaces, see Section 3.0 for discussion)

The results are summarized in Table 6-6.

In order to check the proper application of insolance in MP197HB cask model, the insolance boundary conditions are applied in two separate models. The decay heat loads were ignored in these models. The model "check_Sol_U" is used for insolance over un-finned TC and the model "check_Sol_F" is used for insolance over TC equipped with finned aluminum shell. These model runs are listed in Table 8-2. The reaction solutions in "check_Sol_U" and "check_Sol_F" models are retrieved using "PRRSOL" commands in ANSYS [14] to show the amount of applied insolance.

The retrieved values are then compared to the calculated insolance over neutron shield shell or finned shell. This comparison shows the proper application of insolance boundary conditions as summarized in Table 6-6.

The dissipated heat (convection and radiation) from MP197HB is retrieved from the model using "ETABLE" commands [14] to build up the heat balance for TC. The commands are collected in the input files for each run listed in Table 8-2. The data for TC heat balance are listed in Table 6-7.

Since the MP197HB model is half-symmetric, the retrieved insolance and heat dissipations are multiplied by two in Table 6-6 and Table 6-7.

Table 6-6 Insolation Boundary Conditions for MP197HB – Concluded

Retrieved data from Model “check Sol U”

	(Btu/hr)	(kW)
Solar heat in half-model	6830	2.00
Total solar heat in ANSYS model	13660	4.00
Calculated total solar	13672	4.01
Deviation from calculated values	-0.1%	-0.1%

Retrieved data from Model “check Sol F”

	(Btu/hr)	(kW)
Solar heat in half-model	6255	1.83
Total solar heat in ANSYS model	12510	3.67
Calculated total solar	12497	3.66
Deviation from calculated values	0.1%	0.1%

Note (1): The surface area of exposed thermal shield is very small. Solar heat over this surface is omitted in the model.

Calculation

Calculation No.: MP197HB-0401

Revision No.: 2

Page: 81 of 112

Table 6-7 Heat Balance for MP197HB

Hot Transport Conditions at 100°F Ambient with Insolation									
DSC type	Decay Heat [Table 5-3]	Insolance from ANSYS model [Table 6-6]	Total Heat Load	Heat Dissipation from Rear Impact limiter		Heat Dissipation from Neutron Shield/Finned Shell		Heat Dissipation from Front Impact limiter	
	(Btu/hr)	(Btu/hr)	(Btu/hr)	(Btu/hr)	(Ratio to Total)	(Btu/hr)	(Ratio to Total)	(Btu/hr)	(Ratio to Total)
69BTH, 26 kW	88720	13660	102380	7327	7.2%	88445	86.4%	6597	6.4%
69BTH, 29.2 kW	99639	12510	112149	7264	6.5%	98409	87.7%	6480	5.8%
69BTH, 32 kW	109194	12510	121704	7470	6.1%	107614	88.4%	6606	5.4%
61BTH / 61BTHF Type 1	75071	13660	88731	6989	7.9%	75333	84.9%	6416	7.2%
61BTH / 61BTHF Type 2	81895	13660	95555	7158	7.5%	81873	85.7%	6531	6.8%
61BT	62445	13660	76105	6675	8.8%	63238	83.1%	6201	8.1%
37PTH	75071	13660	88731	6381	7.2%	75407	85.0%	6950	7.8%
32PTH / 32PTH Type 1	88720	13660	102380	6688	6.5%	88535	86.5%	7146	7.0%
32PTH1 Type 1	88720	13660	102380	6688	6.5%	88535	86.5%	7146	7.0%
32PTH1 Type 2	81895	13660	95555	6579	6.9%	81981	85.8%	7001	7.3%
32PT	81895	13660	95555	6602	6.9%	81842	85.7%	7102	7.4%
24PTH / 24PTHF Type 1 & 2	88720	13660	102380	6749	6.6%	88318	86.3%	7302	7.1%
24PT4	81895	13660	95555	7004	7.3%	81552	85.4%	6989	7.3%
Cold Transport Conditions / Hot Transport under Shade									
69BTH, 32kW, -20°F	109194	0	109194	2486	2.3%	105032	96.2%	1664	1.5%
69BTH, 32kW, -40°F	109194	0	109194	2481	2.3%	105034	96.2%	1668	1.5%
69BTH, 32kW, 100°F, Shade	109194	0	109194	2490	2.3%	105061	96.2%	1630	1.5%
37PTH, 22.0kW, -20°F	75071	0	75071	1497	2.0%	71523	95.3%	2044	2.7%
37PTH, 22.0kW, -40°F	75071	0	75071	1514	2.0%	71492	95.2%	2058	2.7%

7.0 CONCLUSION

Heat balance of MP197HB for the hot NCT shows that more than 83% of total heat load (decay heat and insolation) is dissipated to environment from the neutron shield shell or finned shell surface. The heat dissipation from each impact limiter is limited to about 5 to 8%. Heat balance for the cold NCT shows that more than 95% of decay heat load dissipates through the neutron shield or finned shell.

The maximum and average temperatures of major components from Table 6-1 and Table 6-2 are summarized in Table 7-1. As seen in Table 7-1, the maximum temperatures of the MP197HB components calculated for NCT are lower than the allowable limits.

The maximum seal temperature is 352°F at ram closure plate for 32 kW heat load in 69BTH DSC. This temperature is well below the long-term limit of 400°F specified for continued seal function.

The maximum wood temperature for 32 kW heat load is 302°F which is below the considered limit of 320°F for crush structural analysis.

The maximum temperature of gamma shield (lead) is 366°F, which is well below the lead melting point of 621°F.

The highest volumetric average resin temperature in the neutron shield at the hottest cross section is 290°F, which occurs for the maximum heat load of 32 kW. The Vyal B resin temperature is below the temperature limit of 320°F and no degradation of the neutron resin is expected.

The highest volumetric average resin temperature in the trunnion plugs at the hottest cross section is 277°F occurring for the maximum heat load of 32 kW. The polypropylene resin temperature is well below the temperature limit of 445°F and no degradation of the trunnion plug resin is expected.

All materials can be subjected to a minimum environment temperature of -40°F (-40°C) without any adverse effects. The maximum component temperatures for cold NCT are summarized in Table 7-2.

The maximum accessible surface temperatures of MP197HB cask at 100°F without insolation are 121°F for impact limiters and 152°F for personnel barrier. These temperatures are well below the limit of 185°F defined in Section 4.3.

The evaluations of 69BTH and 37PTH DSCs for storage conditions are not available yet. For all other DSC types in MP197HB, the maximum DSC shell temperatures for transport conditions are bounded by the values reported for normal transfer conditions as shown in Table 6-3. Based on discussion in Section 6.1, the DSC shell temperature profiles for normal transfer conditions are bounding for NCT. Therefore, the thermal analysis results for DSCs in

10CFR72 SARs ([3], [4], [5], and [6]) are applicable for NCT and no further DSC thermal analysis is required except for 69BTH and 37PTH DSCs.

All design criteria are herein satisfied.

Table 7-1 Maximum Temperatures of TC Component / DSC Shell for Hot NCT

Conditions	100°F with Insolation			
Heat load	$26 < Q \leq 32 \text{ kW}$	$Q \leq 26 \text{ kW}$		
Inner sleeve	No	No	Yes	
External fins	Yes	No	No	
Component	T_{\max} (°F)	T_{\max} (°F)	T_{\max} (°F)	Limit (°F)
DSC shell	484	451	464	---
Inner sleeve	N/A	N/A	347	---
Cask inner shell	367	351	344	---
Gamma shield	366	349	343	621 [13]
Outer shell	352	337	335	---
Shield shell	305	299	295	---
Finned Shell	229	N/A	N/A	---
Cask lid	267	319 ⁽²⁾	336 ⁽²⁾	---
Cask bottom plate	353	338	322	---
Neutron Shield Resin ⁽¹⁾	290	288	285	320 [2]
Trunnion Plug Resin ⁽¹⁾	277	272	268	445 [24]
Seals	352	337	336	400 [2]
Wood in Impact limiter	302	291	289	320 [2]

Notes:

- (1) The resin temperature is the volumetric, average temperature at the hottest cross section.
- (2) The maximum cask lid temperatures for $26 \text{ kW} < Q \leq 32 \text{ kW}$ and $Q \leq 26 \text{ kW}$ belong to DSCs loaded with BWR and PWR fuel assemblies, respectively. Since a spacer is used for PWR DSCs, the heat load of the PWR fuel assemblies is closer to the cask lid. Due to this configuration, the maximum cask lid temperature for $Q \leq 26 \text{ kW}$ is higher than for $26 \text{ kW} < Q \leq 32 \text{ kW}$. See Table 6-1 for details.

**Table 7-2 Maximum Temperatures of TC Component / DSC Shell
for Cold NCT**

Ambient Temperature	-20°F	-40°F
Component	T_{max} (°F)	T_{max} (°F)
DSC shell	405	392
Cask inner shell	267	250
Gamma shield	265	248
Outer shell	250	233
Shield shell	202	184
Finned Shell	124	105
Cask lid	162	145
Cask bottom plate	252	235
Neutron Shield Resin ⁽¹⁾	187	169
Trunnion Plug Resin ⁽¹⁾	169	151
Wood in Impact limiter	193	175

Note (1): The resin temperature is the volumetric, average temperature at the hottest cross section.

8.0 LISTING OF COMPUTER FILES

A list of the files to create geometries of MP197HB models are shown in Table 8-1.

A summary of ANSYS runs is shown in Table 8-2. All the runs are performed using ANSYS version 8.1 [14] with operating system "Windows XP PRO-SP1", and CPU "Xeon 3.20 GHz".

ANSYS macros, and associated files used in this calculation are shown in Table 8-3.

The spreadsheets for this calculation are listed in Table 8-4.

Table 8-1 List of Geometry Files

File Name (Input and Output)	Description	Date / Time for Output File
MP197HB+BWR_AICS	Macro to create geometry of finned MP197HB with 69BTH DSC	08/25/08 08:10 PM
MP197HB+BWR_N1CS	Macro to create geometry of un-finned MP197HB with 69BTH DSC	08/25/08 08:15 PM
MP197HB+BWR_S1CS	Macro to create geometry of un-finned MP197HB with 61BT/ 61BTH Type 1 DSC	08/25/08 08:20 PM
MP197HB+BWR_S2CS	Macro to create geometry of un-finned MP197HB with 61BTH Type 2 DSC	08/25/08 08:25 PM
MP197HB+PWR_N1CS	Macro to create geometry of un-finned MP197HB with 32PTH, 32PTH Type 1, 32PTH1 Type 1 and Type 2 DSC	08/25/08 08:30 PM
MP197HB+PWR_N2CS	Macro to create geometry of un-finned MP197HB with 37PTH DSC	08/25/08 08:34 PM
MP197HB+PWR_S1CS	Macro to create geometry of un-finned MP197HB with 32PT DSC	08/25/08 08:39 PM
MP197HB+PWR_S2CS	Macro to create geometry of un-finned MP197HB with 24PTH Type 1 and Type 2 DSC	08/25/08 08:43 PM
MP197HB+PWR_S3CS	Macro to create geometry of un-finned MP197HB with 24PT4 DSC	08/25/08 08:48 PM

Table 8-2 Summary of ANSYS Runs

Run Name	Description	Date / Time for Output File	
TC_69BTH_32CS	TC finned with 69BTH and 32 kW	08/26/08	12:47 PM
TC_69BTH_29CS	TC finned with 69BTH and 29.2 kW	08/26/08	01:35 PM
TC_69BTH_26CS	TC un-finned with 69BTH and 26 kW	08/26/08	02:24 PM
TC_61BTHT1_22CS	TC un-finned with 61BTH Type 1 and 22 kW	08/26/08	03:09 PM
TC_61BTHT2_24CS	TC un-finned with 61BTH Type 2 and 24 kW	08/26/08	03:55 PM
TC_61B_18CS	TC un-finned with 61BT and 18.3 kW	08/26/08	04:41 PM
TC_37PTH_23CS	TC un-finned with 37PTH and 23.2 kW	08/26/08	05:22 PM
TC_37PTH_22CS	TC un-finned with 37PTH and 22.0 kW	09/17/08	06:49 PM
TC_32PTH1T1_26CS	TC un-finned with 32PTH, 32PTH Type 1, and 32PTH1 Type 1 with 26 kW	08/26/08	06:07 PM
TC_32PTH1T2_24CS	TC un-finned with 61BT and 18.3 kW	08/26/08	06:48 PM
TC_32PT_24CS	TC un-finned with 32PT and 24 kW	08/26/08	07:35 PM
TC_24PTH_26CS	TC un-finned with 24PTH Type 1 & 2 with 26 kW	08/26/08	08:25 PM
TC_24PT4_24CS	TC un-finned with 24PT4 and 24 kW	08/26/08	09:16 PM
TC_32kW_20CS	TC with 69BTH, 32 kW, -20°F	08/28/08	02:23 PM
TC_32kW_40CS	TC with 69BTH, 32 kW, -40°F	08/28/08	03:17 PM
TC_32kW_ShCS	TC with 69BTH, 32 kW, 100°F, Shade	08/26/08	09:33 AM
TC_23kW_20CS	TC with 37PTH, 23.3 kW, -20°F	08/26/08	10:21 AM
TC_23kW_40CS	TC with 37PTH, 23.2 kW, -40°F	08/26/08	11:20 AM
TC_22kW_20CS	TC with 37PTH, 22.0 kW, -20°F	09/18/08	09:25 PM
TC_22kW_40CS	TC with 37PTH, 22.0 kW, -40°F	09/18/08	10:15 PM
check_Sol_U	Checking of solar heat flux boundary conditions for un-finned cask	08/25/08	09:18 PM
check_Sol_F	Checking of solar heat flux boundary conditions for finned cask	08/25/08	09:36 PM
Heff_Alfin_100 Heff_Alfin_20 Heff_Alfin_40	Effective heat transfer coefficient for external fins	04/15/08 04/15/08 04/15/08	08:46 AM 09:03 AM 09:05 AM
Keff_gap Keff_gc Keff_sl	Effective conductivity for gap between DSC shell and TC inner shell	03/06/08 03/06/08 03/06/08	10:55 AM 11:00 PM 11:02 PM
Mesh_CN	Mesh sensitivity coarse mesh	08/25/08	08:50 PM
Mesh_FN	Mesh sensitivity fine mesh	08/25/08	09:00 PM
TC_69BTH_32CS_R	Sensitivity analysis for slide rail/DSC contact	09/10/08	08:42 AM
TC_69BTH_32U	TC un-finned with 69BTH and 32 kW	10/15/08	09:05 PM
69BTH_32CS_4	69BTH basket w/ 32kW in un-finned TC	10/15/08	11:16 PM

Table 8-3 Associated Files and Macros

File Name	Description	Date / Time
MatMP197HB_CS.inp	Material properties for MP197HB cask models	08/25/08 07:26 PM
HTOT_HCL.mac	Total heat transfer coefficients for horizontal cylindrical surface	04/29/08 09:59 AM
HTOT_VPL.mac	Total heat transfer coefficients for vertical flat surface	11/13/07 12:41 PM
HTOT_HPD.mac	Total heat transfer coefficients for horizontal flat surface facing downwards	11/15/07 06:07 PM
Mat_Alfins.mac	Material properties for finned aluminum shell in Heff_fin runs	01/29/08 05:12 PM
HC_Fin.mac	Convection for external fins used in Heff_fin runs	09/04/07 08:57 PM
HC_Tip.mac	Convection for external fin tips used in Heff_fin runs	05/21/07 04:10 PM
Fins_Gen.inp	Macro to create geometry for external fin sub-model	02/07/08 11:31 AM
DSC_Cask.inp	Macro to create geometry for DSC/Cask radiation sub-model	08/27/07 01:00 PM
Mat_DSC_Cask.inp	Material properties for DSC/Cask inner shell radiation sub-model	03/06/08 10:59 AM
Mat_DSC_SI.inp	Material properties for DSC/Sleeve radiation sub-model	03/06/08 10:56 AM
DSCmid_PWR.txt	Retrieve max DSC shell temp at hottest fuel region for PWR DSCs	10/22/08 09:20 AM
DSCmid_PWR.out		10/22/08 09:28 AM
TempMap_32U.inp	Transfer temp from TC to DSC/Basket model for 69BTH, 32.0 kW w/o fins	10/15/08 07:42 PM
TempMap_32U.out		10/15/08 09:06 PM
Tavg.inp	Retrieve average temperatures for TC model w/o fins, 32 kW	10/20/08 05:07 PM
Tavg.out		10/20/08 05:09 PM

Table 8-4 List of Spreadsheets

File Name	Description	Date / Time
DSC_Data_Nominal.xls	Nominal DSC Dimensions	04/16/08 04:51 PM
MatProp.xls	Material Properties for MP197HB	07/31/08 12:14 PM
Keff_sleeve.xls	Effective conductivity for inner sleeve	11/16/07 12:37 PM
Insolance.xls	Solar heat flux	08/26/08 03:17 PM
HeatFlux.xls	Decay heat flux	09/24/08 02:04 PM
Keff_Radiation.xls	Effective conductivity for gap between DSC/TC	03/10/08 08:45 AM
Heff_Alfin.xls	Effective heat transfer for finned aluminum shell	04/16/08 03:10 PM
Shift_x.xls	Calculation of gap sizes between DSC and TC	02/12/08 11:47 AM
HeatBalance.xls	Heat balance for MP197HB	09/26/08 10:58 AM
ShellContact.xls	Gap between shield shell and finned shell	02/15/08 07:56 PM
Gamma_Gap.xls	Gap between gamma shield and outer shell	01/20/09 10:31 AM
NodalTemp.xls	Nodal temperatures at the slide rail/DSC contact	09/10/08 09:19 AM
Tmax.xls	Maximum Temperatures for Table 7-1	09/24/08 04:13 PM
BL_thk.xls	Boundary layer thinness around cask	02/08/10 06:06 PM

APPENDIX A SHAPES OF EXTERNAL FINS AND INNER SLEEVE

The shapes of the optional external fins and the inner sleeve considered in the TC model are shown in Figure A-1 and Figure A-2, respectively.

The designed external finned shell, shown in Figure A-3 is a continuous shell which covers both of the trunnion plugs up to the skid straps. The considered shape of the external fins in the TC model has fewer fins than the designed finned shell and is therefore conservative for thermal analysis under NCT.

The designed shape of the inner sleeve is shown in Figure A-4. As seen in Figure A-4, there is virtually no gap between the segments of the inner sleeve. The considered shape of the inner sleeve in the TC model includes 120 individual aluminum pieces with 39 radial gaps and three axial gaps. The thicknesses of the radial and axial gaps are respectively 0.25" and 0.188" as shown in Figure A-2. In addition, the material properties of the inner shell elements in contact with the cask slide rails are changed to those of helium to avoid any direct conduction between these two components. Since the considered shape of the inner sleeve in the TC model includes more gaps, it is conservative to use it for thermal analysis of transport cask under NCT.

Proprietary Information Withheld Pursuant to 10 CFR 2.390

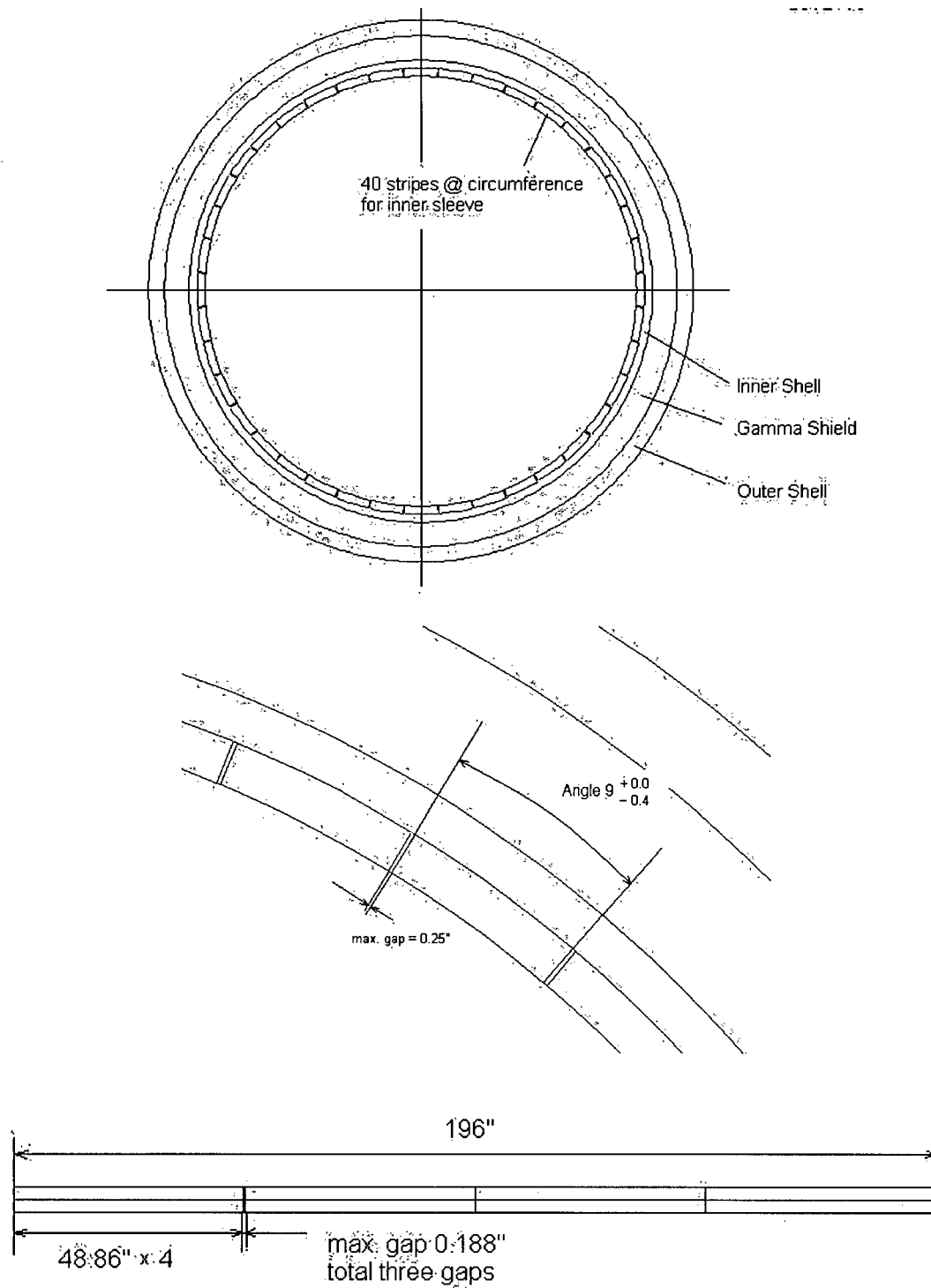


Figure A-2 Assumed Geometry of Inner Sleeve in Thermal Model

Proprietary Information Withheld Pursuant to 10 CFR 2.390

Proprietary Information Withheld Pursuant to 10 CFR 2.390

APPENDIX B TOTAL HEAT TRANSFER COEFFICIENTS

Total heat transfer coefficient, h_t , is used to combine the convection and radiation heat transfer together.

$$h_t = h_r + h_c$$

Where,

h_r = radiation heat transfer coefficient (Btu/hr-in²-°F)

h_c = free convection heat transfer coefficient (Btu/hr-in²-°F)

The radiation heat transfer coefficient, h_r , is given by the equation:

$$h_r = \varepsilon F_{w\infty} \left[\frac{\sigma(T_w^4 - T_{amb}^4)}{T_w - T_{amb}} \right] \text{ Btu/hr-in}^2\text{-}^\circ\text{F}$$

Where,

ε = surface emissivity

F_{12} = view factor from surface 1 to ambient = 1

σ = 0.1714×10^{-8} Btu/hr-ft²-°R⁴

T_w = surface temperature (°R)

T_{amb} = ambient temperature (°R)

Surface emissivity values are discussed in Section 4.2.

The following equations from Rohsenow handbook [7] are used to calculate the free convection coefficients.

For horizontal cylinders:

$$Ra = Gr Pr \quad ; \quad Gr = \frac{g \beta (T_w - T_\infty) D^3}{\nu^2}$$

$$Nu_l = \frac{2f}{\ln(1 + 2f / Nu^T)} \text{ with}$$

$$Nu^T = 0.772 \bar{C}_l Ra^{1/4} \quad ; \quad f = 1 - \frac{0.13}{(Nu^T)^{0.16}} \quad ; \quad \text{with } \bar{C}_l = 0.515 \text{ for gases [7]}$$

$$Nu_t = \bar{C}_t Ra^{1/3}$$

$$\bar{C}_t = 0.103 \text{ for air with } Pr \approx 0.71 \text{ [7]}$$

$$Nu = \left[(Nu_l)^m + (Nu_t)^m \right]^{1/m} \quad \text{with } m = 10 \text{ for } 10^{-10} < Ra < 10^7$$

$$h_c = \frac{Nu \ k}{D} \times 0.1761/144$$

with

g = gravitational constant = 9.81 (m/s²)

β = expansion coefficient = 1/T (1/K)

T = absolute temperature (K)

ν = kinematic viscosity (m²/s)

D = diameter of the horizontal cylinder (in)

k = air conductivity (W/m-K)

The above correlations are incorporated in ANSYS model via macro "HTOT_HCL.mac" listed in Section 8.0.

For vertical flat surfaces:

$$Ra = Gr \ Pr \ ; \ Gr = \frac{g \ \beta (T_w - T_\infty) L^3}{\nu^2}$$

$$Nu_l = \frac{2.0}{\ln(1 + 2.0 / Nu^T)} \text{ with}$$

$$Nu^T = \overline{C}_l \ Ra^{1/4} \quad \text{with } \overline{C}_l = 0.515 \text{ for gases [7]}$$

$$Nu_t = C_t^V \ f \ Ra^{1/3} / (1 + 1.4 \times 10^9 \ Pr / Ra) \text{ with}$$

$$C_t^V = \frac{0.13 \ Pr^{0.22}}{(1 + 0.61 \ Pr^{0.81})^{0.42}} \quad f = 1.0 + 0.078 \left(\frac{T_w}{T_\infty} - 1 \right)$$

$$Nu = \left[(Nu_l)^m + (Nu_t)^m \right]^{1/m} \quad \text{with } m = 6 \text{ for } 1 < Ra < 10^{12}$$

$$h_c = \frac{Nu \ k}{L}$$

with

g = gravitational constant = 9.81 (m/s²)

β = expansion coefficient = 1/T (1/K)

T = absolute temperature (K)

ν = kinematic viscosity (m²/s)

L = height of the vertical surface (in)

k = air conductivity (W/m-K)

The above correlations are incorporated in ANSYS model via macro "HTOT_VPL.mac" listed in Section 8.0.

For horizontal flat surfaces facing downwards:

The following correlations are used only for the outer surface of the bearing block at the lower half of the TC.

$$Ra = Gr Pr \quad ; \quad Gr = \frac{g \beta (T_w - T_\infty) (L^*)^3}{\nu^2}$$

$$Nu_l = \frac{2.5}{\ln(1 + 2.5 / Nu^T)} \quad \text{with}$$

$$Nu^T = \frac{0.527}{\left(1 + (1.9 / Pr)^{9/10}\right)^{2/9}} Ra^{1/5}$$

$$Nu = Nu_l \quad \text{for } 10^3 < Ra < 10^{10}$$

$$h_c = \frac{Nu k}{L^*}$$

with

g = gravitational constant = 9.81 m/s²

β = expansion coefficient = 1/T (1/K)

T = absolute temperature (K)

ν = kinematic viscosity (m²/s)

$$L^* = \frac{A}{p} = \frac{\text{heated area}}{\text{heated perimeter}} = 1.2'' \text{ (shortest surface of bearing block)}$$

k = air conductivity (W/m-K)

The above correlations are incorporated in ANSYS model via macro "HTOT_HPD.mac" listed in Section 8.0.

Air properties are taken from [7] and listed in Table 4-9.

APPENDIX C JUSTIFICATION OF GAMMA SHIELD / OUTER SHELL GAP

A 0.025" radial air gap is assumed between the gamma shield (lead) and the TC outer shell within the finite element model described in Section 4.0. This air gap is due to the differential thermal expansion of the cask body and the gamma shield during the lead pour.

The following assumptions are made for the verification of the gap:

The cask body has nominal dimension at 70°F.

During the lead pour the cask body and lead are at 620°F.

The inner diameter of the gamma shell (lead) is equal to the outer diameter of the inner cask shell at thermal equilibrium.

The average coefficients of thermal expansion for SA-203, Gr. E and lead are listed in Table C-1.

Table C-1 Thermal Expansion Coefficients

Temperature (°F)	SA203, Gr. E α (in/in-°F) [2]	Temperature (°F)	Lead α (in/in-°F) [2]
70	6.40E-06	70	16.07 E-6
200	6.70E-06	100	16.21 E-6
300	6.90E-06	175	16.58 E-6
400	7.10E-06	250	16.95 E-6
500	7.30E-06	325	17.54 E-6
600	7.40E-06	440	18.50 E-6
650	7.60E-06	620	20.39 E-6

The density of lead as a function of temperature is listed in Table C-2.

Table C-2 Density of Lead

Temperature (K)	Density [9] (kg/m ³)	Temperature (°F)	Density (lbm/in ³)
50	11,570	-370	0.4180
100	11,520	-280	0.4162
150	11,470	-190	0.4144
200	11,430	-100	0.4129
250	11,380	-10	0.4111
300	11,330	80	0.4093
400	11,230	260	0.4057
500	11,130	440	0.4021
600	11,010	620	0.3978

The volume within the "lead cavity" is found by determining the cask body dimensions at 620°F. As no gaps will be present between the molten lead and the cask body this volume is also equal to the volume of lead at 620°F. The mass of the lead filled the lead cavity at 620°F is then determined.

The dimensions of the "lead cavity" are calculated based on cask body temperature. A temperature of 360°F is considered for the cask body. This temperature is lower than the maximum cask inner shell temperature shown in Table 6-1. Since the gap size increases at lower temperatures, the above chosen value is conservative. From the mass of the lead and its density at 360°F, the lead volume is determined.

The length of the gamma shield at the cask body temperature is calculated based on thermal expansion coefficients listed in Table C-1. The lead volume is used to determine the maximum size of the air gap adjacent to the lead.

Determination of Lead Mass

$$\alpha_{CS} = 7.44 \times 10^{-6} \text{ in/in-}^\circ\text{F @ 620}^\circ\text{F (via linear interpolation, Table C-1)}$$

$$\rho_{\text{lead}} = 0.3978 \text{ lbm/in}^3 \text{ @ 620}^\circ\text{F (Table C-2)}$$

$$R_{\text{in}} = \text{inner radius of lead cavity @ 70}^\circ\text{F} = 36.50"$$

$$R_{\text{out}} = \text{outer radius of lead cavity @ 70}^\circ\text{F} = 39.75"$$

$$L_{\text{cavity}} = \text{length of lead cavity @ 70}^\circ\text{F} = 195.75"$$

$$R_{\text{in}, 620} = (R_{\text{in}})(1 + (\alpha_{CS})(\Delta T)) = (36.50)[1 + (7.44\text{E-}6)(550)] = 36.6494"$$

$$R_{\text{out}, 620} = (R_{\text{out}})(1 + (\alpha_{CS})(\Delta T)) = (39.75)[1 + (7.44\text{E-}6)(550)] = 39.9127"$$

$$L_{\text{cavity}, 620} = (L_{\text{cavity}})(1 + (\alpha_{CS})(\Delta T)) = (195.75)[1 + (7.44\text{E-}6)(550)] = 196.5510"$$

$$V_{\text{cavity}} = V_{\text{lead}} = (\pi)(R_{\text{out}, 620}^2 - R_{\text{in}, 620}^2)(L_{\text{cavity}, 620}) = 154,274.9 \text{ in}^3$$

$$M_{\text{lead}} = (V_{\text{lead}})(\rho_{\text{lead}}) = (154,274.9 \text{ in}^3)(0.3978 \text{ lbm/in}^3) = 61,363.6 \text{ lbm}$$

Determination of Lead Gap

$$\alpha_{CS} = 7.02 \times 10^{-6} \text{ in/in-}^\circ\text{F @ 360}^\circ\text{F (via linear interpolation, Table C-1)}$$

$$\alpha_{\text{lead}, 620} = 20.39 \times 10^{-6} \text{ in/in-}^\circ\text{F @ 620}^\circ\text{F (Table C-1)}$$

$$\alpha_{\text{lead}, 360} = 17.83 \times 10^{-6} \text{ in/in-}^\circ\text{F @ 360}^\circ\text{F (via linear interpolation, Table C-1)}$$

$$\rho_{\text{lead}} = 0.4037 \text{ lbm/in}^3 \text{ at 360}^\circ\text{F, via linear interpolation from Table C-2}$$

$$R_{\text{in}, \text{cs}, 360} = (R_{\text{in}})(1 + (\alpha_{CS})(\Delta T)) = (36.50)[1 + (7.02\text{E-}6)(290)] = 36.5743"$$

$$R_{\text{out}, \text{cs}, 360} = (R_{\text{out}})(1 + (\alpha_{CS})(\Delta T)) = (39.75)[1 + (7.02\text{E-}6)(290)] = 39.8309"$$

$$L_{\text{lead}, 360} = (L_{\text{cavity}, 620}) / [(1 + (\alpha_{\text{lead}, 620})(620 - 70)) * (1 + (\alpha_{\text{lead}, 620})(360 - 70))] = \\ (196.5510) / [1 + (20.39\text{E-}6)(550)] * [1 + (17.83\text{E-}6)(290)] = 195.3764"$$

$$V_{\text{lead}, 360} = M_{\text{lead}} / \rho_{\text{lead}} = 61,363.6 / 0.4037 = 152,004.6 \text{ in}^3$$

Since $R_{\text{in}, \text{cs}, 360} = R_{\text{in}, \text{lead}, 360}$, then :

$$V_{\text{lead}, 360} = (\pi)(R_{\text{out}, \text{lead}, 360}^2 - R_{\text{in}, \text{ss}, 360}^2)(L_{\text{lead}, 360})$$

It gives:

$$R_{\text{out}, \text{lead}, 360} = 39.8162''$$

$$\text{Air gap} = R_{\text{out}, \text{cs}, 360} - R_{\text{out}, \text{lead}, 360} = 39.8309 - 39.8162 = 0.0147''$$

The assumed air gap of 0.025" is larger than the above calculated gap. Therefore, using a gap of 0.025" is conservative to maximize the DSC shell temperature.

APPENDIX D JUSTIFICATION OF CASK SHIELD SHELL / ALUMINUM FINNED SHELL GAP

An air gap of 0.01" is considered in the model between the cask shield shell (SA-516-70) and the finned aluminum shell (Al 6061) for MP197HB cask with over 26 kW heat load. The following calculation shows that the modeled gap of 0.01" is adequate to bound the existing contact resistance between these two shells.

Yovanovich suggests the following approach in [15] to calculate the thermal contact conductance.

$$h_j = h_c + h_g \quad (D.1)$$

h_j = total thermal contact conductance (m²-K/W)

h_c = contact conductance (m²-K/W)

h_g = gap conductance (m²-K/W)

The thermal contact resistance is:

$$R_j = 1 / h_j \quad (D.2)$$

The contact conductance, h_c , is given in [15] by:

$$h_c = 1.25 k_s \frac{m}{\sigma} \left(\frac{P}{H_c} \right)^{0.95} \quad (D.3)$$

Where

$k_s = 2 k_1 k_2 / (k_1 + k_2)$ Harmonic mean thermal conductivity of interface (W/m-K)

$m = \sqrt{m_1^2 + m_2^2}$ Effective mean absolute asperity slope of interface

$\sigma = \sqrt{\sigma_1^2 + \sigma_2^2}$ Effective RMS surface roughness of contacting asperities (m)

P = Contact pressure (MPa)

H_c = Microhardness of the softer of the two contacting solids (MPa) = $H_{C,Al}$ in this evaluation

The mean absolute asperity slope for each plate can be approximated by the following correlation from [15]:

$$m_i = 0.125 (\sigma_i \times 10^{-6})^{0.402} \quad \text{for } 0.216 \mu m \leq \sigma \leq 9.6 \mu m \quad (D.4)$$

As seen in equation (D.3), the contact conductance, h_c , depends heavily on contact pressure, P. Assuming a very small contact pressure of 10⁻⁶ psi, gives a negligible contact

conductance, h_c and eliminates this term in calculation of the total thermal contact conductance in equation (D.1).

A contact pressure of 10^{-6} psi is equivalent to having no friction between the two shells, which is very conservative.

Due to elimination of h_c in equation (D.1), the conductivities of the contacting plates are not required for this calculation.

The gap conductance, h_g , is given in [15] by:

$$h_g = k_g / (Y + M) \quad (D.5)$$

Where

k_g = thermal conductivity of the gap substance (W/m-K)

Y = effective gap thickness (m)

M = gas parameter (m)

Based on [15], the effective gap thickness, Y , shown in Figure D-1, can be calculated as follows:

$$Y = 1.53 \sigma (P / H_c)^{-0.097} \quad \text{for } 10^{-5} < P / H_c < 2 \times 10^{-2} \quad (D.6)$$

The gas parameter M accounts for the rarefaction effects at high temperatures and low gas pressure. This gas-surface parameter depends on the thermal accommodation coefficients, the ratio of specific heats, the Prandtl number, and the molecular mean free-path of the gas. This complex gas-surface parameter depends on gas pressure and temperature according to the following relationship:

$$M = M_0 \frac{T}{T_0} \frac{P_{g,0}}{P_g} \quad (D.7)$$

Where M_0 denotes the gas parameter value at the reference values of gas temperature and pressure, T_0 and $P_{g,0}$, respectively. T and P_g are temperature and pressure of the contact gas. The gas parameter for air is 0.373×10^{-6} m at 50°C and 1 atm, as reported in [15].

An operating temperature of 200°F (378K) is considered for T and k_g in equations (D.5) and (D.7). The assumed operating temperature is well below the cask shield shell and the finned aluminum shell temperatures in Table 6-1 and is therefore conservative.

A pressure of 1 atm is considered for air between the two shells.

Based on Table 4-9, the air conductivity is 0.0015 Btu/hr-in- $^\circ\text{F}$ or 0.031 W/m-K at 200°F .

The following data in Table D-1 are considered for roughness and hardness of the shells.

Table D-1 Surface Properties for Aluminum and Stainless Steel Plates

Material	Roughness (μm)	Hardness	Microhardness ⁽¹⁾ (MPa)
Aluminum	0.2 to 6.3 [16]	25 to 95 Brinell 500kg [17]	440 to 1079
SA 203, Gr. E	0.2 to 6.3 [16]	(2)	---

Note (1): For conversion of roughness units see reference [19]

Note (2): Based on [15], the hardness of the softer plate, aluminum here, is taken for evaluation.

Surface roughness is mainly determined by the production method. The roughness values in Table D-1 correspond to average values for cold rolling / drawing process.

The contact resistances are calculated based on the average roughness and hardness from Table D-1 and listed below.

$$\sigma_{\text{Al}} = 3.25 \mu\text{m}, \quad H_{\text{c,Al}} = 760 \text{ MPa}$$

$$\sigma_{\text{CS}} = 3.25 \mu\text{m}$$

The calculated contact resistance is listed in Table D-2.

Table D-2 Contact Resistances between Shield Shell and Finned Aluminum Shell

Contact Type	Al / SA203
σ (μm)	4.60E-06
P (MPa)	6.891E-09
H_c (MPa)	760
P_g (atm)	1.0
T (K)	378
k_g (W/m-K)	0.031
P/H_c	9.073E-12
Y (μm)	8.283E-05
M (μm)	4.361E-07
h_c (W/m ² -K)	0.00
h_g (W/m ² -K)	374
h_j (W/m ² -K)	374
R_j (m ² -K/W)	2.7E-03

The equivalent thermal resistance for the air gaps across the shells considered in the MP197HB is:

$$R_{j,model} = \frac{\Delta x_{gap}}{k_g} \quad (D.8)$$

$$\Delta x_{gap} = 0.01'' = 2.54E-4 \text{ m}$$

$$R_{j,model} = \frac{2.54E-4}{0.031} = 8.2E-3 \text{ m}^2\text{-K/W}$$

The above thermal resistance considered in the model ($R_{j,model}$) is about three times larger than the calculated contact resistances ($R_{j,i}$) shown in Table D-2. This indicates that the air gap of 0.01" considered in the model is more than adequate to bound the contact resistance between the cask shield shell and the finned aluminum shell.

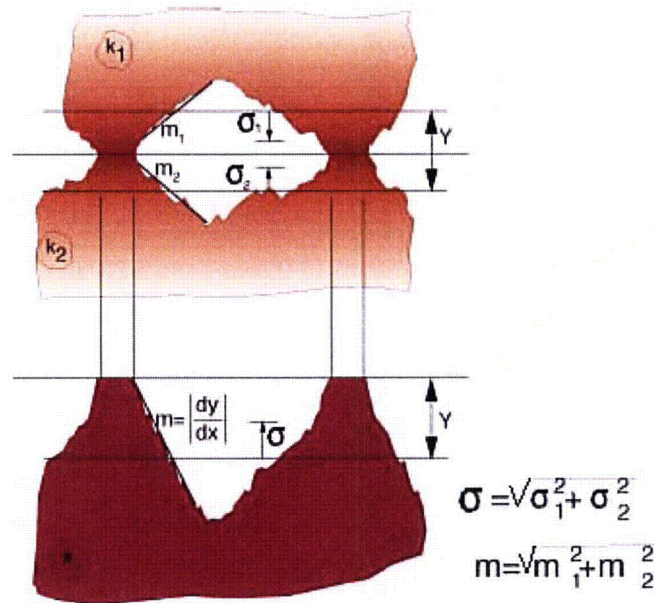


Figure D-1 Conforming Rough Surfaces [15]

APPENDIX E MESH SENSITIVITY

A slice of the TC model containing 69BTH DSC shell is recreated for mesh sensitivity analysis (Mesh_CN run listed in Table 8-2). The length of the TC slice model is 24" and includes the DSC shell and cask shells. The mesh density of this model is the same as the mesh density of the geometry model "MP197HB+PWR_N" listed in Table 8-1 from z=30.5" to z=60.34" except that the element size is decreased from 3.73" to 3.0" in the axial direction. The slice model contains 26,744 elements and 29,574 nodes. The number of nodes and elements in the slice model are identical to the model "MP197HB+PWR_N" from z=30.5" to z=60.34".

For the purpose of mesh sensitivity analysis, the mesh density of the slice model is increased to more than five folds of its original value so that the number of elements and nodes are increased to 147,376 and 154,564, respectively (Mesh_FN run listed in Table 8-2).

Ambient temperature of 100°F with insolation and a decay heat of 26 kW are considered as boundary conditions for both TC slice models with coarse and fine meshes. The boundary conditions are applied using the same methodology as described in Section 5.0. The maximum temperatures are retrieved from these models and listed in Table E-1 for comparison.

As seen in Table E-1, the differences between the maximum temperature for coarse and fine mesh models are less than 1°F. It concludes that the TC model described in Section 5.0 is mesh insensitive and the results reported in Sections 6.0 and 7.0 are adequately accurate for evaluation.

Table E-1 Maximum Temperatures for Coarse and Fine Model of MP197HB TC

DSC type	69BTH, 26 kW, 100°F, Insolation TC without External Fins and Inner Sleeve		
Mesh Type	Coarse	Fine	
Component	T _{max} (°F)	T _{max} (°F)	Difference (T _{Fine} - T _{Coarse}) (°F)
DSC shell	426.5	427.3	0.8
Cask inner shell	307.4	308.3	0.9
Gamma shield	305.9	306.8	0.9
Outer shell	269.1	270.0	0.9
Shield shell	218.8	218.8	0.0
Neutron Shield Resin ⁽¹⁾	239.9	240.4	0.5

Note (1): The resin temperature is the volumetric, average temperature at the hottest cross section.

APPENDIX F SENSITIVITY ANALYSIS FOR TEMPERATURES
AT CONTACT AREA BETWEEN SLIDE RAILS AND DSC SHELL

As stated in Section 3.0, a 0.01" gap is considered between the TC slide rail and the DSC shell. Although this gap is conservative regarding the maximum DSC temperatures, it decreases potentially the temperature gradient through the circumference of the DSC shell at the location of its contact with the TC slide rail. To capture the maximum circumferential temperature gradient, it is assumed in this sensitivity analysis that perfect contact exist between the slide rails and the DSC shell at 168° and 192° orientations.

MP197HB TC loaded with 69BTH DSC and 32 kW heat load under hot NCT (100°F ambient and insolation) is selected for sensitivity analysis.

The above assumption is implemented by changing the effective conductivity of the TC slide rails (calculated in Section 5.4) to conductivity of SA-240, type 304 (see Table 4-2 for the properties). Since the upper nodes of the TC slide rail are connected to the DSC shell, this modification creates a perfect contact between these two components. The ANSYS run for the modified model "TC_69BTH_32CS_R" is listed in Table 8-2.

The maximum DSC shell temperature for the model with 0.01" gap between the TC slide rail and the DSC shell is 483.8°F as shown in Figure 6-1. The maximum temperature of the DSC shell for the modified model is 483.8°F and remains unchanged.

The local temperatures of the contact area between the TC slide rail and the DSC shell are listed in Table F-1.

As seen in Table F-1, the DSC shell temperature at the contact area decrease at most by 12.7°F when perfect contact is assumed between the TC slide rail and the DSC shell.

The following commands are used to select the nodes in the contact area between the TC slide rail and the DSC shell:

```
esel,s,mat,,10  
nsle,s  
esel,s,mat,,1  
nsle,r
```

The nodal temperatures are listed using the PRNSOL command in ANSYS post processor (/post1).

Table F-1 Temperatures at Contact between TC Rail and DSC Shell for Sensitivity Analysis

With 0.01" gap				w/o gap			
Run Name	TC_69BTH_32CS	TC_69BTH_32CS_R		Run Name	TC_69BTH_32CS	TC_69BTH_32CS_R	
Node No.	T _{32CS} (°F)	T _{32CS_R} (°F)	ΔT (°F)	Node No.	T _{32CS} (°F)	T _{32CS_R} (°F)	ΔT (°F)
230470	385.3	374.1	11.2	379357	360.3	348.3	12.0
233980	385.5	374.3	11.2	381138	359.6	347.6	12.0
234452	385.6	374.4	11.2	382945	357.2	345.1	12.1
234924	385.7	374.5	11.2	385911	287.4	284.5	2.9
235396	385.8	374.6	11.2	387542	289.5	285.8	3.7
235868	385.9	374.8	11.2	389173	309.7	299.9	9.8
236340	387.0	376.0	11.0	390804	309.7	300.0	9.8
236812	386.8	376.2	10.7	392435	318.6	306.5	12.1
237284	383.7	374.4	9.4	394066	320.9	308.5	12.4
237756	371.5	367.3	4.2	395847	320.9	308.5	12.4
238662	366.2	363.6	2.6	397628	326.1	313.4	12.7
239351	362.1	360.0	2.1	399409	329.3	316.7	12.6
240040	360.8	359.1	1.7	401190	331.6	319.0	12.6
240729	359.9	358.1	1.8	402971	333.2	320.6	12.6
293401	285.5	283.1	2.4	404752	333.2	320.6	12.6
295752	284.7	282.5	2.1	406533	334.4	321.8	12.6
296224	283.9	282.0	1.9	408314	334.4	321.8	12.6
296696	283.7	281.8	1.9	410095	334.6	322.1	12.6
297168	283.0	281.3	1.7	411876	334.8	322.3	12.6
297640	282.3	280.8	1.5	413507	355.0	342.9	12.1
298112	277.0	276.5	0.5	415314	353.0	340.8	12.1
298584	273.8	273.6	0.2	417121	351.2	339.0	12.2
299056	271.6	271.4	0.1	418928	349.5	337.3	12.2
299528	270.1	270.0	0.1	420735	348.0	335.7	12.3
300434	268.9	268.7	0.2	422542	346.6	334.3	12.3
301123	268.5	268.2	0.3	424349	345.3	333.0	12.3
301812	267.9	267.6	0.3	426156	344.0	331.6	12.4
302501	267.6	267.3	0.3	427963	342.8	330.4	12.4
303190	267.3	267.0	0.3	429770	341.7	329.2	12.4
355173	385.0	373.8	11.2	431571	340.8	328.3	12.5
356804	384.7	373.5	11.3	433336	340.0	327.5	12.5
358435	382.4	371.1	11.4	435101	339.5	327.0	12.5
360066	382.4	371.0	11.4	436902	339.2	326.7	12.5
361697	380.0	368.6	11.4	438709	338.9	326.4	12.5
363328	378.9	367.5	11.5	440516	338.6	326.1	12.5
365109	378.9	367.4	11.5	442323	338.3	325.8	12.5
366890	375.1	363.5	11.6	444130	338.0	325.5	12.5
368671	371.3	359.6	11.7	445937	337.6	325.1	12.5
370452	367.6	355.8	11.8	447744	337.2	324.6	12.5
372233	364.2	352.3	11.9	449551	336.7	324.2	12.5
374014	364.1	352.3	11.9	451358	336.2	323.6	12.5
375795	361.0	349.1	12.0	453165	335.6	323.0	12.6
377576	361.0	349.0	12.0	ΔT _{max} = 12.7°F			

Note (1): ΔT = (T_{32CS} - T_{32CS_R})

**APPENDIX G THERMAL ANALYSIS RESULTS FOR MP197HB LOADED WITH 37PTH DSC
AND 23.2 KW HEAT LOAD FOR STRUCTURAL ANALYSIS INPUT**

MP197HB loaded with 37PTH DSC and 23.2 kW heat load is analyzed only for the structural evaluation purposes. The maximum component temperatures for NCT at various ambient conditions are listed in Table G-1.

Table G-1 Maximum Component Temperatures for MP197HB loaded with 37PTH DSC and 23.2 kW Heat Load

DSC type	37PTH, 23.2 kW, TC without External Fins or Inner Sleeve		
Ambient Conditions	100F with Insolation	-20°F, No Insolation	-40°F, No Insolation
Component	T_{max} (°F)	T_{max} (°F)	T_{max} (°F)
DSC shell	421	342	329
Cask inner shell	324	229	214
Gamma shield	323	228	212
Outer shell	311	215	199
Shield shell	279	182	166
Cask lid	310	214	198
Cask bottom plate	252	154	137
Neutron Shield Resin ⁽¹⁾	270	172	156
Trunnion Plug Resin ⁽²⁾	255	152	135
Wood in Impact limiter	270	165	148

Note (1): This temperature is the volumetric, average temperature of the elements located at hottest cross section of the neutron shield resin.

Note (2): This temperature is the volumetric, average temperature of the elements located at hottest cross section of the trunnion plug resin.

**APPENDIX H THERMAL ANALYSIS RESULTS FOR MP197HB LOADED WITH 69BTH DSC
AND 32 KW HEAT LOAD WITHOUT EXTERNAL FINS**

This section provides the thermal analysis for MP197HB loaded with 69BTH DSC and 32 kW heat load when no external fins are used for the cask. The geometry model developed for un-finned cask "MP197HB+BWR_N1CS" listed in Table 8-1 is used for this analysis.

The heat load for this model is set to 32 kW. All other boundary conditions, assumptions, conservatism, and material properties are the same as those used for the un-finned cask model "TC_69BTH_26CS" listed in Table 8-2. The boundary conditions for TC model are described in Section 5.0. The finite element model of un-finned cask with 32 kW heat load is documented in "TC_69BTH_32U" run listed in Table 8-2.

The DSC shell temperature profile is retrieved from the TC model using the macro "TempMap_32U.inp" listed in Table 8-3. The retrieved DSC shell temperatures are applied as boundary conditions on the DSC/basket model of 69BTH DSC described in [25]. All other boundary conditions, assumptions, conservatism, and material properties remain the same as those described in [25] for 69BTH DSC.

The maximum TC and DSC component temperatures are listed in Table H-1 for MP197HB with no external fins loaded with 69BTH DSC and 32 kW heat load under NCT at 100°F ambient.

The temperature profiles for TC and DSC components are shown in Figure H-1 and Figure H-2, respectively.

**Table H-1 Maximum Component Temperatures of TC and 69BTH DSC
with 32 kW Heat Load within MP197HB with No External Fins**

Component	T _{max} (°F)	Limit (°F)
Fuel Cladding	674	752 [2]
Basket (compartment)	638	---
Al / Poison Plate	622	---
Basket Rails	534	---
Top Shield Plug	302	---
Bottom Shield Plug	470	---
DSC shell	510	---
DSC shell @ mid-length ⁽¹⁾	496	---
Cask inner shell	398	---
Gamma shield	397	621 [13]
Outer shell	382	---
Shield shell	335	---
Cask lid	295	---
Cask bottom plate	383	---
Neutron Shield Resin ⁽²⁾	276	320 [2].
Trunnion Plug Resin ⁽³⁾	303	445 [24]
Cask lid seal	296	400 [2]
Ram plate seal	382	400 [2]
Drain port seal @ bottom	381	400 [2]
Test seal @ bottom	379	400 [2]
Vent & test seal @ top	295	400 [2]
Wood in Impact limiter ⁽⁴⁾	208	320 [2]

Note (1): This value is the maximum DSC shell temperature in the region where the fuel assemblies have the maximum peaking factor.

Note (2): This temperature is the volumetric, average temperature of the elements over the entire length of the neutron shield resin.

Note (3): This temperature is the volumetric, average temperature of the elements located at hottest cross section of the trunnion plug resin.

Note (4): This temperature is the volumetric, average temperature of the elements located at hottest cross section of the wood.

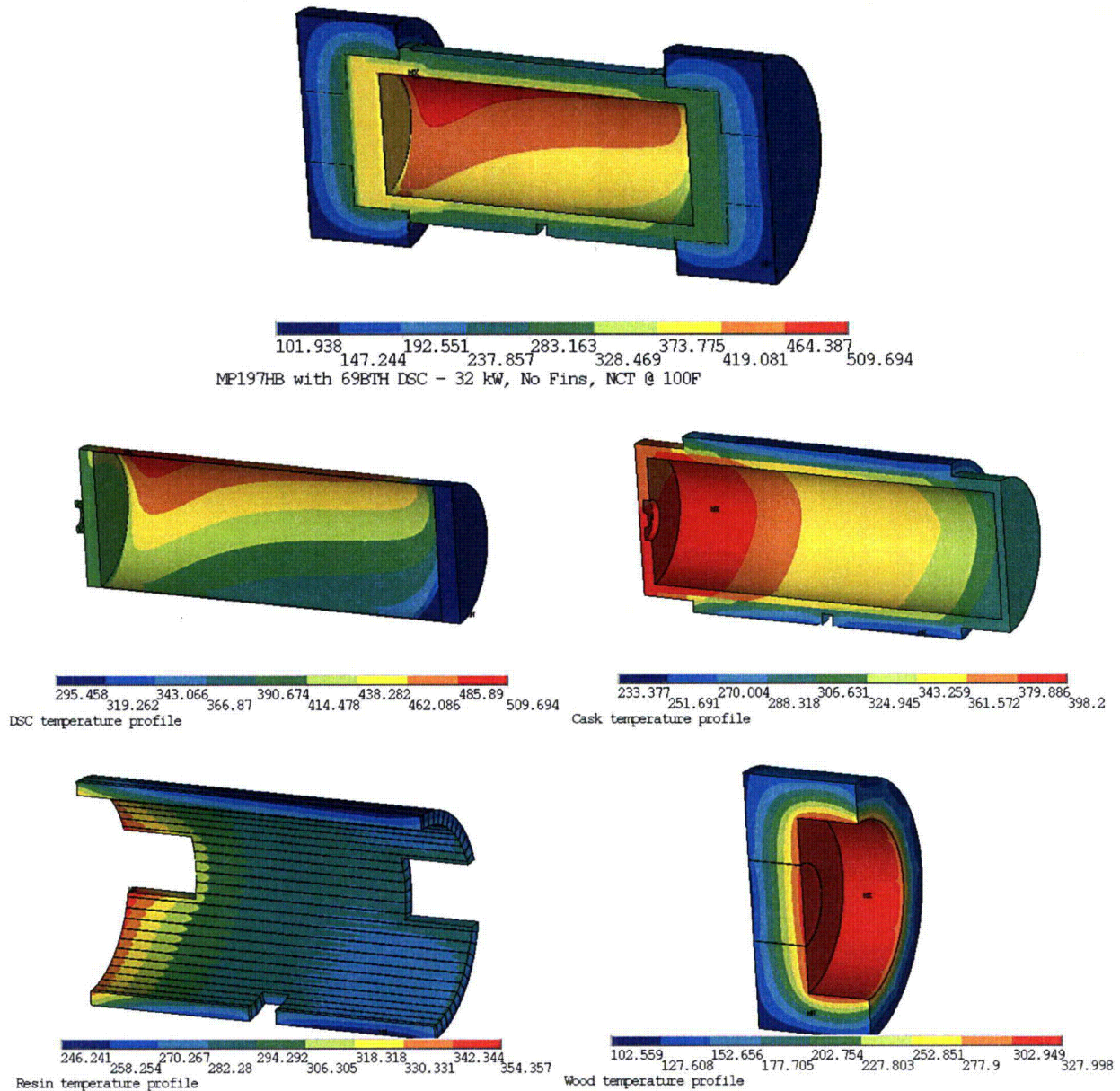


**Figure H-1 Temperature Profiles for MP197HB Transport Cask
NCT, 100°F, Insolation, 69BTH DSC, 32 kW, No External Fins**

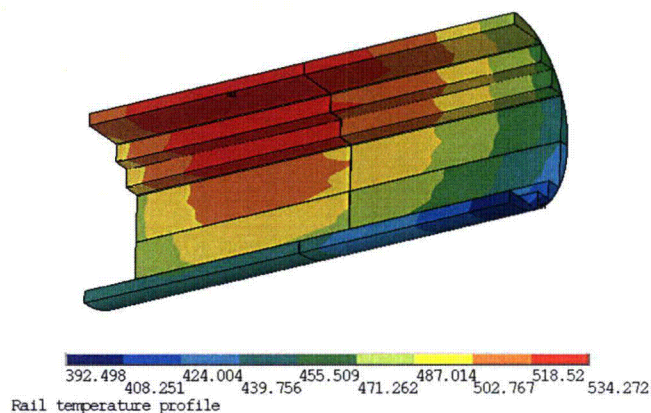
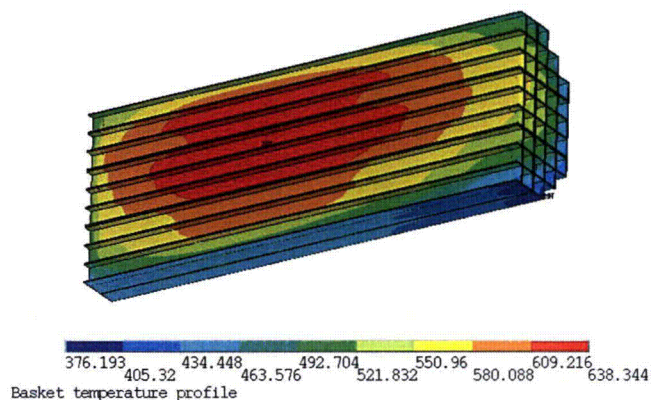
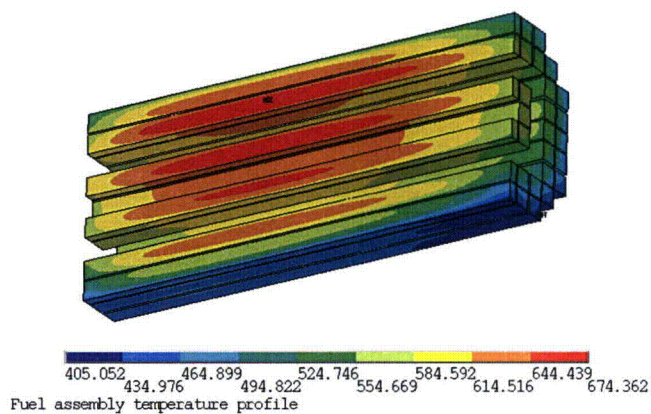


**Figure H-2 Temperature Profiles for 69BTH DSC Components
NCT, 100°F, HLZC #4 [25] in TC w/o External Fins**

As seen in Table H-1, the maximum (average when applicable) temperatures of the MP197HB components calculated for NCT are lower than the allowable limits.

The maximum fuel cladding temperature is 674°F and remains well below the allowable fuel cladding temperature limit of 752°F established in [2].

The maximum seal temperature is 382°F belonging to ram closure plate. This temperature is well below the long-term limit of 400°F specified for continued seal function.

The maximum wood temperature retrieved from the model (TC_69BTH_32U.out, see Figure H-1) is 328°F. This high temperature is local and spread only in a thin layer of wood as shown in Figure H-1. The average wood temperature at the hottest cross section is 208°F, which is well below the limit of 320°F for crush structural analysis.

The maximum temperature of gamma shield (lead) is 397°F (see Table H-1), which is well below the lead melting point of 621°F.

The highest volumetric average resin temperature in the neutron shield at the hottest cross section is 322°F (TC_69BTH_32U.out), which is slightly over the selected limit of 320°F. The highest average resin temperature is concentrated in a thin segment located at the bottom of the neutron shield as shown in Figure H-1. The average resin temperature over the entire length of the neutron shield resin is 276°F (see Table H-1), which is well below the limit of 320°F. It concludes that the overall shielding effect of the resin remains intact.

The highest volumetric average resin temperature in the trunnion plugs at the hottest cross section is 355°F. The polypropylene resin temperature is well below the temperature limit of 445°F and no degradation of the trunnion plug resin is expected.

All materials can be subjected to a minimum environment temperature of -40°F (-40°C) without any adverse effects.

Based on discussions in Section 6.2, the maximum accessible surface temperature belongs to personnel barrier. Table H-1 shows that the maximum temperature of the cask outer surface for TC without external fins under insolation is 335°F. This temperature bounds the cask outer surface temperature without insolation. Using the methodology described in Section 5.6, the maximum temperature of the personnel barrier is calculated based on the maximum cask outer surface temperature of 335°F. The maximum temperature of the personnel barrier is 163°F. This temperature is well below the limit of 185°F defined in Section 4.3.

All design criteria are herein satisfied for MP197HB without external fins loaded with 69BTH DSC with the maximum heat load of 32 kW for NCT.